Nonlinear Analysis of Waves Induced Motions and Loads in Large Amplitude Waves

Giuseppe Mortola (MSc, BSc)

Department of Naval Architecture and Marine Engineering,

University of Strathclyde, Glasgow, UK

This thesis is submitted in fulfilment of the requirements for the degree of PhD in Naval Architecture and Marine Engineering

2013

Copyright Statement

Signed:

Date:

Acknowledgements

After these wonderful years of postgraduate studies in Glasgow it is difficult to thank all the people that, in a way or another, contribute to the making of this thesis and without whom I could not succeed. I will try to do my best to acknowledge all of them.

First of all I would like to express all my gratitude to my supervisor, Prof. Atilla Incecik, who helped me with his knowledge and experience. I will never forget the encouragement, kindness and positive attitude during our long meetings, thank you.

I would like to thank also Prof. Osman Turan for his advices and the opportunities that he gave me to expand my experience in these years.

I thank the Lloyd's Register of Shipping and EPSRC for the financial support during my studies and the EPSRC funded ARCHIE-WeSt High Performance Computer for the countless core hours.

I'm also very thankful to all the people that helped me and support me:

Dr. Spyros Hirdaris, for sharing his experience and ideas during the review meetings of this project. and Dr. Yongwon Lee for helping me with the data of the Wils-II container ship.

All the students and researchers of the research area at NAME who made these challenging years unforgettable, and Thelma for her cares and guide through the academical life.

All my family that helped me to pursuit my passion.

Chicca, to give me strength and determination with her infinite support and patience, from the first sentence to the last correction. Thank You.

to my father

Abstract

An ocean going vessel, sailing in severe seas, experiences motions and loads that are largely affected by nonlinear phenomena. These effects deviate the responses from the linear prediction, modifying their magnitudes, symmetry and frequency characteristics. The change of the actual wetted geometry due to motions and large ambient waves elevation and the occurrence of impulsive phenomena, such as bottom impact, are some of the main sources of nonlinearities.

Current state-of-art in seakeeping, applied to ship design, is based on the assumption of small amplitude motions and linearity between the excitation and the response. These techniques have been proved, during the years, to be reliable for small and moderate sea states, but they are not effective in large amplitude waves. The understanding and prediction of the behaviour of the vessel in rough seas is of crucial importance for its design, and therefore there is a need for better methods and practices.

Application of nonlinear seakeeping methods in a every-day design situations is limited. The complexity and the computational cost of some methodologies, together with the absence of standardised procedures, are the main causes for the reduced use of such a methodologies.

The work presented in this thesis aims to develop a practical nonlinear seakeeping approach that can be used in a design content to model wave induced motions and loads in large amplitude waves.

The wave-body interaction problem is solved using a time domain nonlinear two dimensional approach, that considers the actual wetted hull portion and the relative velocity between the structure and the waves. The vessel is modelled as a flexible body to allow structural dynamics. The proposed formulation takes into account impulsive phenomena due to water impact, on both the bottom and the

flare of the hull, using a combination of analytical and empirical techniques.

The proposed methodology is applied to the S-175 and the Wils II 13,000 TEU container ships. The validation of the proposed method, conducted in both small and large amplitude regular waves, shows the capability of the technique to correctly predict the behaviour of the vessel also when linear methodologies fail. The analysis demonstrates the importance and the reliability of hydroelastic methods for the prediction of wave induced loads, especially when whipping is relevant.

A procedure, which applies the proposed methodology for the evaluation of maximum expected values of wave induced motions and loads is presented. Long term analyses are conducted, using both linear and nonlinear method, to study the effect of nonlinearities. The comparison between linear and nonlinear approaches shows an increase of maximum load responses when nonlinear hydroelasticity is applied. This study highlights also the dependency of the results on the selection of the return period and operational velocity profile of the vessel.

Contents

List of Figures

List of Tables

Chapter 1

Introduction

1.1 Background

The design and construction of a new class of ultra large container ships has brought into the spotlight the necessity to improve our understanding of wave induced motions and loads in severe seas. These vessels are characterised by large dimensions ($L > 300m$), significant bow flare, that enhances nonlinear effects, relatively high Froude number and flexible structures which increases the amplitude of high frequency vibrations due to periodic and impulsive fluid actions.

Seakeeping methods based on linear assumptions partially model or do not consider all these previously described characteristics, resulting often in an not accurate evaluation of motions and loads in large amplitude waves. Linear methodologies are the industry standard for seakeeping analysis, due to their simplicity and calculation speed. In order to apply nonlinear based methods in a design content, it is necessary to develop a methodology that is able to take into account the principal nonlinear effects associated to large amplitude waves and that is fast enough to be used in everyday ship design.

Nonlinear wave-body interaction techniques have been developed for more than

twenty years. The research in this topic has been driven by two different objectives: a first one, that aimed to improve the knowledge in the field studying and applying complex methodologies and a second one, that focuses on the applications, trying to find an engineering compromise between accuracy and computational cost.

As previously stated, the principal nonlinearities are related to the change of wetted geometry due to the motions of the vessel, and to impulsive loads.

In order to properly model the wave-body interaction problem, a time domain approach is chosen, this allows to remove the assumption of harmonic responses. The effects associated with the change in time of the wetted hull portion are calculated at each time step finding the actual geometry of the hull as function of the motions of the vessel.

Loads induced by slamming phenomena are of crucial importance in the design of a container ship vessel, due to the significant bow flare, the sailing speed and the flexibility of the structure. To properly model them, the hull should be described as flexible body, using an hydroelastic approach. In this thesis the fluid-structure interaction problem is solved using the Timoshenko beam model and modal superposition. Impulsive loads are described using both analytical and empirical methods.

The proposed methodology is validated against experimental results, and other numerical techniques, in both small and large amplitude waves. The well known S-175 container ship is used as benchmark. Since the aim of this thesis is to apply the proposed methodology in a practical design problem, long term analysis of maximum expected values for wave induced loads is conducted for container ships of different sizes, with the aim of understanding the importance and feasibility of using a nonlinear tool to asses wave induced motions and loads.

1.2 Aims and Objectives of the Thesis

The aim of this thesis is to develop a nonlinear techniques and associated computational tools able to correctly predict wave induced motions and loads for container ships sailing in rough seas. The proposed methodology should be able to take into account the principal nonlinear effects associated with large amplitude motions,

The main objectives of the proposed methodology are two:

- Model principal nonlinear effects associated with motion and load responses in large amplitude waves
- Ensure a relatively low computational cost to allow an utilisation of the developed tool in design content

1.3 Contents of the Thesis

This thesis begins with a critical review that describes and comments on the previous works conducted in the subjected area. The development of the proposed method required to review and study publications from different fields, therefore the literature review is divided in five sections: linear wave-body interaction , nonlinear wave-body interaction, wave-structure interaction, water entry modelling and extreme loads estimation from nonlinear analysis. The first two sections review seakeeping methodologies and collect them upon their degree of nonlinearity. The third section describes the hydroelasticity for ships, focusing on the fluid-structure interaction problem. The water entry section comments on the state of art in slamming analysis. The last section analyses the methodologies used to obtain extreme responses from nonlinear approaches.

The proposed methodology to predict the nonlinear motion and load responses in

regular seas is described in Chapter 3. This chapter describes the formulation of the equations of motion, along with the numerical techniques used to solve them. The forces are firstly described for a rigid system and then applied to a flexible body.

Chapter 4 describes the validation in regular waves. The proposed methodology is compared against other numerical techniques and experimental results in both small and large amplitude waves. The S-175 container ship is used as a case study due to the large number of data in the literature.

Results in irregular waves and analysis of maximum expected responses in long term are reported in Chapter 5. A methodology to extrapolate extreme values from the time histories of nonlinear wave induced motions and loads is presented and applied to two different container ship of different size: the S-175 and the WILS II 13,000 TEU container ship.

Study of the probability of exceedance for wave induced vertical bending moments is conducted. Different return periods and velocity profiles are considered, in order to understand the effect of such parameters over the expected extremes calculated using a nonlinear method.

Chapter 6 summarises this thesis and draws the conclusions. This section describes the achievements and points the direction that in the author's opinion should be followed to improve and take forward this work.

Chapter 2

Literature Review

2.1 Introduction

In the current chapter a review of the previous works, related to the topic of this thesis, is presented. The publications that mostly contribute to the field of wave-body interaction are described and commented, trying to highlight the contribution of each work. The literature review is divided into five main subjects namely:

- Linear wave-rigid body interaction: the most relevant works in the field of linear seakeeping analysis are reviewed, the different assumptions on which the methods are based on are described and their limitations analysed.
- Nonlinear wave-rigid body interaction: this section outlines the state of art of nonlinear seakeeping methods; these are collected upon the nonlinear effects that they consider.
- Wave-flexible body interaction: here the different approaches to the fluid-structure interaction problem are discussed.
- Water-entry modelling: here the different methodologies used to assess

slamming in ship applications are described.

- Extreme loads estimation from nonlinear analysis: the principal procedures used to evaluate extreme responses from nonlinear methods are reported, focusing also on the effect of nonlinearities on the extreme loads.

2.2 Linear Wave-Rigid Body Interaction

The study of ship behaviour in rough seas has always been one of the most important and fascinating aspects of naval architecture. Since the second half of the nineteenth century, countless papers, discussing the wave-body interaction, have been published. A series of rigorous analytical theories, empirical formulations and numerical schemes have been presented, all of them sharing the same intention: to model wave induced motions and loads.

The first attempts to model the dynamics of a vessel in waves can be attributed to Froude (1861) and Krylov (1896). They formulated the equations of motion for a floating body considering only the inertial, restoring and exciting forces. The excitation was associated with the pressure due to the undisturbed ambient wave field, described using first-order perturbation theory (Froude-Krylov force). In their work the effects associated with the disturbances due to the ship presence were not considered.

St Denis and Pierson (1953) described the irregular seas using spectral analysis. In this approach the sea is defined as a superposition of regular waves. Their approach opened the way to the modern seakeeping applications in ships and marine structures design, allowing the introduction of linear methodology in practical design contents. The work of St Denis and Pierson also clearly showed the importance of the frequency domain analysis.

Due to the limited computational capabilities of computers, until the end of

the 70s, researchers tried to solve the wave-body interaction problem following analytical approaches. From the 40s to the end of 70s several analytical techniques have been introduced; some of these methods imposed restrictions on the geometry and characteristics of sea-going vessel (L/B ratio or Froude number) or limitations on the ambient waves. This period of time is probably the most important for the theoretical understanding of fluid-body interactions.

Some of the first studies on the disturbances in the fluid due to hull presence and motions can be found in Michell (1898) and Lewis (1929). Lewis studied added mass of two dimensional bodies oscillating at high frequency (to avoid any gravitational effects) and applied his results to ship motions considering a slender ship and a strip theory approach to integrate longitudinally the sectional contributions. Michell studied the wave resistance problem using the thin-ship assumption. The thin-ship assumption implies that the breadth is small compared to the draft and the length of the vessel ($B \ll D, L$), this approach is similar to thin-wing theory. The thin-ship first-order theory leads to an unbounded resonant ship system since the exciting forces are balanced by restoring and mass inertial forces, hydrodynamics effects associated with the motions of the vessel are usually of higher order.

An other interesting paper related to the thin-ship theory was published by Haskind (1946). Haskind used Green's theorem to introduce the velocity potential due to the presence of the ship hull and introduced the thin-ship assumption to solve the resulting integral equations. One of the most interesting novelties of Haskind's work was the subdivision of the velocity potential in diffraction and radiation potentials, as it is nowadays used.

One of the last attempts to formulate a thin-ship theory that takes correctly into account effects of hull disturbances was conducted by Newman (1961). The author reformulated the boundary condition on the moving ship hull and used a

systematic expansion in multiple small parameters to avoid the trivial formulation in which the Froude-Krylov forces are the only first-order hydrodynamic actions, however results did not compare well with experiments.

Typical hull-forms of ocean going vessel are elongated with breadth and draft of the same order of magnitude compared to the length; this characteristic geometrical shape is the base of the slender-body assumption. Originally developed to analyse steady-state wave resistance problem by Cummins (1956). Slender-body theories are based on the assumption that the ship is slender compared to the incoming wavelength, therefore the minimum wavelength acceptable to satisfy the initial assumptions should be of $O(L)$; for this reason the slender body theories are also called long-wavelength theory (Newman, 1978).

Some of the slender-body theories for the solution of the unsteady problem were derived by Ursell (1962), Joosen (1964), Newman (1964), Newman and Tuck (1964) and Maruo (1967). Under the long wavelength assumption the slender-body theory leads to solution similar to the thin-ship ones. The majority of hydrodynamic actions are of higher-order in comparison to the Froude-Krylov and restoring forces resulting in non resonant equations of motion. In the case of a vessel without forward speed, subjected to long waves (compared to its length), the dominant terms in the equations of motions are the exciting and the restoring forces, the excitation frequencies are far from the natural frequency of the body, thus the slender-body theory gives a reasonable prediction. If the vessel is sailing with a forward speed, the shift of the excitation frequencies due to the higher frequency of encounter permits the exciting forces to have frequencies that are close to the natural frequency of the ship, resulting in a wrong prediction of the wave induced motions.

In the same period Cummins (1962) formulated the general equations of motion for a floating body using impulse response functions in terms of convolution inte-

grals. The velocity potential is decomposed into an impulsive term and a memory effect part; in the paper, the related boundary value problems for each potential are formulated. In the conclusion the author highlighted the fact that he did not consider this model a good analytical tool to investigate hydrodynamic actions, but he was more interested to formulate a practical computational technique. This sentence can be justified by noting that using a convolution integral to model the terms associated with the fluid gravitational effects we lost details of the single components and preclude an accurate analysis of the effects of each term, but on the other hand convolution integrals and impulse response functions are a powerful tool to model the behaviour of a complex system in time domain.

Ogilvie (1964) presented a work similar to the Cummins'. He formulated the equations of motion in time domain decomposing the radiation and diffraction problems in impulsive and memory effect terms. He rigorously formulated the boundary value problems for a sailing vessel and imposed the time continuity between the two velocity potentials (impulsive potentials and memory potentials) using the free-surface kinematic boundary condition. Ogilvie also derived a mathematical relation between the frequency domain coefficients and the time domain terms involved in the convolution integral.

Since rigorous three-dimensional theories such as the thin- and slender-ship methods did not ensure an accurate prediction of wave induced motions and loads, the interest of some researchers moved to a more simplified two dimensional approach: the strip theory. The first comprehensive work on strip theory method was presented by Korvin-Kroukovsky, B.V. (1955). This methodology, based on the slender-ship assumption and on the negation of mutual interaction between different transverse hull sections, was capable to give an acceptable prediction for heave and pitch motions.

One of the most successful refinement of Korvin-Kroukovsky theory was presented

by Salvesen et al. (1970). This work, based on slender-ship and high encounter frequency assumptions (to ensure that the length of the waves generated by the motions of the ship are of $O(B)$) was formulated to evaluate sway, heave, roll pitch and yaw motions and associated wave induced loads. Their formulations resulted in a set of frequency- and speed-dependent two dimensional hydrodynamic coefficients that were numerically evaluated using the close fit method proposed by Frank (1967). The results compared very well with the experiments, especially for vertical motions and loads. The methodology proposed by Salvesen Tuck and Faltinsen is still one of the most used design tools in the evaluation of wave induced motions and loads.

Jensen and Pedersen (1979) proposed a second order frequency domain strip theory based on the formulation of relative displacement and expansion of the terms up to the second order. This simple but efficient methodology allows to model asymmetrical behaviour of vertical bending moment with a frequency domain procedure. A comparison for the sectional hydrodynamic forces (radiation plus diffraction) against experimental results validates the proposed second order formulations. The vessels are firstly modelled as a rigid body and then considered flexible and described as a Timoshenko beam (see section 2.4). Analysis of the vertical responses of a 270 meters long container ship shows the capability of the methodology to predict second harmonic effects on the amidship vertical bending moment.

The strip theory approach was a successful design tool, but was not fully accepted by the scientific community because its lack of rigorous mathematical foundation. The concerns about the theoretical approach behind two dimensional methods were mainly based on two considerations (Newman, 1978). Firstly, the formulation of the radiation problem was not correct in the low encounter frequency region and this is clearly visible, for example, in the trend of the sectional added

mass coefficient in heave (two dimensional solution tends to infinity as the exciting frequency tends to zero). The second problem was related to the forward speed formulation: in the strip theory, forward speed effects are included as higher order corrections proportional to (U/ω) and $(U/\omega)^2$. Both those arguments are valid and define the main theoretical limitations of strip theories: applicable only for short-wavelength and limited to low Froude numbers. Despite the limits due to their mathematical formulation strip theories give results in the long-wavelength region of engineering accuracy. For long-wavelengths the dominant effects are associated to the restoring and the Froude-Krylov forces that, in a two dimensional approach, are correctly formulated without any restriction associated with the geometry of the body. For a linear system, added mass forces are proportional to the square of the wave frequency and therefore are less important when the wavelength is long. Strip theory can also be used to study motions for a vessel with forward speed. The majority of ships sails at $F_n \leq 0.3$, which is inside the range of validity of two dimensional approaches since limit of applicability for high speed is reached at $F_n \simeq 0.4$ (Faltinsen, 1987).

The arrival of fast computers allowed to implement new methodologies that could avoid the limitations of analytical approaches. The body is treated as a three-dimensional object preserving its details and geometrical characteristics. The boundary of the fluid domain (or part of it) is discretised in a set of elements named panels; special functions that satisfy the governing fluid equations and boundary conditions are collocated on each panel; the velocity potential at any point inside the fluid domain is obtained using the Green's theorem along the boundary of the fluid domain. This class of method is usually called Boundary Element Methods (BEM).

Boundary element methods differ from each other for the type of singularity (Green's function) that they use, and for the different linearisation of the bound-

ary conditions. The majority of BEM, used to study the interaction between vessels with forward speed and waves, can be divided in Neumann-Kelvin and Double Body methods.

Considering the problem of a ship sailing with forward speed in a sea state defined by small amplitude waves, it is possible to divide the velocity potential associated with fluid kinematics into three principal components: a first one associated with the problem of the ship sailing at a constant forward speed in calm water (that can be divided into a basis flow of $O(1)$ Φ and a first-order perturbation φ), a second one related to the unsteady motions of the vessels ϕ_D and a last one related to the ambient waves ϕ_I, as described in Equation (2.1)

$$\Psi = (\Phi + \varphi) + \phi_I + \phi_D \tag{2.1}$$

If the small steepness waves assumption is introduced ($ka \ll 1$) and the ship is stable it is possible to state that the unsteady motions are $O(A)$; therefore the only first order potential is the one that describes the basis flow. Following this line of thought it is possible to justify the linearisation of the unsteady velocity potential around the basis flow. The previously described analytical models (thin- and slender-ship theories) were formulated to ensure small steady state disturbances. Neumann-Kelvin and Double body methods differ from each other by their basis flow formulation.

In the Neumann-Kelvin method the steady flow is formulated as the sum of a free stream velocity field $-Ux$ and a perturbation due to the presence of the body $U\tilde{\varphi}$. Equation (2.2) describes the velocity potential associated with the steady problem.

$$\Phi + \varphi = U(\tilde{\varphi} - x) \tag{2.2}$$

This simple formulation of the steady potential gives the possibility to apply Green's functions that automatically fulfil the free-surface boundary condition (Wehausen and Laitone, 1960). One of the first researchers to propose this approach was Chang (1977); the author presented the mathematical statements of the boundary value problem and the analytical formulation of the singularity used to solve the velocity potential. The presented results, for the wave making resistance of a Wigley hull and for the unsteady motions with and without forward speed of a Series 60 hull, show good agreement with experiments. The zero speed versions of these methods are very popular in offshore engineering since they allow to calculate first- and second-order slow varying drift forces on a floating body applying free-surface Green's functions, for example the WAMIT code (Korsmeyer et al., 1988) is one of the most used seakeeping software in the offshore sector.

If the subject of the analysis is a vessel with forward speed the Neumann-Kelvin approach can be used if the vessel is fine, but if the underwater geometry has a large and rapid longitudinal variation of its forms the disturbance in the fluid induced by the presence of the hull is too large to justify a linearisation of the unsteady potential around the free stream flow. A second drawback of the Neumann-Kelvin method applied to a vessel sailing with forward speed is the formulation of the forward speed free-surface Green's function. Zero speed free-surface Green's functions are easy to evaluate numerically especially in the case of infinite depth, the exact forward speed free-surface Green functions (Beck, 2001) are more complicated to evaluate and their calculation increases the computational cost of the technique.

In the double body approach the steady flow is linearised on the double body flow. The double body flow is the velocity field obtained by the solution of an equivalent

infinite fluid problem where the body is composed by the submerged geometry of the vessel and its symmetric image on the $z > 0$ half plane; this methodology was first proposed by Dawson (1977). The author presented the method for two- and three-dimensional problems and produced results for a Wigley hull and a Series 60 ship.

Free-surface Green's functions developed for the Neumann-Kelvin approach cannot be used to solve the boundary value problem that rises from the Dawson's method, therefore the Rankine source Green's function was used to numerically solve the double body approaches. The Rankine source is a simple singularity that satisfies the field equations of ideal fluids (Laplace equation), differently from the free-surface Green's function it does not automatically fulfil the free-surface boundary conditions, thus a finite region of the free-surface must be included into the computational domain.

The introduction of a finite and discretised portion of the free-surface in the integral formulation of the boundary values problem presents some numerical challenges related mainly to two issues. The first one is the possibility to properly model the propagation of the wave disturbances on a discrete free surface; the second one is connected with the reflection of the radiated waves at the end of the computational domain, since the truncation of the free-surface is numerically seen as a wall for the propagated waves.

One of the first complete works on three-dimensional Rankine panel methods was presented by Nakos (1990). The author formulated the mathematical problem with the related linearised boundary conditions, defined the numerical scheme and its challenges. Results for the steady and unsteady problem were presented for a Wigley and a Series 60 hull. Comparison with experimental points and with strip theory and Neumann-Kelvin methods proofs the validity of the double body approach.

2.3 Nonlinear Wave-Rigid Body Interaction

All the methodologies described in the previous section have something in common: they are linear methods, based on the assumptions of small amplitude waves and linearity between the excitation and the response. Since research on nonlinear seakeeping methods started after the development of linear theories, some nonlinear methods can be seen as a modification or an extension of the linear ones.

Nonlinearities in the wave-body interaction problem depend on factors: some nonlinear effects are, for example, associated with the ambient waves and others are function of the flare of the vessel. Therefore nonlinear theories differ from each other based on which type of nonlinearities they model. Numerical solution of the equations of motion for a nonlinear system is usually conducted in time domain using a time marching scheme.

In the literature several reviews of nonlinear seakeeping methods exist; for example: the seakeeping report of the 26^{th} International Towing Tank Conference (ITTC, 2011), the 17^{th} International Ship and Offshore Structures Congress (ISSC, 2009) and Beck (2001). The critical reviews that were more relevant for this project are from the ISSC (2009) and the seminar paper from professor Beck (2001). In the first review nonlinear methodologies are classified upon their degree of nonlinearities in a practical manner; in the second one seakeeping methods are subdivided considering the different sets of boundary conditions involved. The second classification follows a more theoretical rigorous approach; unfortunately the focus of professor Beck's lecture was the numerical method for seakeeping in general, therefore, also if non linear methods are a significant part of the review, differences between the methodologies were often lost in his taxonomy and a large group of different methodologies were collected under the definition of "blending methods".

For these reasons the following critical review of nonlinear seakeeping methods is conducted following the classification given by the ISSC (2009), but the methodologies themselves will be described in a theoretical manner. The following analysis is limited to the approaches that are based on the assumption of ideal fluid. Methods that model the fluid using the Euler equations or the Navier-Stokes equations (RANS, LES and DNV methods) are not considered here, since the numerical solution of the governing equations and the related challenges are not of interest to the aim of this thesis. The described techniques are divided into four groups, namely: nonlinear Froude-Krylov, body exact, weak scatterer and fully-nonlinear ideal fluid methods.

2.3.1 Froude-Krylov Nonlinear Methods

The simplest class of nonlinear methods is called Froude-Krylov nonlinear. For this type of approaches the nonlinearities are associated with the calculation of the Froude-Krylov and restoring forces (difference between the hydrostatic and weight force) on the actual hull portion at each time step. The radiation and diffraction boundary value problems are defined using linear boundary conditions and usually solved in the frequency domain and related to the time domain using the procedure proposed by Ogilvie (1964). The horizontal plane of the mean wave elevation is used to describe the free-surface and the wetted hull portion is calculated as the part of the hull below the linearised free-surface. These methodologies are usually referred as "blending techniques" because they are an engineering compromise of linear (radiation and diffraction) and nonlinear (Froude-Krylov and restoring) assumptions.

In large amplitude motion problem, the effects associated with the calculation of the Froude-Krylov forces and with the integration of the hydrostatic pressure components along the actual wetted hull portion (considering the linearised free-

surface) are some of the most relevant nonlinear contributions, therefore this simple class of techniques can help to improve the responses prediction. On the other hand other equally relevant nonlinear effects are neglected; for example the bow flare slamming effects are not considered because they are associated with the rate of change in time of the fluid added mass, that in a Froude-Krylov nonlinear method is zero.

Fonseca and Guedes Soares (1998) presented a Froude-Krylov nonlinear strip theory. The proposed method solves the radiation and diffraction problems considering the linear free-surface and body boundary conditions. Sectional hydrodynamic coefficients are calculated in the frequency domain using multi-parameters conformal mapping and related to the time domain using inverse Fourier transform and convolution integrals. The complex amplitude of the diffraction forces is calculated before the simulation and considered harmonic during the time evolution of the system. Froude-Krylov and restoring forces are evaluated on the actual wetted hull portion at each time step. Forward speed effects are considered using the corrections to the zero speed sectional hydrodynamic coefficients proposed by Salvesen et al. (1970) and by introducing C^m terms that take into account the interaction between the steady and unsteady flow, following the formulation introduced by Ogilvie (1964). The methodology models vertical motions and wave induced loads. Results for the S-175 container ship are presented for $F_n = 0.25$ and for head sea condition; this simple analysis highlights the asymmetry between positive and negative nonlinear responses, and the reduction of motions responses when wave elevation rises. The results seems to correctly model the physical behaviour of the vessel, but the reduction of the nonlinear responses for the larger waves seems too marked.

In the following paper from the same authors (Fonseca and Guedes Soares, 2002) the previously described approach is compared against the experimental results

for the S-175 container ship by O'Dea et al. (1992) and Watanabe et al. (1989), in head seas for different wave frequencies and heights and for different Froude numbers ($F_n = 0.20$ and 0.275). Numerical results for the vertical motions show a good agreement with the experimental points for the lower forward speed and satisfactory agreement for the higher speed. This is probably due to the type of forward speed correction used. The comparison for the vertical bending in severe irregular seas ($H_S = 8.33m$ and $T_0 = 11.1s$) shows a good agreement with experimental results at $F_n = 0.25$.

Bruzzone and Grasso (2007) used a three-dimensional Rankine panel method to solve the radiation and the diffraction problems in the frequency domain. Froude-Krylov and restoring forces are calculated in the time domain considering the actual three-dimensional discretised hull, the system of equations of motion follows the formulation proposed by Fonseca. The implementation of the Rankine panel method ensures a better prediction of the forward speed effects; fluid actions are calculated considering the calm water level as free-surface. Simulations were performed for hulls derived from the NPL series and the analysis was focused on the prediction of motions at high froude number, therefore only comparisons with experimental results and linear methods for $Fn = 0.65$ and $Fn = 0.67$ are presented, considering a maximum wave steepness of $ka = 0.07$ (see Bruzzone and Grasso, 2007 for details). Results seem to improve the prediction given by a linear Rankine panel method, also if the presented analysis is too limited to understand the effectiveness of the proposed methodology.

In the following paper by Bruzzone et al. (2011) a modification of the previously described approach is used to assess vertical motions and loads for the S175 container ship in head seas at $Fn = 0.25$. The modified approach follows the same concept of the previously described one, but introduces two major novelties. Firstly the nonlinear Froude-Krylov and restoring forces are evaluated in the

time domain at each time step, but the equations of motions are solved in the frequency domain and iteratively passed to the time domain until convergence; this numerical scheme allows to avoid the transitory part of the solution at the beginning of the simulation. Secondly the Froude-Krylov and restoring forces are analytically evaluated in time via bi-cubic function that are used to describe the actual wetted hull portion. Vertical wave induced motions and loads are compared with experimental results published by Fonseca and Guedes Soares (2004); the analysis showed a general good agreement with experimental data except around resonant region where both motions and loads are over-predicted. This could be due to the calculation of the kernel of the convolution integral, that describes the damping forces. A good evaluation of the damping forces is crucial around the resonance region.

During the first half of the 90s a research group leaded by Woei-Min Lin and Nils Salvesen produced several papers related to the development of a software to predict large amplitude motions and loads considering different type of modelling. The so-called LAMP-2 version was a blended method where the linear radiation and diffraction problems are solved using a time domain three-dimensional free surface Green function method. Lin et al. (1994) presented a comparison for the different methodologies in order to assess the importance of nonlinear modelling in large amplitude wave. The vessels chosen for the analysis are a Series 60 hull ($C_B = 0.70$) and the $S175$ Container ship. The paper collects a vast set of numerical and experimental results showing the importance of nonlinear modelling for large amplitude wave problems, especially when the ship presents a large bow flare. From the comparison of vertical bending moment at midship in regular waves for the Series 60 hull with $\lambda/L = 1.00$ and $F_n = 0.20$ between LAMP-1 (linear three-dimensional time domain method), LAMP-2 and LAMP-4 (nonlinear weak scatterer method) it is possible to notice that both LAMP-2 and LAMP-4 improve the prediction from the linear methodology and the two

approaches give very similar results. Analysis for the $S175$ container ship with $\lambda/L = 1.20$ and $F_n = 0.275$ shows that in this case the relative different between the predictions given by the LAMP-2 and the LAMP-4 methods is larger respect the case of the $S60$ series hull. This could be due to the nonlinear hydrodynamic effects due to the bow flare which are just partially modelled in the LAMP-2 approach.

2.3.2 Body Exact Nonlinear Methods

Nonlinear body exact methods are an improvement of the Froude-Krylov nonlinear methods. The body exact word describes the fact that all the forces are calculated on the actual (exact) wetted hull portion in the time domain. The radiation and diffraction problems are solved considering the calm water level as free surface and the linearised set of related kinematic and dynamic boundary conditions and the actual wetted hull geometry up to the still water level as body surface with related nonuniform Neumann boundary condition. Restoring and incoming wave forces are calculated in a similar manner to the Froude-Krylov nonlinear methods.

The rigorous approaches consist in the direct solution of the radiation and diffraction problems in time domain considering the hull kinematics to identify the exact hull boundary surface. The most common numerical techniques used to evaluate the velocity potentials are: time domain free surface Green function methods and Rankine panel methods. Since the underwater geometry is changing with time, the numerical boundary needs to be evaluated and discretised at each time step, the forces acting on the body are then usually found by integrating the Bernoulli equation along the wetted surface. This procedure results in an elevated computational cost.

A modified Cummins approach (Cummins, 1962) can be also used to evaluate

the radiation and diffraction components of the global forces using frequency domain results. This approach is based on the linear superposition of effects, since the potential is divided into impulsive and memory effect components, but it is widely used to solve body exact methods due to the smaller amount of time required compared to direct solution of the radiation and diffraction problems in time domain. This type of methods belong to the group of momentum based methods, since they calculate fluid action on the body using the rate of change of momentum in the fluid with time, instead integrating the Bernoulli equation. That is due to the fact the these methods partially use frequency domain coefficient, therefore only the integral of the velocity potential along the hull is a known quantity instead of its punctual value along the body surface.

Also if the Cummins' approach is generally used to model linear wave-body interaction problems its extension to weakly nonlinear methodologies can be justified by the fact that the nonlinearities in the radiation and diffraction problems are in general of small magnitude and they vary relatively slowly with time. This is not valid for the impulsive phenomena, such as water entry or bow flare slamming. On the other hand, in these cases the gravitational effects can be neglected (except for the water exit case), since the acceleration in the fluid due to hull motions is higher than the gravitational one. For this reason, memory effects, associated with the gravitational component of the potential, are of smaller magnitude compared to the impulsive terms. This results in a reduction of the effects of the simplification introduced by the superposition principle between impulsive and memory effect velocity potentials.

Singh and Debabrata (2007) presented a comparison between several different three-dimensional nonlinear techniques. One of the methodologies is a body exact theory (in the paper it is referred to as body nonlinear method); the hydrodynamic problem is solved applying transient free-surface Green function. The

paper describes the formulation of the algebrical system used to solve the discrete integral radiation problem. The comparison is performed for a Wigley hull and for the S175 container ship, studying vertical motions of the centre of gravity and relative vertical motions of the bow. The aim is to understand the effect of each level of modelling on the prediction of relative velocity at the bow, used to evaluate slamming forces. The comparison clearly shows the difference of response between Froude-Krylov nonlinear and body exact methods, especially for the relative vertical displacement and velocity. For these quantities the phase angle of the motion is important and this difference could be due to a different prediction of the phase angles.

A two-dimensional body exact method was developed at the University of Michigan (Zhang and Beck, 2007; Zhang et al., 2007; Bandyk, 2009). The radiation and diffraction boundary value problems are solved in two-dimensions in time domain using a desingularised source method and two dimensional Rankine source Green's function. The wetted hull and a finite portion of the free surface are considered in the computation. One of the main advantages of this methodology is that in a desingularised method, the sources are distributed outside the fluid domain, therefore the integrals are never singular (Beck, 1994). In order to avoid any wave reflections at the end of the computational free surface panel length and desingularised distance increase with the increasing of distance from the body, this configuration allows to postpone wave reflection by increasing the length of the computational domain. Bandyk (2009) described accurately the methodology and the numerical techniques focusing on the use of radial basis function to approximate the $\partial\phi/\partial x$, for the evaluation of forward speed effects. Particular attention is given also to the application of the acceleration potential to solve the $\partial\phi/\partial t$ term in the pressure equation. Bandyk's Ph.D. thesis (2009) presented motion analysis for several hull geometries; the proposed methodology gives, in small amplitude waves, prediction of motions of the same level of

accuracy of other two-dimensional techniques. Not sufficient results have been presented to understand the effectiveness of the proposed methodology in large amplitude waves, but Zhang and Beck (2007) discussed results of the water entry and exit problem, obtained with the earlier described method, that showed the capability of correctly predicting asymmetric forces in the water entry and exit phase.

Another two-dimensional body exact method was introduced by Xia (2005). This paper presents a momentum based formulation to evaluate sectional fluid actions in time domain; velocity potential is decomposed into an impulsive term and a memory effect component. Sectional hydrodynamic coefficients are evaluated for each section at each time step considering the actual wetted hull portion and the linearised free-surface. Relative vertical velocity is used to evaluate hydrodynamic forces along the body. The formulation of the sectional radiation forces given by this methodology allows to easily identify each component of the nonlinear forces, in particular it is possible to asses bow flare and water entry slamming in the limits of the assumptions of the methodology (a Von Karman type method). The paper presents few results for the S175 container ship displaying heave, pitch, bow acceleration and vertical bending moment for different wave heights and frequencies. The result shows the capability of the methodology to predict motion reduction and increase in the load response compared to the linear prediction when wave elevation rises.

2.3.3 Weak Scatterer Nonlinear Methods

The nonlinear weak scatterer methods are techniques based on the assumption that the radiated waves generated by the vessel movements are of smaller order compared to the ambient waves. This is the so called weak scatterer hypothesis firstly introduced by Pawlowski and Bass (1991) using the following formulation:

"The disturbance induced by the moving ship in the wave flow is considered to be of a smaller magnitude than the wave flow quantities which are proportional to the wave height, but at least of the same magnitude as the wave flow quantities proportional to the square of the wave height."(Pawlowski and Bass, 1991).

Lets consider the following decompositions for the velocity potential and free-surface elevation

$$\Phi(\vec{x},t) = \Psi(\vec{x},t) + \phi_I(\vec{x},t) + \phi(\vec{x},t) \tag{2.3}$$

$$\eta(x,y,t) = \zeta_I(x,y,t) + \zeta(x,y,t) \tag{2.4}$$

where Ψ is the potential associated with the steady forward motion of the vessel, ϕ_I is the velocity potential due to the incoming wave field and ϕ describes the perturbation due to the motions of the vessel and its interaction with the incoming potential; ζ_I is the free-surface elevation of the undisturbed incoming wave and ζ is the disturbance wave elevation due to the potentials Ψ and ϕ. Following the weak scatterer hypothesis the orders of the terms of equations 2.3 and 2.4 are defined as follow

$$\Psi \sim \mathcal{O}(1); \quad \phi_I \sim \mathcal{O}(1); \quad \phi \sim \mathcal{O}(\epsilon), \tag{2.5}$$

$$\zeta_I \sim \mathcal{O}(1); \quad \zeta \sim \mathcal{O}(\epsilon), \tag{2.6}$$

where $\epsilon \ll 1$. The weak scatterer hypothesis, summarised in equations 2.5 and 2.6, modifies the free-surface boundary conditions, that now should be linearised on the incoming undisturbed wave profile ζ_I. A second difference from the previous formulations is given by the terms that compose the free-surface boundary conditions: ϕ_I is $\mathcal{O}(1)$ and therefore terms of the incoming wave potential that

in the previous cases are of $\mathcal{O}(\epsilon^2)$, under the current assumption are of $\mathcal{O}(\epsilon)$ and must be considered in the linearised problem.

A comparison for the kinematic and dynamic free-surface boundary conditions between a linear and weak scatterer formulation is well presented by Kim et al. (2011). The free-surface boundary conditions of the linear problem are also applied in the nonlinear Forude-Krylov and body exact methods, therefore this comparison is very useful to understand and appreciate the mathematical and numerical complexity introduced by the weak scatterer assumption.

The weak scatterer hypothesis was firstly introduced by Pawlowski and Bass (1991). In this paper the authors discuss the theoretical model related to the weak scatterer hypothesis and presented a numerical analysis with a comparison against experimental results for a series 60 hull and a stern trawler. The numerical technique used to solve the radiation and diffraction problem is a boundary elements method with zero speed free-surface Green's function. The zero speed results are corrected to take into account forward speed in a strip theory manner (Salvesen et al., 1970). The methodology was chosen for its reliability also if the authors were aware of its limitations. Results show a reasonable good agreement especially for the series 60 hull. The most important component of this work is the clear theoretical formulation of the weak scatterer hypothesis and the related boundary value problem.

Due to the mathematical formulation of the free-surface boundary conditions the Rankine panel methods seem to be the most suitable technique to numerically tackle the weak scatterer hypothesis. Huang (1997) presented a numerical solution for a nonlinear weak scatterer method using higher order Rankine singularity in the boundary element method. This work follows the thesis of Kring (1994) where a linear time domain Rankine panel method was firstly introduced. Huang's Ph.D. thesis presents the mathematical and numerical scheme of the

methodology and a comparison against experimental results as well as other numerical procedures for a series 60 hull and the S175 container ship. The numerical methodologies used in the comparison are a linear and a Froude-Krylov nonlinear Rankine panel methods. The comparison shows an excellent agreement against experimental results for the weak scatterer method for both vessels. The comparison against other level of modelling is very useful to understand the improvements for the prediction of the motions when the level of complexity of the model increases. The proposed weak scatterer method almost always gives the best predictions. It is also very interesting that the drastic decrease of the response around the resonant region occurs in the weak scatterer method. The presented technique improves the motion predictions also for small amplitude waves, demonstrating that this mathematical formulation is a general improvement from the linearised one and the weak scatterer assumption, almost mandatory in large amplitude waves, can be successfully applied also for problems involving small amplitude waves.

An approach similar to the one of Huang (1997) was presented by Kim et al. (2011). The proposed methodology follows the Huang's formulation, but the novelty in this paper is the coupling of the seakeeing and the maneuvering problem to highlight the flexibility of time domain methods. Another important features of this methodology is the use of a flexible body model to study springing and whipping (this topic will be described in section 2.4). Comparisons against experimental results and numerical predictions of a linear and a Froude-Krylov nonlinear method are presented for a 6500 TEU container ship and for the S175 container ship. The comparison in small amplitude waves reports a good agreement between the weak scatterer method and the experimental points. On the other hand a brief analysis for large amplitude waves shows that the nonlinear Froude-Krylov method gives the best prediction for heave and pitch motions.

A different approach to the weak scatterer hypothesis was proposed by Singh and Debabrata (2007). The radiation problem is solved numerically using a transient free-surface Green's function. Transient free-surface Green's functions should be applied using an horizontal plane as free-surface, therefore the wetted hull under the incoming wave profile is mapped under a flat free-surface. Then, the boundary value problems are solved in the transformed space using the same formulations of the body exact methods. This approach considers the weak scatterer hypothesis only as a change of the wetted hull portion that is included in the calculation; no interaction between the radiation and the incoming wave potential is considered.

A different interesting formulation of the weak scatterer approach was proposed by Sclavounos (2012). Sclavounos presented a formulation that expresses hydrodynamic forces and moments on the body using the rate of change of fluid impulse with time instead of the direct pressure integration via Bernoulli equation. The main advantages of this approach should be the related relative simple mathematical formulation against the numerical evaluation of the Bernoulli equation: for large amplitude motions the gradients of the velocity potential must be considered to find the hydrodynamic pressure, leading to a complex numerical procedure for the evaluation of the spacial derivatives of the potential. The author describes in details the mathematics, ending with a formulation analogous to the one of the previous methodologies but expressed in an integral form. The free-surface is identified as the undisturbed incoming wave profile and the ambient wave potential is considered of $\mathcal{O}(1)$. This methodology can be useful to apply the weak scatterer hypothesis with momentum based methods.

2.3.4 Fully Nonlinear Methods

All the previous methodologies are a combination of linear and nonlinear assumptions; also weak scatterer methods are based on the hypothesis of superposition

of effects, that is a valid for a linear system, but is not acceptable for a nonlinear one. The present techniques are the most complex among all (if ideal fluid is considered), they are nonlinear methods without any linear simplification. For this class of techniques the Laplace equation still governs fluid dynamics, but the boundary conditions are not linearised; therefore the free-surface boundary conditions must be satisfied on the unknown free-surface profile and the body boundary conditions must be imposed on the actually wetted hull portion at each time step. The principal complexity of these methodologies lies in the fact that the nonlinear kinematic and dynamic free-surface boundary conditions must be imposed on a time evolving unknown surface; for this reason a time marching scheme is used to predict free-surface profile at each time step.

The numerical solution of the boundary value problem can be achieved using different techniques, such as finite-difference or finite-elements methods (see Yeung, 1982, for an accurate review). In the research area of nonlinear wave-body interaction the most common numerical techniques are the so called Mixed Eulerian-Lagrangian methods (MEL). The MEL approach was first introduced by Longuet-Higgins and Cokelet (1976); this methodology is characterised by two phases, namely an Eulerian one and a Lagrangian one. In the Eulerian phase the velocity potential is found by solving the mixed boundary value problem, at this stage all the fluid kinematics are calculated; in the Lagrangian phase the time evolution of the water particles on free-surface is calculated using the free-surface boundary conditions, thus the location of the free-surface and the value of the potential on it are known and are used as input value for the next time step.

These methodologies have some numerical problems due to their assumptions and numerical formulations. First of all, the calculation stops when wave breaking occurs, this is due to the definition of the free-surface and usually wave breaking is prevented using numerical damping on the free-surface. A second disadvantage is

given by the motions of the Lagrangian particles on the free-surface that generates a so-called "sawtooth" instability. The water particles are free to move and after several time steps numerical points tend to accumulate in the regions with higher gradient; therefore in some other region the Courant stability condition is violated (Dommermuth and Yue, 1987). This inconvenience is avoided applying a smoothing scheme on the free-surface during time marching.

A MEL application to the wave body interaction problem was proposed by Beck (1994). In this paper a three-dimensional fully nonlinear method is used to study ship unsteady motions; the singularity used to determine the velocity potential is a desingularised Rankine source applied over the underwater body geometry and the free-surface. The author accurately describes the mathematical formulation of the methodology focusing on the time marching of the free-surface points and on the description of the desingularised source method. Numerical results for several body geometries show the capability of the methodology to model nonlinear forces and motions. No results or comparisons in large amplitude waves have been presented.

Instead of modelling full scale wave-ship interactions fully nonlinear methods are often used to simulate the motion of a vessel in a towing tank creating what is called a numerical wave tank. This research area is wide and deserves a separate and accurate review but it is worth to be mentioned because it is a clear example of how fully nonlinear methods are used to predict ship motions. Numerical wave tanks are the computational equivalent of a towing tank: the boundary of the domain is completely included in the computation (free-surface, body surface, side walls and tank bottom), ambient waves are generated from the oscillation of a side wall (or equivalent imposed velocity potential) and wave reflection from other walls is avoided introducing numerical damping or imposing a piston-like movement on the reflecting side walls (see Clement, 1996 for more details).

Koo and Kim (2004) defined a two dimensional numerical wave tank to study the unsteady motion of a cylindrical body using the previously described fully nonlinear MEL approach. A second order Stoke's wave is used as incoming wave and motions are compared against linear and experimental results. The comparison shows the discrepancies between the linear and the nonlinear modelling highlighting the nonlinear behaviour of motions around resonance region where the second and third harmonic of the response have a significant magnitude. This paper is a clear example of how a numerical wave tank can be used to study unsteady motions of a floating body.

In order to avoid the accumulation of numerical points of the free surface in some region partial MEL methods can be used. The difference with the previously described methodology is that in a partial MEL methods water particle are allowed to move only vertically, in this way theoretically no smoothing scheme is necessary. An example of this approach can be found in Faltinsen (1978) where a partial two dimensional MEL is used to study sloshing in a rectangular tank.

2.4 Wave-Structure Interaction

All the methodologies described in section 2.2 and 2.3 model the ship as a rigid body and evaluate wave induced loads considering the equilibrium between external forces and internal loads for a portion of the hull. In the reality the ship is a flexible body and its interaction with the sea environment produces structural vibrations and deflections.

In severe seas slamming events due to water entry or bow flare generate high frequency transient hull vibrations; this phenomenon is called whipping and is important to assess the strength of the vessel. A different type of hull vibration is springing; springing is continual hull girder vibration induced by wave excita-

tions that are in resonance with the hull natural frequencies. Springing is very important for the analysis of the fatigue life of a ship with low first structural natural frequencies.

In order to correctly model these dynamic phenomena the hydrodynamic problem should be coupled with the structural one. This area of fluid mechanic is generally called fluid structure interaction (FSI) but when the analysis concerns the responses of a vessel in a seaway it goes under the name of hydroelasticity.

All the described seakeeping methods can, theoretically, be coupled with the equations of motion of the hull structure and therefore a review similar to the previous one can be conducted. Since repeating the difference between the several seakeeping theories is pedantic and does not add any value to this survey the hydroelastic methods will be presented and described with the intention to highlight the differences in term of fluid structure coupling and modelling, with the aim to understand the effects of the different assumptions on the results obtained.

The structural dynamics can be modelled following two principal methodologies: modal superposition or direct integration of the equations of motions.

In the modal superposition method structural hull kinematics are subdivided into a set of orthogonal time independent mode shapes. Under the assumption of linear structural response the degrees of freedom of the system are composed by the set of principal co-ordinates that is used to define the amplitude of each mode shape and characterise the time response of the hull; this methodology is the most common since it ensures a rapid and accurate solution of the equations of motions with a relatively small number of mode of shapes, Bishop and Price (1979) accurately describe this approach and its application to different type of vessels.

A second approach is the direct solution of the equations of motions of the hull girder. The structure is discretised with a finite number of points or elements

(depending on the numerical method applied) and displacements and rotations of each one of them define the degrees of freedom of the system. This approach is definitely more time consuming since the number of degrees of freedom is larger compared to the modal analysis one, but allows the solution of more complex problems. Direct solution methods differ from each other based on the coupling with the fluid domain problem, that can be strong if the balance between fluid and structure is mutually satisfied each time step or weak if fluid and structure exchange alternatively information from time step to time step. Matthies and Steindorf (2003) described strong fluid structure interaction algorithms that can be used in wave-body interaction problems. Strong coupled algorithms are more robust and accurate, but require more time due to internal iterations at each time step, while weak coupled methods are more easy to implement and faster, but due to their explicit formulation they can suffer from numerical instabilities.

Bishop and Price (1979) accurately describe modal superposition hydroelastic method where the fluid problem is solved using a linear frequency domain strip theory based on the relative velocity formulation. They define the structural problem considering both an Euler and Timoshenko beam model in six degrees of freedom and presented a methodology to study transient loads, based on momentum based slamming modelling and memory effect functions. This book is without doubt one of the most important publication in hydroelasticity research area and it shows how an hydroelastic approach can take the place of the classical seakeeping methods without losing any accuracy or detail in the analysis.

Hirdaris et al. (2003) presented a comparison between results obtained by linear two- and three-dimensional hydroelasticity theories for a 280 meters long bulk carrier. In the two dimensional model the structure is represented by Timoshenko beam theory and the fluid actions are calculated using a strip theory approach (Bishop and Price, 1979). For the three dimensional case finite shell

elements are used to model the hull and hydrodynamic forces are evaluated using a pulsating free-surface Green's function source distribution under the calm water level. Comparison is conducted for both symmetric (vertical modes) and anti-symmetric (horizontal and torsional modes) modes. The analysis shows that two- and three-dimensional modelling give similar results for vertical modes, but the comparison for horizontal and torsional modes presents differences in the results, claiming the incapability of the Timoshenko beam model to properly represent highly non-prismatic hull girders that allow for the effect of warping.

Kim et al. (2009a) and Kim et al. (2009c) developed a fully coupled time domain hydroelasticity method based on hybrid boundary element method and finite element method (FEM) scheme. The fluid domain is modelled by a BEM based on higher-order B-spline Rankine panel method; structural domain is handled via FEM using different beam theory: Timoshenko beam theory (Kim et al., 2009a) and Vlasov beam theory (Kim et al., 2009c). The Vlasov method is more complicated, but allows to capture warping effects of container ships open sections. Instead of modelling the time evolution of the structural displacements and rotations via modal superposition the proposed method solves the structural equations of motions using a direct integration approach: a β-Newmark method is used to evolve the system with time and nonlinear effects associated with the fluid coupling and internal iteration to ensure a correct fluid-structure coupling are conducted following the method proposed by Matthies and Steindorf (2003). Kim et al. (2009a) presented a comparison against experiment for vertical motions of a pontoon like body showing a good agreement with experimental results. Kim et al. (2009c) compared results from the hydroelastic method against rigid body one, displaying the importance of hull flexibility.

Since hydroelastic effects are important in large amplitude waves several nonlinear hydrodynamic methods have been applied to a flexible hull, both two- (Jensen

and Pedersen, 1979; Jensen and Dogliani, 1996; Xia et al., 1998; Park, 2006) and three-dimensional (Kim et al., 2009b; Tuitman, 2010).

Jensen and Pedersen (1979) applied a second-order frequency domain strip theory to hull modelled using Timoshenko beam theory, this results in a frequency domain methodology able to model asymmetric response of vertical bending moment between sagging and hogging condition. In a following paper Jensen and Dogliani (1996) presented a theoretical study of statistical properties of the nonlinear vertical bending moment of a flexible ship hulls. The proposed methodology uses Hermite series to approximate the non-Gaussian distribution of the vertical bending moment response. This approach presents the advantage of frequency domain analysis and is partially able to model geometrical nonlinearties; one of the main drawback is that it is not possible to model whipping using a frequency domain approach.

Xia et al. (1998) presented a hydroelastic method where the fluid actions are evaluated using a nonlinear strip theory method coupled with a Timoshenko beam to represent the flexible hull, sectional hydrodynamic coefficients are evaluated using a multi-parameters conformal mapping technique. The aim of the research is to study nonlinear responses of fast vessels and comparison of vertical motions and loads responses for the S175 container ship shows good agreement with experimental data from O'Dea et al. (1992). One of the novelties of this approach is the evaluation of the memory effect terms via state space model instead of memory effect functions. The state space model seems promising when the radiation and diffraction problems are treated in a linear manner, but it does not present any advantages when the hydrodynamic forces are considered nonlinear since a solution of a system of the higher order differential equation is needed at each time step.

Park (2006) proposed a two dimensional hydroelastic approach similar to the one

presented by Xia et al. (1998), in this methodology the governing equations are divided in a linear and nonlinear part, while the linear components are solved in frequency domain the nonlinear ones are solved in time domain using a β-Newmark method. Sectional hydrodynamic coefficients are evaluated at each time step using Lewis form conformal mapping method. An empirical formulation is used to calculate impulsive forces due to water entry (Ochi and Motter, 1973). Comparison for the S175 container ship shows good agreement with experimental results from O'Dea et al. (1992). This approach seems promising also if no details are given about the coupling of the empirical formulation for water entry with the nonlinear strip theory; this details are important since a wrong coupling can lead to over prediction of the water entry impulsive forces, resulting in an excessive and prolonged whipping excitation.

Tuitman (2010) presented a hydroelasticity theory based on a nonlinear Froude-Krylov method that uses zero speed free-surface Green's function with forward speed correction to evaluate the radiation and diffraction potential. Both three- and one-dimensional structural FEM model are considered. Impulsive loads are represented by using both a generalised Wagner method (see section 2.5) and an empirical approach. Results show a good agreement against experimental points except for the highest speed where stresses are over predicted. This can be related to the range of applicability of a nonlinear Froude-Krylov method based on corrected zero speed free-surface Green's function or to the slamming model used.

Kim et al. (2009b) presented a nonlinear extension of a BEM-FEM coupled method (Kim et al., 2009c). The Vlasov beam model of the ship hull is coupled with a nonlinear Froude-Krylov method that uses a modified Rankine panel approach to evaluate hydrodynamic fluid actions, resulting in highly oscillatory response in the wave frequency regime; this is claimed to be related to the higher

order frequency components that are implicitly related to the nonlinear model and that end up exciting the natural frequencies of the hull structure.

2.5 Water Entry Modelling

In section 2.4 the importance of hydroelasticity, and especially of nonlinear hydroelasticity, in large amplitude waves has been reported. This is due to the fact that hydroelastic approaches allow to model girder hull vibrations due to water impacts; therefore it is straightforward that an equivalent important element for the evaluation of loads is the mathematical approach used to model the impact phenomena.

Several methodologies to model hydrodynamic impacts exist, as well as several type of slamming, thus it is crucial to select the appropriate formulation. The most relevant types of slamming for monohull vessels are namely: bottom impact, bow flare and green water on deck. Since the work of this thesis is focused on modelling bottom and bow flare impact, only those two events are considered in the following review.

Numerical methods to evaluate forces from water impact can be divided into three main groups: empirical methods, analytical based and numerical based methods. Empirical methods are formulated from the analysis of observations and they are the most widely used methodologies for their reliability and rapid execution. Analytical methods are more accurate and have theoretical rigour, but they can be applied only in the restrict range of validity of their assumptions. Numerical procedures are time consuming, but they can give a better and accurate insight of the fluid, compared to empirical methods and can stretch the applicability limits imposed by analytical solutions.

Stavovy and Chuang (1976) proposed a semi-empirical formulation to evaluate

maximum impact pressure on the hull bottom considering relative velocity between body and fluid, based on the experimental observations on wedge impacts and analytical impact theories (Wagner and cone impact theories). In their work the authors presented also an analytical expression to find the actual impact angle between the moving section and the wave profile. Ochi and Motter (1973) developed a methodology to assess slamming forces using empirical formulation proposed by Stavovy and Chuang (1976) (but it can be applied with any empirical method). In this procedure, the time evolution of the maximum pressure is a function of the Froude number of the vessel. The methodology provides also an useful expression to evaluate pressure distribution on the hull bottom, where the pressure peak is located at the keel and an the pressure distribution varies linearly with the vertical coordinate (maximum at the bottom and zero on the intersection between the section and the free-surface). Also if those expressions can be applied only to bottom impact and the pressure distribution formulated by Ochi and Motter (1973) is not in agreement with experimental trials this methodology gives results within engineering accuracy and it is probably the most reliable method to evaluate bottom impact forces.

Analytical methods are generally divided into two classes: Von Karman type and Wagner type methods. Von Karman (1929) methods do not consider the flow caused by the impact in the calculation of the body free-surface intersection. Impact forces are function of the rate of change with time of the fluid added mass and relative normal velocity between the body and the fluid surface, while Wagner (1932) approaches consider these effects for the evaluation of the wetted length.

This discrepancy of the assumptions mainly results in the fact that von Karman approaches can be applied to both water entry and exit phase, but they miss the prediction of the actual wetted length. Wagner based methods are very effective

in the water entry phase for bodies with small deadrise but are not suitable for the water exit phase (Dessi and Mariani, 2008). The different formulations for the wetted length result in an under-prediction of the impact pressure and force for von Karman based approaches; an interesting comparison can be found in Zhao et al. (1997).

Zhang and Beck (2007) presented a numerical method to evaluate water impact on a two dimensional body in both water entry and exit phase. The procedure is based on a boundary element method with Rankine source on the body and on the free-surface, the free-surface discretisation is based on desingularised panel method. The free-surface and boundary conditions are linearised along the calm water level and the body boundary condition is satisfied on the actual wetted body portion. Results for the water entry and exit for wedges with different deadrise angles show the capability of the method to predict impulsive force asymmetry in water entry and exit phases when the linearised free-surface is considered instead of zero potential boundary condition (usually used for body oscillating at high frequency). Since, like a von Karman method, the pile up of the water is not considered in the calculation, the pressure and forces are under predicted; but a stretching technique is used to extend the wetted length, increasing the accuracy of the results.

A nonlinear boundary method with jet flow approximation was published by Zhao and Faltinsen (1993) the body and free-surface are discretised using panels with constant source strength, the problem is solved considering nonlinear free-surface boundary conditions without including gravity since fluid accelerations due to the motions of the body are higher then the gravitational acceleration. Jet flows at the body free-surface interceptions are modelled introducing panels perpendicular to the body over which the pressure is set equal to the atmospheric one. Comparison with the numerical similarity solution by Dobrovol'skaya (see

Zhao et Faltinsen, 1993 for details) show good agreement in both maximum pressure value and pressure distribution.

Zhao et al. (1997) presented a generalised Wagner approach based on the solution of the outer flow domain as defined by Wagner. The zero potential kinematic free-surface boundary condition is applied to a horizontal plane passing by the intersection between the free-surface and the body; exact body condition is applied and free-surface evolution in time is predicted using the free-surface dynamic condition. Without solving the inner jet region flow the pressure at the free-surface body interception is negative and is neglected in the presented methodology. Comparisons for a wedge with 30° degrees deadrise and a bow flare section show a general good agreement for pressure distribution against experimental and numerical results (Zhao and Faltinsen, 1993), pressure values seems slightly over predicted compared to experimental results.

2.6 Extreme Loads Estimation from Nonlinear Analysis

Estimation of long- and short-term extremes of motions and hull girder loads in ship design is usually conducted using linear frequency domain methodologies and spectral analysis. Since linear methods have been proven to be not accurate in extreme sea states (see section 2.3), extreme prediction via linear analysis can lead to incorrect results. The linear approximation can be however accepted for vessels like tankers that are not significantly affected by nonlinear behaviour, but cannot be applied to long vessels that have a large bow flare and sail at a relative high speed, such as container ships.

In their interaction with waves, container ships are largely affected by nonlinearities due to their hull forms and length. The sectional flare (especially at the bow

and at the stern) leads to a large asymmetrical response of vertical bending moment and can produce large impact forces resulting in whipping of the hull girder. Springing is also an issue for large container ships, especially in oblique seas, due to their U-shape hull girder open sections. A nonlinear method allows to assess the asymmetric behaviour of loads and if it coupled with a flexible hull structure model gives the possibility to predict whipping effects; therefore the application of nonlinear hydroelastic methodologies is crucial for the correct assessment of extreme responses for large container ships.

The IACS $S11$ "Longitudinal strength standard", which forms the basic structural requirement for hull strength, represent the current standard for hull girder design loads for ships and summarised the philosophy behind wave induced loads assessments. The IACS requirement and technical background is presented by Nitta et al. (1992). These formulations take into account nonlinearities associated with the asymmetry of vertical bending moment between sagging and hogging condition, calculated using a correction factor that is a function of the block coefficient of the ship. It does not include vibrational phenomena of the hull girder; however the authors highlight that these rules should not be applied to vessels having a large bow flare.

The inclusion of whipping and springing on extreme loading is very important especially for ultra large container ships. Storhaug et al. (2010) presented the results of an experimental campaign for a 13000TEU container ship model. The author's analysis extreme responses in different type of severe sea states. The conclusions highlight that the vertical bending moment, considering whipping, may exceed the IACS rule moment by a factor up to 1.8.

The assessment of wave induced loads via nonlinear methods is definitely more time consuming compared to the classical approach. Nonlinear methods solve the equations of motion in the time domain and therefore long and numerous

simulations in irregular seas are required to calculate the long-term maximum expected value for a given return period. For this reason several papers are focused on simplified analysis of extreme responses using nonlinear seakeeping methods.

Baarholm and Moan (2000) proposed a methodology to evaluate extreme loads using a nonlinear time domain method and a limited number of sea states. The use of reduced combinations of significant wave heights and zero crossing periods within the nonlinear seakeeping method is made by selecting the sea state that mostly contribute to the extreme responses calculated using a linear approach. This procedure is found to be very effective in the reduction of the number of sea states to be used, but it is based on the strong assumption that the sea states that give the higher contribution to the long-term extreme response in the nonlinear case are the same as the linear one. The authors concluded the paper stating that the results obtained by the proposed approach show a reasonable accuracy compared to the one calculated using the whole wave scatter diagram. In this work only rigid body hull is considered, the authors do not mention the effect of hydroelasticity on the procedure presented.

When whipping is considered, an important issue is the approach used to count the extremes of the time signal, because since the whipping vibration frequency is higher than the wave frequency the number of extremes (considered as local maxima and minima of the time history) is higher when whipping is considered then when are not included in the modelling. Tuitman (2010) compared the extreme response of a vessel using different methods to count the extremes. The approaches used were three: mean crossing, rigid body zero crossing and full count. In the mean crossing approach one maximum and one minimum are taken into account for each zero crossing period, the rigid body zero crossing approach takes one extreme (positive and negative) for each zero crossing period of the

response calculated using a rigid-body model and the full count considers all the local maxima and minima of the time history. The comparison shows that all the three methodologies unexpectedly give similar results, showing an independence of the extreme responses from the way the extremes are counted.

Wu and Hermundstad (2002) presented an analysis for the long term probability of exceedance in vertical sagging and hogging moments amidships based on a time-domain nonlinear hydroelastic simulation. Extreme nonlinear responses are extrapolated from the time history considering one maximum and minimum response per zero crossing period; then, they are fitted with a generalised Gamma function density probability distribution. The analysis presents the nonlinear results for a return period of twenty hours and compares them against the DNV rule, showing that the extreme responses calculated considering whipping are higher than the rule values. Also if a comparison against linear calculation is not presented, the amplification factor (ratio between the nonlinear extremes and the linear ones) can reach a value of two for sagging response, when the extremes are compared to the results of a linear analysis (frequency domain hydroelastic strip theory).

White et al. (2012) presented guidance notes for the whipping and springing assessment for large container ships. The paper analyses extreme loads for a 350 metres long container ship (13000TEU) considering nonlinear rigid body and whipping model. The time domain analysis is conducted using the rigid body three-dimensional nonlinear Froude-Krylov code PRETTI (CRS hydrodynamics), whipping responses are found by superimposing slamming induced vibrations over the "quasi-static" wave induced loads time history. Whipping loads are calculated using a nonuniform Timoshenko beam and a slamming momentum based method (von Karman approach). Results show that the nonlinear correction factors for hogging and sagging (rigid body) for a return period of three hours are 1.43 for

sagging and 0.94 for hogging, the values given by the IACS standard rules are 1.25 and 0.94 respectively. This highlights the fact that the sagging correction factor is underestimated by the IACS standard rules for this type of vessel. When whipping is considered the ratios between the hydroelastic results against the linear ones for sagging and hogging are 1.98 and 1.42 respectively. These results together with the ones obtained by Storhaug et al. (2010) clearly highlight the importance of whipping for large container ships.

Chapter 3

Methodology

3.1 Introduction

The characteristics of the proposed methodology are developed following the critical review presented in Chapter 2. The aim of this thesis is to present a practical time domain computational tool able to model nonlinear motion and load responses for a container ship sailing in rough seas.

The principal nonlinear effects, for an ocean going vessel, sailing in large amplitude waves, are associated with nonlinearities in the Froude-Krylov and restoring forces. This nonlinear effects are related to the actual change in time of the wetted hull portion. For container ships the flexibility of the structure and the shape of the hull enhance whipping effects and therefore it is essential to proper model hull girder vibrations associated with water impacts.

In order to model the principal nonlinear effects, all the forces acting on the vessel are evaluated using the actual wetted body portion, calculated using the calm water level as free-surface, and the vertical relative displacement between the hull and the ambient wave. The fluid actions on the vessel are defined using the classical subdivision into radiation, diffraction, restoring and exciting forces.

Following the classification proposed in the literature review, this level of modelling corresponds to a so-called "body exact" method. It is consider a good compromise between accuracy and computational cost, it allows to model the change in time of wetted hull portion using well-know and rapid numerical procedure. The "body exact" approach permit also to model water impact forces associated with bottom and flare slamming in a more rigours manner. A novel approach for the study of impulsive forces, that couples momentum based and empirical based methods is presented. Hull girder vibrations are studied using an hydroelastic approach that couples structure and fluid dynamic in time domain. These characteristics permit to study whipping effects.

In the current chapter the mathematical method used to study the dynamics of the vessel is described; all the formulations necessary to find fluid actions on the body are reported and explained along with the numerical procedures implemented.

3.2 Coordinate System and Equations of Motions

The motions of the vessel and the forces acting on it are originally described in an inertial coordinate system translating at constant velocity U along the positive direction of the x-axis. The coordinate system has its centre on the interception between the calm water level plane, the symmetry plane of the vessel and a plane perpendicular to the x-axis where the centre of gravity of the vessel is located; the details of the reference frame are pictured in Figure 3.1.

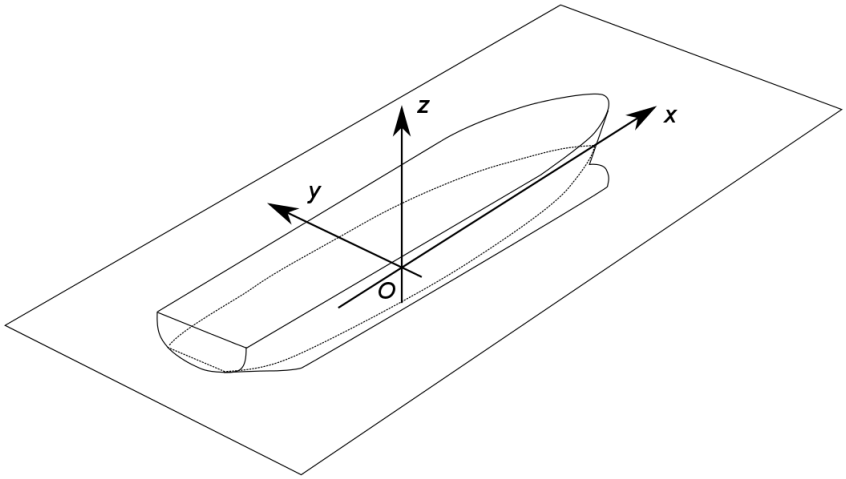

Figure 3.1: Coordinate system.

The focus of this thesis is to model vertical motions and wave induced loads, therefore the system of equations of motions of the vessel, considered as rigid body, is composed by two equations for heave and pitch respectively. The equations of motions for a rigid body, following Newton's second law, are described in Equation 3.1.

$$\begin{cases} m\ddot{z}(t) = \sum_i F_i(t) \\ I_{yy}\ddot{\Theta}(t) = \sum_i M_i(t) \end{cases} \tag{3.1}$$

Where m is the mass of the vessel, z is the heave displacement, F_i is the *i-th* external force acting on the body and M_i is its moment, I_{yy} is the mass moment of inertia and Θ is the pitch displacement.

In large amplitude waves hydroelastic effects are important for load estimations, therefore in the present study the vessel is considered as a flexible body. The first effect of this assumption is a drastic change in the formulations of the equations of motion, the degrees of freedom of a flexible system are defined by the translations and rotations of each point of the structure. If the system is discretised into a set of finite number of points the equations of motion can be written in matrix

form:

$$\mathbf{M}\ddot{\mathbf{X}} + \mathbf{B}\dot{\mathbf{X}} + \mathbf{C}\mathbf{X} = \mathbf{F}(t) \tag{3.2}$$

In the above equation, **M**, **B** and **C** are the matrices of mass, damping and stiffness respectively; **X** is the vector of the nodal displacements and rotations and **F** is the vector of the external forces. The Timoshenko beam theory is used to model the hull girder and, under the assumption of small structural displacements, modal superposition is used to define the dynamics of the system. In modal superposition methods the displacement of a point of the hull is described as the sum of displacements in its principal modes, as described in Equation 3.3

$$W(x;t) = \sum_{r=0}^{\infty} \Big[w_r(x) p_r(t) \Big] \tag{3.3}$$

W is the vertical displacement of a section of the hull, w_r and p_r are the $r-th$ principal mode shapes and coordinate respectively. The set of modes of shapes must be orthogonal, therefore the $r-th$ and $s-th$ mode shapes have to satisfy the following condition.

$$\int_L \mu(x) w_s(x) w_r(x) dx = 0 \quad r \neq s \tag{3.4}$$

L is the length of the vessel and μ the mass per unit of length. Equation 3.3 provides also the existence of rigid body motions (Bishop and Price, 1979). Under those hypothesis Equation 3.2 can be written as:

$$\sum_r \Big[a_{sr}\ddot{p}_r + b_{sr}\dot{p}_r + c_{sr}p_r \Big] = F_s(t) \quad s = 0, 1, 2, \ldots \tag{3.5}$$

a_{sr}, b_{sr} and c_{sr} are the components of the generalised mass, damping and stiffness matrices respectively; F_s is the generalised external force in the *s-th* mode of

shape. The elements of the structural generalised matrices can be found from:

$$\begin{cases} a_{sr} = \delta_{sr} \int_L (\mu w_s(x) w_r(x) + I_y \theta_s(x) \theta_r(x)) dx \\ b_{sr} = \delta_{sr} 2 a_{sr} \omega_r \nu_r \\ c_{sr} = \delta_{sr} a_{sr} \omega_r^2 \end{cases} \tag{3.6}$$

Where ω_r is the *r-th* natural frequency of the dry hull (without considering fluid added mass), θ_r is the *r-th* mode of shape of the sectional rotations and ν_r is the *r-th* damping factor. The generalised external forces F_s that excite the system in Equation 3.5 are calculated decomposing the external forces into components along each principal mode of shape. $F^k(t)$ is the vertical component of the $k-th$ force vector acting on the hull defined as follow.

$$F^k(t) = \int_L f^k(x;t) dx \tag{3.7}$$

Where f^k is the sectional vertical force component; therefore the associated generalised force $F_s^k(t)$ is defined as:

$$F_s^k(t) = \int_L f^k(x;t) w_s(x) dx \tag{3.8}$$

Equation 3.8 defines the generalised force F_s^k that can be interpreted as the projection of F^k on the *s-th* mode of shape w_s.

3.3 Forces Acting on The Vessel

Equation 3.5 is an initial formulation of the equations of motion for a flexible hull. In order to obtain an expression that can be used to calculate the motions of the body, the vector of the generalised external forces must be evaluated. This

requires the forces acting on the vessel to be defined in the physical reference frame described in Figure 3.1, and then projected onto the principal mode shapes using Equation 3.3. The forces acting on the body are evaluated using a strip theory approach, longitudinal effects and forward speed effects are considered in the calculation and they rise from the mathematical formulation of the external forces.

In the following sections all the forces that excite the vessel are formulated and described.

Following Bishop and Price (1979) the generalised force F_s can be written as follow

$$F_s^k(t) = \int_L (Z(x;t) - \mu(x)g)w_s(x)dx \tag{3.9}$$

Where Z describes the vertical fluid actions on the body and μg represents the sectional weight force of the vessel. The fluid is considered to be incompressible, inviscid, uniform, irrotational, and ideal; therefore it is possible to define the velocity field using the velocity potential. Considering the first order terms of the Bernoulli equation for an ideal flow, the sectional fluid actions Z can be formulated as follow.

$$Z(x;t) = -\rho \int_{S_B(x;t)} (\frac{D\phi(y,z;t)}{Dt} + gz)n_z(y,z;t)dx \tag{3.10}$$

S_B represents the actual wetted hull section and ϕ is the velocity potential, where $D/Dt = (d/dt - U\partial/\partial x)$. Following the classical decomposition of the velocity potential into radiation, diffraction and ambient wave field potentials is it possible to expand Equation 3.10.

$$Z(x;t) = -\rho \int_{S_B(x;t)} \left[\frac{D}{Dt}\left(\phi_{hd} + \phi_0\right) + gz\right] n_z dx \tag{3.11}$$

The vertical relative velocity is used to define hydrodynamic sectional forces; therefore the term ϕ_{hd} in Equation 3.11 collects both the radiation and diffraction potentials, while ϕ_0 describes the velocity potential related to the ambient waves field. Equation 3.11 can finally be written as:

$$Z(x;t) = f_{hd}(x;t) + f_0(x;t) + f_{hs}(x;t) \tag{3.12}$$

where

$$\begin{aligned} f_{hd}(x;t) &= -\rho \int\limits_{S_B(x;t)} \frac{D\phi_{hd}}{Dt} n_z dx \\ f_0(x;t) &= -\rho \int\limits_{S_B(x;t)} \frac{D\phi_0}{Dt} n_z dx \\ f_{hs}(x;t) &= -\rho \int\limits_{S_B(x;t)} g z n_z dx \end{aligned} \tag{3.13}$$

Equations 3.12 and 3.13 describe the sectional fluid actions in terms on f_{hd} hydrodynamic, f_0 exciting andf_{hs} hydrostatic forces.

3.3.1 Hydrodynamic Forces

In this nonlinear time domain approach the velocity potential associated with the radiation and diffraction problems (hydrodynamic potential) is expressed using the formulation proposed by Cummins (1962). The velocity potential is divided into two components: an impulsive part, related to the instantaneous impulse of displacement, and a memory effect function, that describes the radiated waves field. The resulting formulation for the hydrodynamic velocity potential is expressed in Equation 3.14.

$$\phi_{hd}(\vec{x};t) = \Psi(y,z;t)\frac{DW_{rel}}{Dt}(x;t) + \int\limits_{-\infty}^{t} \chi(y,z;t-\tau)\frac{DW_{rel}}{Dt}(x;\tau)d\tau \tag{3.14}$$

In the above equation Ψ represents the impulsive potential and χ defines the memory effect one. τ is the integration variable in the history of motion; W_{rel} is the vertical relative displacement between vessel and waves. Equation 3.14 requires the solution of two distinct boundary value problems described in Equations 3.15 and 3.16.

$$\begin{cases} \nabla^2\Psi = 0 & \text{In the fluid} \\ \frac{\partial}{\partial n}\Phi = \frac{DW_{rel}}{Dt} & \text{on } S_B(x;t) \\ \Phi = 0 & \text{on } z = 0 \end{cases} \tag{3.15}$$

$$\begin{cases} \nabla^2\chi = 0 & \text{In the fluid} \\ \frac{\partial^2}{\partial t^2}\chi + g\frac{\partial}{\partial z}\chi = 0 & \text{on } z = 0 \\ \frac{\partial}{\partial n}\chi = 0 & \text{on } S_B(x;t) \\ \chi(0) = 0 & \\ \frac{\partial}{\partial \tau}\chi(0) = -g\frac{\partial}{\partial z}\Psi & \text{on } z = 0 \end{cases} \tag{3.16}$$

These set of boundary conditions are more extensive than the ones for the classical formulation. This is due to the subdivision of the velocity potential into two components. New conditions are required to ensure the continuity of the potentials in time; this is stated in the last initial condition of Equation 3.16, where it is assumed that at the initial instant the amplitude of the radiated waves must be equal to the z derivative of the impulsive potential at $z = 0$.

The impulsive boundary value problem is solved in analogy to the problem of a body oscillating vertically at infinite frequency. The solution leads to the evaluation of the sectional added mass coefficient at infinite frequency a_z^∞.

$$a_z^\infty(x;t) = \rho \int\limits_{S_B(x;t)} \Psi n_z ds \tag{3.17}$$

The memory effect part can be solved following the approach presented by Ogilvie (1964); therefore the integral of the memory effect potential along the sectional

hull surface is related to the frequency dependent hydrodynamic damping coefficients via inverse Fourier transform.

$$\rho \int\limits_{S_B(x;t)} \left[\int\limits_0^t \chi(t-\tau) \frac{DW_{rel}}{Dt}(\tau) d\tau \right] n_z ds = \int\limits_0^t K_z(x;t-\tau) \frac{DW_{rel}}{Dt}(\tau) d\tau \quad (3.18)$$

Where the kernel of the memory effect function K_z is evaluated as follow

$$K_z(x;t) = \frac{2}{\pi} \int\limits_0^\infty \frac{b_z(\omega) - b_z(\infty)}{\omega} \sin \omega t d\omega \quad (3.19)$$

Where b_z is the sectional frequency domain damping coefficient. Considering Equations 3.17, 3.18 and 3.19, it is possible to reformulate Equation 3.13 introducing the sectional added mass and convolution integral.

$$f_{hd}(x;t) = -\frac{D}{Dt} \left[a_z^\infty(x;t) \frac{DW_{rel}}{Dt}(x;t) + \int\limits_0^t K_z(x;\tau) \frac{DW_{rel}}{Dt}(x;t-\tau) d\tau \right] \quad (3.20)$$

Before analysing Equation 3.20 the vertical relative displacement should be defined.

The sectional relative displacement W_{del} is defined as the difference between the vertical displacement of the vessel due to its motions and the wave displacement at a given section.

$$W_{rel}(x;t) = W(x;t) - \zeta(x;t) \quad (3.21)$$

All the terms of Equation 3.20 are nonlinear and evaluated on the actual wetted hull portion of the vessel. The sectional vertical motion of a strip of hull follows Equation 3.21. This leads to a nonlinear formulation of the sectional

hydrodynamic forces that takes into account the exact body geometry.

$$\begin{aligned} f_{hd}(x;t) = &- a_z^{\infty}\frac{D^2W_{rel}}{Dt^2} - \frac{da_z^{\infty}}{dt}\frac{DW_{rel}}{Dt} + U\frac{\partial a_z^{\infty}}{\partial x}\frac{DW_{rel}}{Dt} + \\ &- \left(\frac{d}{dt} - U\frac{\partial}{\partial x}\right)\left[\int_0^t K_z(\tau)\frac{DW_{rel}}{Dt}(t-\tau)d\tau\right] \end{aligned} \tag{3.22}$$

Equation 3.22 describes the sectional nonlinear hydrodynamic force; the first term is an inertial term related to the acceleration of the body, the second one represents the impulsive momentum slamming (von Karman method) and the third component is a higher-order forward speed correction proportional to U and U^2 (from the formulation of the material derivative of the sectional relative displacement). The memory effect terms describe the frequency depended part of the force related to the free-surface gravitational effects.

f_{hd} collects both radiation and diffraction component, this is possible because the relative vertical velocity is used to defined fluid momentum and therefore the components related to the kinetics of Equation 3.22 represent the radiation part and the terms function of the wave particle velocity are the sectional nonlinear diffraction forces. The water particle velocity is not uniform along a section, therefore an average value is taken using the well-known Smith's correction.

$$sc(x;t) = 1 - k\int_{-T(x;t)}^{0} e^{kz}\frac{y(x,z;t)}{y_0(x;t)}dz \tag{3.23}$$

Equation 3.23 describes the Smith's correction for a section at a given time instant, k is the wavenumber of the ambient wave, T is the sectional instantaneous immersion and y_0 is the half breadth at the free surface interception.

Equation 3.22 can be further modified if the Leibniz rule is used together with the properties of the time derivative of the convolution integral, therefore, neglecting

the difference of the extremes of the integral, it is possible to write

$$\begin{aligned} f_{hd}(x;t) = &- a_z^\infty \frac{D^2 W_{rel}}{Dt^2} - \frac{da_z^\infty}{dt}\frac{DW_{rel}}{Dt} + U\frac{\partial a_z^\infty}{\partial x}\frac{DW_{rel}}{Dt} + \\ &- \int_0^t \dot{K}_z(\tau)\frac{DW_{rel}}{Dt}(t-\tau)d\tau + U\frac{\partial}{\partial x}\int_0^t K_z(\tau)\frac{DW_{rel}}{Dt}(t-\tau)d\tau \end{aligned} \tag{3.24}$$

Where

$$\dot{K}_z(x;t) = \frac{2}{\pi}\int_0^\infty (b_z(\omega) - b_z(\infty))\cos\omega t d\omega \tag{3.25}$$

A last modification of Equation 3.24 is introduced by reformulating the time derivative of the sectional added mass in the second term of the right-hand side as follow

$$\frac{da_z^\infty}{dt} = -\frac{\partial a_z^\infty}{\partial T}\frac{dw}{dt} \tag{3.26}$$

The derivative respect T should be considered as the rate of change of sectional added mass within the sectional immersion. Introducing Equation 3.26 into Equation 3.24 it is possible to write:

$$\begin{aligned} f_{hd}(x;t) = &- a_z^\infty \frac{D^2 W_{rel}}{Dt^2} + \frac{\partial a_z^\infty}{\partial T}\frac{dw}{dt}\frac{DW_{rel}}{Dt} + U\frac{\partial a_z^\infty}{\partial x}\frac{DW_{rel}}{Dt} + \\ &- \int_0^t \dot{K}_z(\tau)\frac{DW_{rel}}{Dt}(t-\tau)d\tau + U\frac{\partial}{\partial x}\int_0^t K_z(\tau)\frac{DW_{rel}}{Dt}(t-\tau)d\tau \end{aligned} \tag{3.27}$$

Equation 3.27 is the final formulation of the nonlinear sectional hydrodynamic force and it is used in section 3.4.1 to develop an expression for the generalised hydrodynamic force.

3.3.2 Restoring Forces

The term f_{hs} in Equation 3.13 defines a sectional hydrostatic force. In a linear theory, this term is represented together with the sectional weight force into the elements of the stiffness matrix. In a nonlinear approach the sectional hydrostatic

force changes with time as function of the vessel instantaneous immersion; therefore the stiffness matrix cannot be used anymore to represent the restoring forces. They are now formulated as the instantaneous difference between the sectional hydrostatic and weight forces as shown in Equation 3.28.

$$f_r(x;t) = -\int\limits_{S_B(x;t)} (\rho g z n_z + g\mu) dx \tag{3.28}$$

3.3.3 Exciting Forces

The ambient wave field is defined by a first-order sinusoidal wave. The associated velocity potential is defined using the well-known formulation reported in Equation 3.29

$$\phi_0(x,y,z;t) = \Re\left\{ i\frac{a_w g}{\omega} e^{kz} e^{ik(x\cos\beta + y\sin\beta) - i\omega_e t + i\epsilon} \right\} \tag{3.29}$$

Equation 3.29 describes a linear plane deep water progressive wave, this expression is used to model the ambient wave field. Finite depth effects can be considered without introducing any further complexity. The force acting on the body due to the ambient waves, calculated using the present formulation, is the so called Froude-Krylov force. In the present work the exciting force is evaluated from a direct integration of the ambient wave potential on the actual wetted body portion and stated in Equation 3.30.

$$f_0(x;t) = \rho g a_w \Re\left\{ \left[\frac{\omega_e}{\omega} e^{ikx\cos\mu} \int\limits_{S_B(x;t)} e^{kz} e^{iky\sin\mu} n_z dx \right] e^{i\omega_e t + \epsilon} \right\} \tag{3.30}$$

3.3.4 Bottom Impact Forces

In severe seas, slamming induced forces are extremely important for the integrity and safety of the vessel. As described in section 2.5, different methodologies can

be used to model forces due to bottom impact and bow flare slamming.

The second term in the right hand side of Equation 3.27 describes the impulsive component of the sectional hydrodynamic forces. This term can be associated with a von Karman approach and therefore can lead to an underestimation of impulsive effects for water entry for sections with small deadrise angle. On the other hand, this methodology is able to estimate flare slamming and it gives satisfactory results for water entry of sections with large deadrise angle.

For these reasons the approach described in section 3.3.1 is used in conjunction with an empirical approach proposed by Ochi and Motter (1973) to model water entry of sections with small deadrise angle. Since both methods describe the same force in a different manner it is important to create a numerical procedure that allows to use one approach or the other without summing their effects (Section 3.5).

The formulation of the maximum impulsive pressure acting on a section, given by the empirical approach, is function of the deadrise angle of the section and of the relative velocity as described in Equation 3.31

$$p_{max}(x;t) = \frac{1}{2}\rho K(x)\frac{DW_{rel}}{Dt}^2 \tag{3.31}$$

K is a shape factor function of the section deadrise angle formulated by Stavovy and Chuang (1976). The formulation of the sectional impulsive force based on Ochi and Motter (1973) is described below.

$$f_{bs}(x;t) = \frac{1}{2}\rho K\frac{DW_{rel}}{Dt}^2 G(x) f_T(t) \tag{3.32}$$

$G(x)$ is a shape factor that takes into account a pressure distribution on the hull sections. The pressure distribution profile is described in Figure 3.2 and varies linearly with the z coordinate, from the value of p_{max} from the lower point to

zero at a sectional immersion equal to $T_D/10$ where T_D is the sectional design immersion.

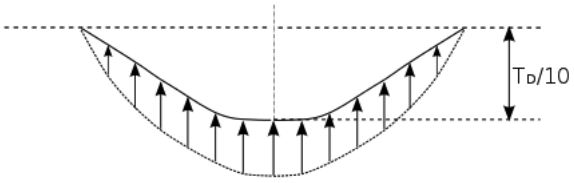

Figure 3.2: Distribution of impulsive pressure due to bottom impact on a section described by $G(x)$.

f_T is a time dependent function that describes the time evolution of the maximum pressure, its formulation is reported in Equation 3.33. Its shape is described in Figure 3.3 where f_T is plotted against the non-dimensional time variable (t/t_{max}).

$$f_T(t) = \frac{t}{t_{max}} e^{1-\frac{t}{t_{max}}} \tag{3.33}$$

The value t_{max}, used in Equation 3.33, describes the time instant of the peak of the impulsive pressure; it is function of the length of the vessel: $t_{max} = 0.00088\sqrt{L_{BP}}$ (Ochi and Motter, 1973). This function in the current approach is very important to merge in time the empirical and the momentum based formulation.

3.4 Generalised Forces

In this section the formulations for the generalised forces are described and explained.

The equations for the sectional forces, derived in the previous sections are used, in conjunction with Equation 3.7, to calculate their associated generalised forces

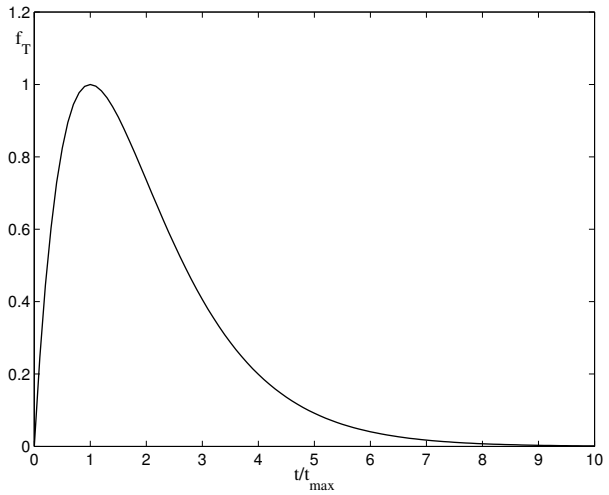

Figure 3.3: Time evolution function of the maximum impulsive pressure.

3.4.1 Generalised Hydrodynamic Forces

Before presenting the formulation for the generalised hydrodynamic forces it is important to understand the definition of relative displacement between the body and the wave. The vertical displacement of a strip of hull $W(x;t)$ is expressed using Equation 3.3; therefore the relative vertical displacement $W_{rel}(x;t)$ is formulated as follows:

$$W_{rel}(x;t) = W(x;t) - \zeta(x;t) = \sum_{r=0}^{\infty} \Big[w_r(x) p_r(t) \Big] - \zeta(x;t) \tag{3.34}$$

where $\zeta(x;t)$ describes the wave elevation due to the undisturbed ambient velocity potential. Thus the relative velocity and acceleration of a section of the hull is evaluated applying the material derivative to the right-hand side of Equation 3.34 once and twice respectively.

$$\frac{DW_{rel}}{Dt}(x;t) = \sum_{r=0}^{\infty} \Big[w_r(x) \dot{p}_r(t) - U w_r'(x) p_r(t) \Big] - \dot{\zeta}(x;t) - U\zeta'(x;t) \tag{3.35}$$

$$\frac{D^2W_{rel}}{Dt^2}(x;t) = \sum_{r=0}^{\infty}\left[w_r(x)\ddot{p}_r(t) - 2Uw_r'(x)\dot{p}_r(t) + U^2w_r''(x)p_r(t)\right] + \\ - \ddot{\zeta}(x;t) + 2U\dot{\zeta}'(x;t) - U^2\zeta''(x;t) \tag{3.36}$$

To evaluate the equations for the generalised fluid actions Equations 3.27, 3.35 and 3.36 are applied to Equation 3.8. The formulations are rather complex and the mathematical process to obtain them is described in Appendix A. In this section only the main steps are reported.

To obtain the final formulation of the generalised hydrodynamic force, the relative vertical velocity and displacement in the first and third terms in the right-hand side of Equation 3.27 must be evaluated using modal superposition.

$$\begin{aligned} F_s^{HD}(t) = &\sum_{r=0}^{\infty}\left[-\int_L a_z^{\infty}w_rw_sdx\ddot{p}_r\right] + \\ &+\sum_{r=0}^{\infty}\left\{U\int_L\left[2a_z^{\infty}w_r' + (a_z^{\infty})'w_r\right]w_sdx\dot{p}_r\right\} + \\ &+\sum_{r=0}^{\infty}\left\{-U^2\int_L\left[a_z^{\infty}w_r'' + (a_z^{\infty})'w_r'\right]w_sdxp_r\right\} + \\ &+\int_L(a_z^{\infty}\frac{D^2\zeta}{Dt^2} - (a_z^{\infty})'U\frac{D\zeta}{Dt})w_sdx + \\ &+\int_L\frac{\partial a_z^{\infty}}{\partial T}\frac{dw}{dt}\frac{DW_{rel}}{Dt}w_sdx + \\ &-\int_L\dot{\tilde{K}}w_sdx + U\int_L\tilde{K}'w_sdx \quad s = 0,1,2,\ldots \end{aligned} \tag{3.37}$$

where the terms $\dot{\tilde{K}}$ and $\tilde{K}'$ describe the components of the convolution integrals.

$$\begin{aligned} \dot{\tilde{K}} &= \int_0^t \dot{K}(t-\tau)\frac{DW_{rel}}{Dt}(\tau)d\tau \\ \tilde{K}' &= \frac{\partial}{\partial x}\int_0^t K(t-\tau)\frac{DW_{rel}}{Dt}(\tau)d\tau \end{aligned} \tag{3.38}$$

Equation 3.37 collects all the components of the hydrodynamic generalised forces. To simplify the understanding of the effect of each single component, the right-

hand side of Equation 3.37 can be grouped into four main contributions. The first three lines form the generalised added mass radiation force F_s^{RAD}, the fourth row describes the generalised added mass diffraction component F_s^D, while the fifth term defines the momentum slamming generalised force F_s^I and in the end the last line is the memory effect generalised force F_s^M.

The generalised added mass radiation force in the s-th mode is formulated as the sum of the contributions among all the modes of shape, with terms that are directly proportional to the principal coordinate displacement, velocity and acceleration.

For this reason it is possible to express the generalised added mass radiation forces using matrices and coefficients to multiply with the principal coordinate displacements, velocities and accelerations. These coefficients are called generalised hydrodynamic coefficients.

$$\begin{aligned} A_{sr}(t) &= \int_L a_z^\infty w_r w_s dx \\ B_{sr}(t) &= -U \int_L a_z^\infty (w_r' w_s - w_r w_s') dx - U a_z^\infty w_r w_s|_0^L \\ C_{sr}(t) &= -U^2 \int_L a_z^\infty w_r' w_s' dx + U^2 a_z^\infty w_r' w_s|_0^L \end{aligned} \tag{3.39}$$

Equation 3.39 is also an improvement of Equation 3.37 since the x derivative of a_z^∞ and the second x derivative of w_r have been removed, via integration by parts, ensuring a better numerical accuracy. The same modifications can be implemented into the formulation of the generalised momentum slamming, added mass diffraction and memory effects forces.

$$F_s^I(t) = \int_L \frac{\partial a_z^\infty}{\partial T} \frac{dw}{dt} \frac{DW_{rel}}{Dt} w_s dx \tag{3.40}$$

$$F_s^D(t) = \int_L a_z^\infty \left[(\ddot{\zeta} - U\dot{\zeta}') w_s + U \frac{D\zeta}{Dt} w_s' \right] dx - U a_z^\infty \frac{D\zeta}{Dt} w_s|_0^L \tag{3.41}$$

$$F_s^M(t) = -\int_L \left(\dot{\tilde{K}} w_s + U\tilde{K} w_s'\right) dx + U\tilde{K} w_s|_0^L \tag{3.42}$$

With the introduction of Equations 3.39 the system of equations of motion described in Equation 3.5 needs to be modified. The generalised hydrodynamic coefficients are introduced and the system of equations of motion becomes as follows.

$$\sum_r \left[\left(a_{sr} + A_{sr}\right)\ddot{p}_r + \left(b_{sr} + B_{sr}\right)\dot{p}_r \left(c_{sr} + C_{sr}\right) p_r \right] = \tilde{F}_s(t) \quad s = 0, 1, 2, \ldots \tag{3.43}$$

Where A_{sr}, B_{sr} and C_{sr} represent the elements of the generalised added mass, damping and stiffness matrix respectively. $\tilde{F}_s$ is the vector of the generalised external forces without the added mass radiation forces.

The numerical evaluation of all the components of Equations 3.39, 3.41 and 3.42 is described in section 3.5.

3.4.2 Generalised Restoring and Exciting Forces

The generalised restoring F_s^R and exciting F_s^E forces are directly formulated from Equations 3.28 and 3.29 respectively. The equations below represent their final implementation.

$$F_s^R(t) = \int_L f_r(x;t) w_s(x) dx \tag{3.44}$$

$$F_s^E(t) = \int_L f_0(x;t) w_s(x) dx \tag{3.45}$$

3.4.3 Final Formulation of the Equations of Motion

In the section the final formulations of the equation of motions are recovered using the results from sections 3.4.1 and 3.4.2. The system of second order differential equations that describes the dynamics of the vessel is formulated using the modal

superposition method as described in Equation 3.5. Hydrodynamic, restoring and exciting forces acting on the floating body are formulated using the approaches described in the previous sections.

In order to obtain the final formulation of the equations of motion Equation 3.43 is further modified introducing the actual formulation for each generalised force. The result is reported in Equation 3.46.

$$\sum_r \left[\left(a_{sr} + A_{sr}\right)\ddot{p}_r + \left(b_{sr} + B_{sr}\right)\dot{p}_r \left(c_{sr} + C_{sr}\right)p_r \right] = \\ = F_s^D + F_s^M + F_s^R + F_s^E + F_s^S \quad s = 0, 1, 2, \ldots \tag{3.46}$$

Where F_s^S described the generalised slamming force. The momentum slamming component, defined in Equation 3.40, is partially used to evaluate slamming forces on a section; when a strip of hull has a deadrise angle smaller than 30 degrees and enters into the water with a relative vertical velocity higher than a threshold value the empirical equations presented in section 3.3.4 are used to evaluate impulsive forces. The coupling between these two formulations is described in section 3.5.

3.4.4 Linear Formulation of the Equations of Motion

In the previous sections the equations of motion for a nonlinear system have been formulated, and equation 3.46 summarises their final form. In order to compare and validate results obtained by the proposed nonlinear method a linear methodology, based on the same mathematical approach, is obtained. In a linear method, the fluid actions acting on the body are evaluated assuming small amplitude motions and wave steepness. Therefore the equations of motions, and related boundary value problems, are linearised considering the calm water level as free surface and the vessel fixed on its equilibrium position (in calm water).

These assumptions result in a set of equations similar to the ones described from

section 3.4.1 to section 3.4.3, but in this case the hydrodynamic coefficients are not time dependent and the excitation and diffraction forces are harmonic functions. Equation 3.47 describes the equations of motion for a linear system.

$$\sum_r \Big[\big(a_{sr} + A_{sr}\big)\ddot{p}_r + \big(b_{sr} + B_{sr}\big)\dot{p}_r \big(c_{sr} + C_{sr}\big)p_r \Big] = \\ = F_s^D + F_s^M + F_s^E \quad s = 0, 1, 2, \ldots \tag{3.47}$$

where the elements of the generalised hydrodynamic stiffness matrix are defined considering also the hydrostatic components

$$C_{sr} = \rho g \int_L B(x) w_r w_s dx - U^2 \int_L a_z^\infty w_r' w_s' dx + U^2 a_z^\infty w_r' w_s |_0^L \tag{3.48}$$

In equation 3.47 the momentum slamming term F_s^S vanishes.

3.5 Numerical Methods

In the present section the numerical methods used to solve equation 3.46 are described. The principal elements reported here are: the evaluation of modes shape and structural natural frequencies, the solution of the system of equations of motion, the calculation of the sectional forces and the coupling between the momentum and the empirical formulations for slamming.

A finite element method is used to evaluate mode of shapes for the vertical translations and rotations using a nonuniform free-free Timoshenko beam model (Kwon and Hyochoong, 1997). The principal input required for the calculations are the longitudinal distribution of mass μ, flexural rigidity EI, shear rigidity kAG and rotary inertia I_y.

The system of equations of motion is numerically solved in time domain using a 4-th order Runge-Kutta method. The initial values $\dot{p}$ and p for the problem of a

vessel sailing in a seaway are given considering the vessel sailing in calm water at constant forward speed.

Using this procedure a preliminary calculation is needed, but it allows to reduce the transient phase during the seakeeping analysis. A linear ramp function is used to attenuate environmental forces at the beginning of the calculation. The duration of the ramp function is usually three or four wave encounter periods.

The sectional hydrodynamic coefficients, needed to evaluate the radiation and diffraction forces, are found using a two dimension boundary element method obtained modifying the approach proposed by Andersen and Wuzhou (1985) (described in Appendix B). This approach discretises all the boundary of the domain and uses a simple logarithmic Green's function with potential eigenvalues expansion on the radiation boundaries. The principal advantages respect a free-surface Green's function approach and a mapping technique are that this methodology allows a correct calculation hydrodynamic coefficients for complex geometries without been affected by the problem of irregular frequencies. On the other hand the matrix of the coefficients of influence is larger and therefore it requires more time to be inverted. To reduce computational time, hydrodynamic coefficients are evaluated before the time domain calculation for several sectional immersions and their values are stored. During the time analysis the actual values of sectional hydrodynamic coefficients are evaluated from the stored ones via interpolation.

Exciting and restoring forces are calculated integrating the pressure field over the body. At each time step the actual wetted hull strips are evaluated and discretised in a set of linear panels over which the pressures are integrated to compute the exciting and restoring forces.

Sectional slamming forces are calculated using a momentum based formulation (Equation 3.27) and an empirical approach (Equation 3.32). Water entry forces for sections with small deadrise angle are better modelled using the empirical

based approach, while the momentum theory gives a better prediction for bow flare slamming and water entry for sections with large deadrise angle. Therefore the sectional impulsive force f^S, used to calculate the generalised force F_s^S, is computed by coupling the two methodologies as described below.

$$f^s(x;t) = \begin{cases} f_{bs}(x;t) & \text{If } \tilde{t} \leq 5t_{max} \\ \frac{\partial a_z^\infty}{\partial T}\frac{dw}{dt}\frac{DW_{rel}}{Dt} & \text{If } \tilde{t} > 5t_{max} \end{cases} \tag{3.49}$$

where $\tilde{t}$ is the time instant at which the section reenters the water. Equation 3.49 is used for sections that have a deadrise angle larger than 30 degrees, otherwise the momentum based method is used alone in the water entry phase.

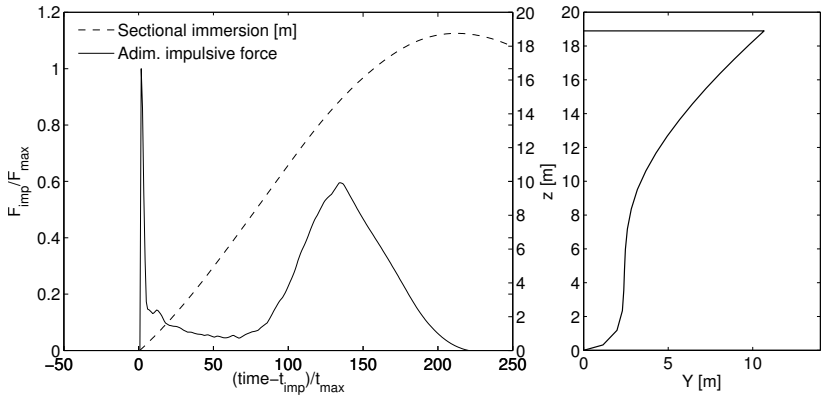

Figure 3.4: (Left) Example of the time history of sectional impulsive forces. (Right) Geometry of the section under analysis.

An example of sectional impulsive force, calculated using this procedure, is shown in Figure 3.4(Left). Here the time history of a single water entry event is reported. At $\tilde{t} = 0$ the sections enter the water and the forces are evaluated using the empirical approach; the first spike results from the water entry pressure peak. When $\tilde{t} > 5t_{max}$ the sectional impulsive force is calculated using the momentum theory and the bow flare event is computed accordingly, this approach gives the second peak present in the time history, associated with the flare of the hull.

From Figure 3.4(Left) it is also possible to appreciate the importance of model the impulsive forces using different methods. The characteristics and time scale of water entry and bow flare phenomena are different, but both events produces a high sectional force.

Since the sectional added mass is evaluated considering the boundary value problem of Equation 3.15, during the water exit phase this momentum based approach gives results that are symmetrical to the water entry phase, resulting in a wrong force estimation. Thus, during the water exit phase, the sectional impulsive force f_S is set equal to zero.

The described methodology and numerical techniques have been implemented in the MATLAB environment. The developed tool is divided into three subprogram:

- Pre-processor: it calculates the hydrodynamic coefficients for different sectional immersions and the parameters for the empirical slamming calculation and it saves them into an "hydrodynamic" database.
- Time marching scheme: this part of the tool solves the equations of motion in time domain for both regular and irregular seas.
- Post-processor: these subroutines analyse the output of the simulation and evaluate responses characteristics and statistics.

The time required by the code is 4.5 times the actual simulated time (60 seconds of simulation require 4.5 minutes). This means that a several short term calculation (3 hour duration) can be performed within a day. It is important to notice that at the current stage of development the tool it has not been optimised yet to reduce the computational cost.

A parallelisation of the calculation can allow to run several simulation at the same time and to perform operations on different section simultaneously and it

will sensibly reduce the computational cost, improving the efficiency of the tool.

Chapter 4

Application of the Methodology in Regular Seas

4.1 Introduction

The proposed nonlinear time domain hydroelastic strip-theory is applied to the S-175 container ship in regular waves. Wave induced motions and loads are compared against experimental points from published papers and results from other numerical methodologies. Simulations are conducted in both small and large amplitude waves with the purpose of validating the methodology and assess the nonlinear effects for large amplitude motions. An analysis to understand the effect of the different flexural principal coordinates on the wave induced loads is presented.

4.2 S-175 Container Ship

In this section numerical results for the S-175 container ship are presented. The vertical responses of the vessels are analysed in both small and large amplitude

waves.

Computations for small amplitude waves are compared against experimental points from ITTC (2010) and Fonseca and Guedes Soares (2004) and against numerical methodologies. The techniques used in the comparison are a linear frequency domain strip theory implemented into the VERES software and a linear frequency domain seakeeping code based on free-surface Green's function named PRECAL. These types of methodologies are the most widely used for wave induced motions and loads assessment and provide a good comparison to understand the effectiveness of the proposed nonlinear hydroelastic method for small amplitude waves. Simulations for the S-175 container ship in small amplitude waves are conducted for the following:

- $Fn = 0.25$ for head seas
- $Fn = 0.275$ for head and following seas

The two analysed speeds are similar in magnitude, but they have been chosen because the literature provides a large number of experimental results for both cases allowing an accurate validation of the proposed method.

Results in large amplitude waves are compared against experimental campaign published by ITTC (2010), Fonseca and Guedes Soares (2004), O'Dea et al. (1992) and Watanabe et al. (1989). The analysis is conducted to validate the predicted motions and loads when the wave steepness increases. This comparison is important to assess the accuracy of the current nonlinear hydroelastic method for large amplitude waves. The analysis is conducted for head seas for the following Froude numbers:

- $Fn = 0.20$
- $Fn = 0.25$
- $Fn = 0.275$

The experiments used in the validation of the proposed methodology come from different research projects. They differ from each other by the model used, wave conditions and response analyses. Also if they are some of the most used references, it has not been possible to numerically replicate the same experimental conditions. Not enough details have been found to exactly model the mass properties of the vessel and the structural characteristics of the hull girder for each study setting. The longitudinal distributions of mass and stiffness are fundamental parameters for a correct loads evaluation. This lack of a complete set of informations did not allow the author to assess all the uncertainties associated with the experimental points. For example in Figures 4.28 and 4.29 the experimental points present a large scatter and it has not been possible for the author to identify the source of such uncertainty.

The main particulars of the S-175 container ship are summarised in Table 4.1, while the hull geometry is described in Figure 4.1. Structural properties of the hull girder are based on the values used by Park (2006). In order to evaluate the natural frequencies of the structure of the hull and the related mode shapes (for symmetric modes), the longitudinal distributions of mass, flexural rigidity, shear rigidity and rotary inertia are required. The distributions used in the present analysis are described in Figures 4.2, 4.3, 4.4 and 4.5 respectively. The structural damping is taken as 5% in agreement with previous works (Xia et al., 1998; Park, 2006).

Parameters	Values
Length between the perpendiculars	175.00 m
Beam amidships	25.40 m
Depth amidships	15.40 m
Draught amidships	9.50 m
Displacement	24792 tonnes
LCG from MP	-2.40 m
Pitch radius of gyration	43.75 m

Table 4.1: S-175, main particulars.

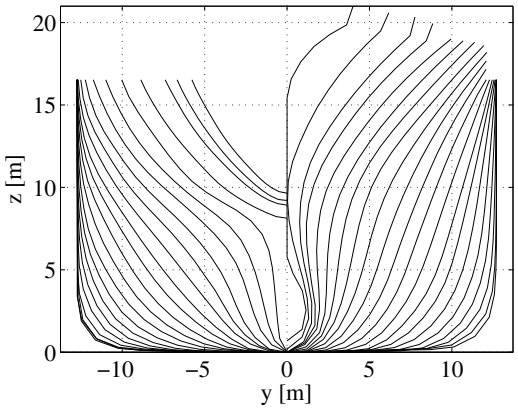

Figure 4.1: S-175, lines plan.

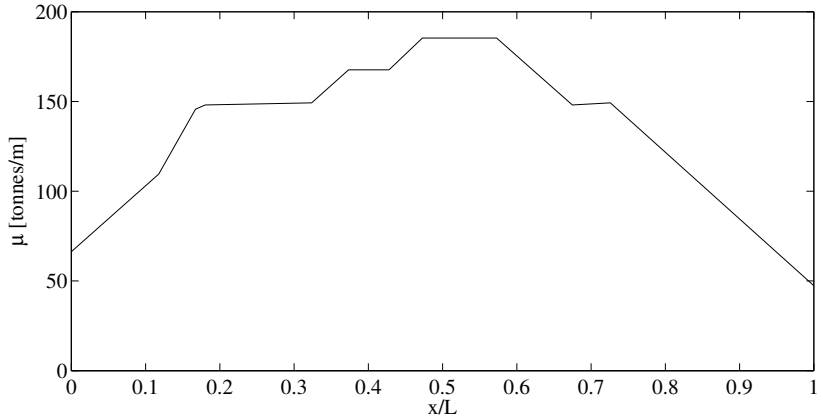

Figure 4.2: S-175, longitudinal mass distribution.

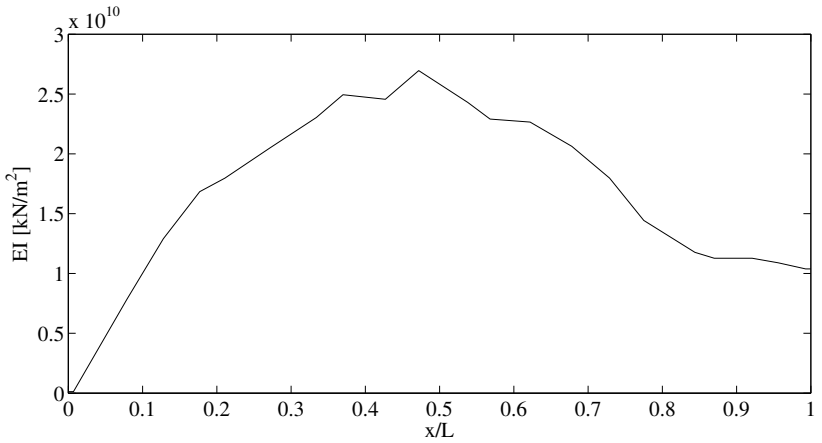

Figure 4.3: S-175, longitudinal flexural rigidity distribution.

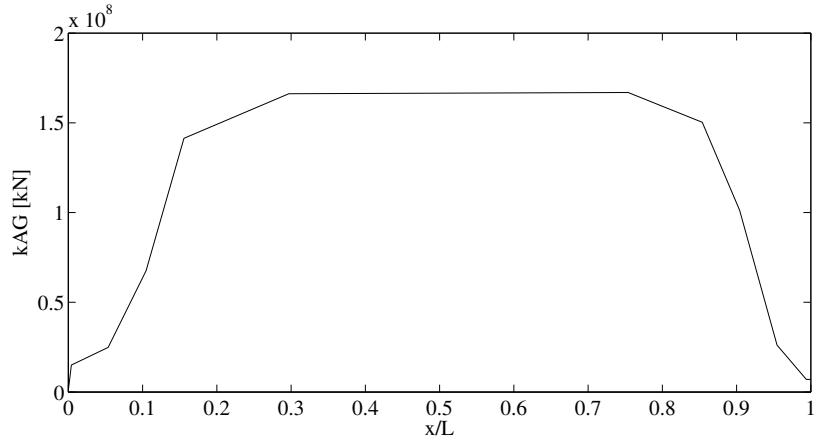

Figure 4.4: S-175, longitudinal shear rigidity distribution.

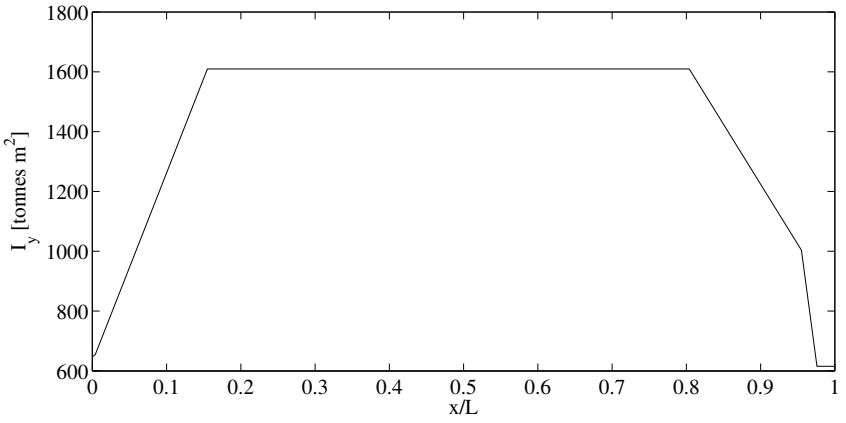

Figure 4.5: S-175, longitudinal rotary inertia distribution.

Natural frequencies and mode of shapes are calculated for the dry hull using 50

equally separated sections and using the Timoshenko beam theory, numerically solved using a finite element scheme. The number of sections is enough to properly characterise the first four flexural modes (from mode 2 to 5). Table 4.2 reports the calculated natural frequencies of the dry hull;

Modes	Values [rad/s]
2	9.268
3	21.362
4	35.815
5	52.130

Table 4.2: S-175, dry hull natural frequencies.

In Figure 4.6. 4.7 and 4.8 the first six mode of shapes for the vertical displacement, shear force and bending moment are reported. In the figures the mode of shapes are discretised in 20 points; the calculation was conducted, as previously stated, for 50 sections; the number of points in the charts has been reduced only for graphical reasons.

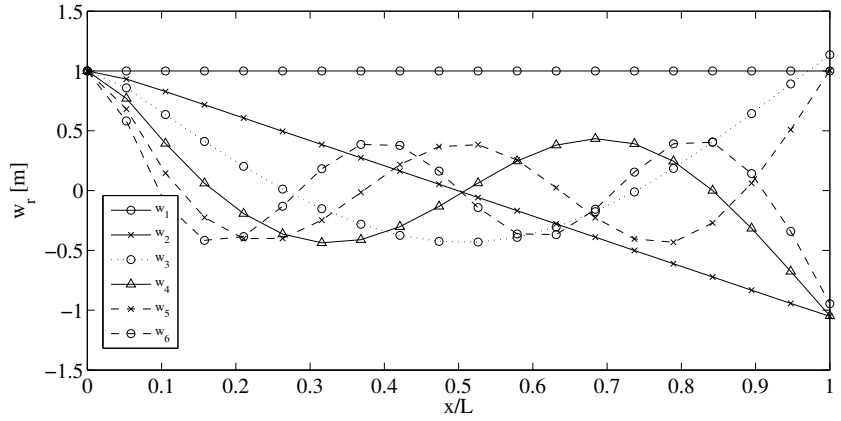

Figure 4.6: S-175, mode of shapes of the vertical hull displacement.

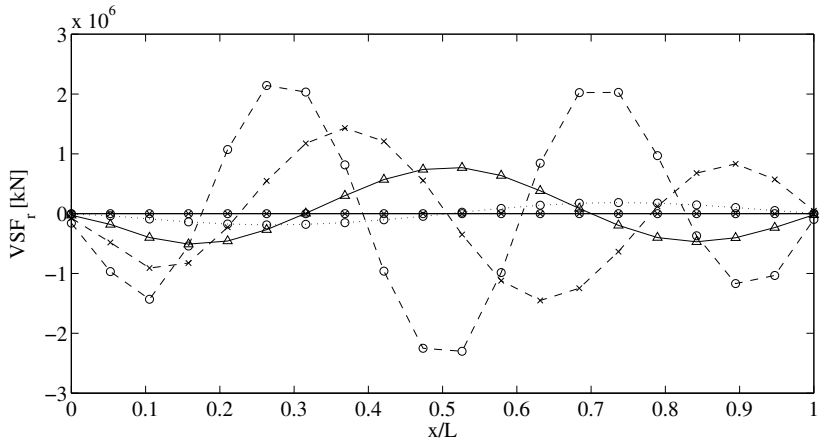

Figure 4.7: S-175, mode of shapes of the vertical shear force.

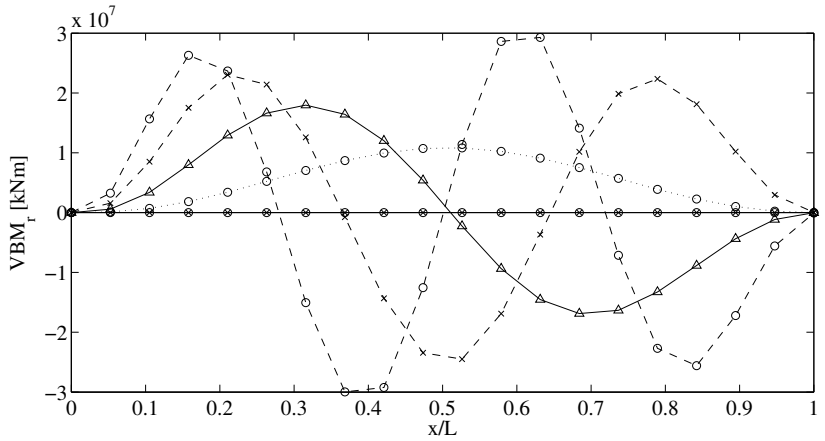

Figure 4.8: S-175, mode of shapes of the vertical bending moment.

Figure 4.9 shows the non dimensional heave response at $F_n = 0.250, 0.275$. The effect of Froude number can be observed by the shifting of the peak towards smaller wave frequencies when vessel forward speed increases. Similar behaviour, also if less visible, can be seen in Figure 4.10 where the non dimensional pitch response, at the same values of Froude number, is reported.

The predicted heave and pitch motions are compared against experimental results (Fonseca and Guedes Soares, 2004) in Figures 4.11 and 4.12 respectively, for Froude number $F_n = 0.25$ and wave steepness $H_w/\lambda = 1/120$. Comparisons show a good agreement with experimental points especially for pitch. Heave response results over predicted around resonant region; this phenomenon is typical

of methods based on inviscid flows in small amplitude waves and it is due to a lack of damping

A similar comparison against experiments (ITTC, 2010) is presented in Figures 4.13 and 4.14. Figure 4.13 shows the results for the non dimensional heave response and Figure 4.14 reports the comparison for pitch. The comparison is conducted at $F_n = 0.275$, also if wave steepness for the experimental points was not specified, numerical simulations have been conducted for $H_w/\lambda = 1/120$ in order to satisfy the criteria of small wave steepness. This comparison leads to the same observations of the previous case.

Figures 4.15 and 4.16 show a comparison between experimental (ITTC, 2010) and calculated heave and pitch for stern seas ($\mu = 0$ degrees) at $F_n = 0.275$ in small amplitude waves. Numerical results are in agreement with experimental points in the whole frequency range.

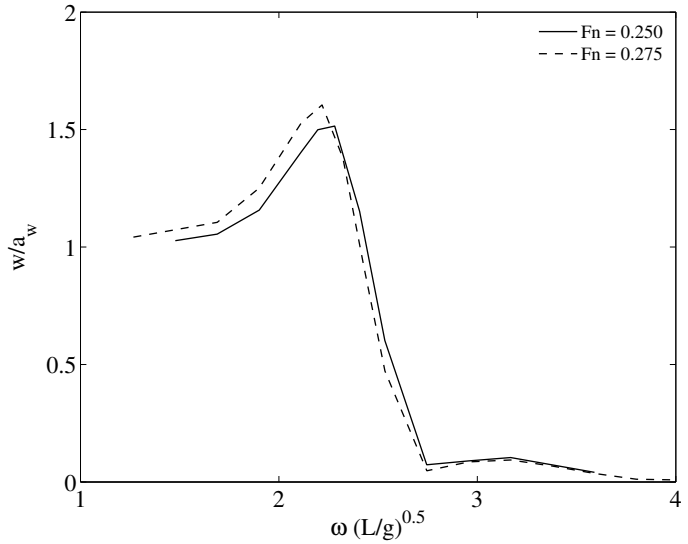

Figure 4.9: S-175, non dimensional heave response in head sea for different Froude numbers for $H_w/\lambda = 1/120$.

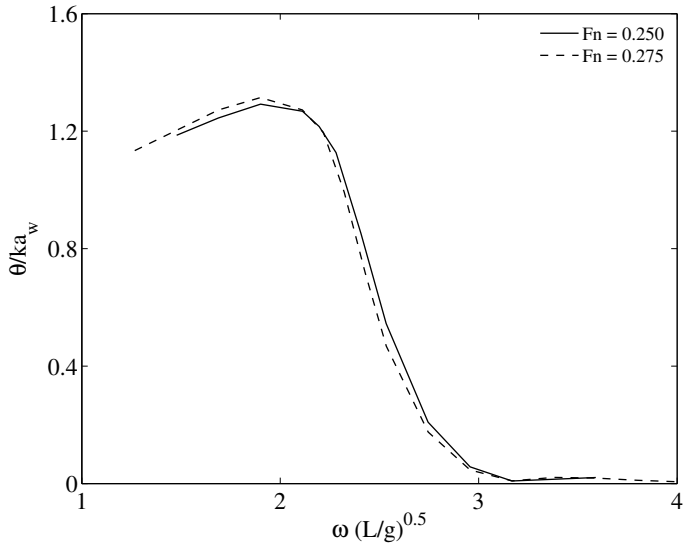

Figure 4.10: S-175, non dimensional pitch response in head sea for different Froude numbers for $H_w/\lambda = 1/120$.

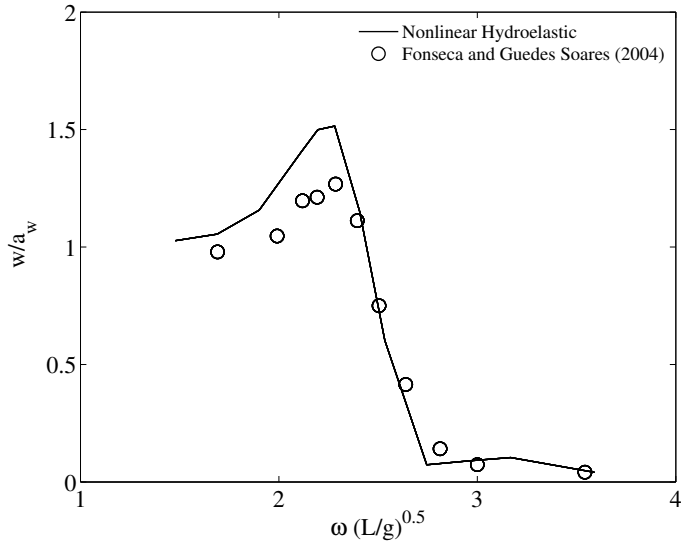

Figure 4.11: Comparison for the non dimensional heave response for the S-175, in head sea at $F_n = 0.25$ and $H_w/\lambda = 1/120$, against experimental points (Fonseca and Guedes Soares, 2004).

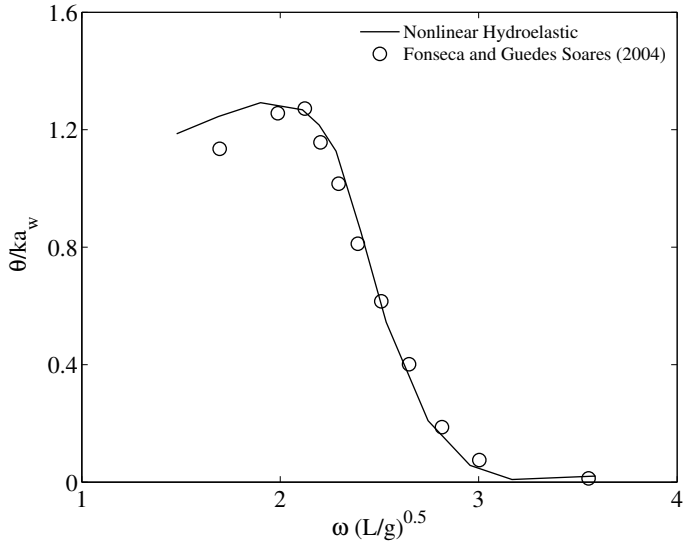

Figure 4.12: Comparison for the non dimensional pitch response for the S-175, in head sea at $F_n = 0.25$ and $H_w/\lambda = 1/120$, against experimental points (Fonseca and Guedes Soares, 2004).

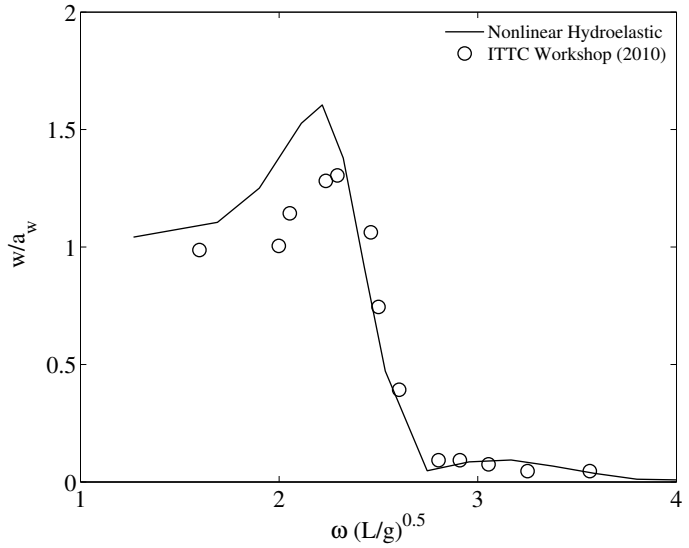

Figure 4.13: Comparison for the non dimensional heave response for the S-175, in head sea at $F_n = 0.275$, against experimental points (ITTC, 2010).

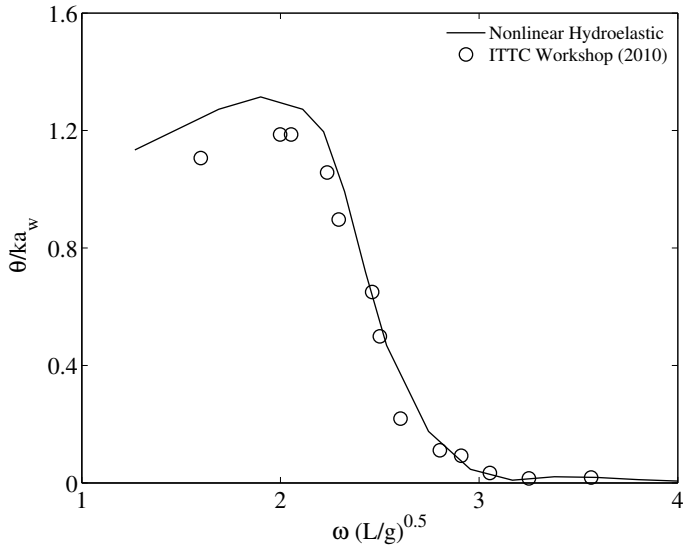

Figure 4.14: Comparison for the non dimensional pitch response for the S-175, in head sea at $F_n = 0.275$, against experimental points (ITTC, 2010).

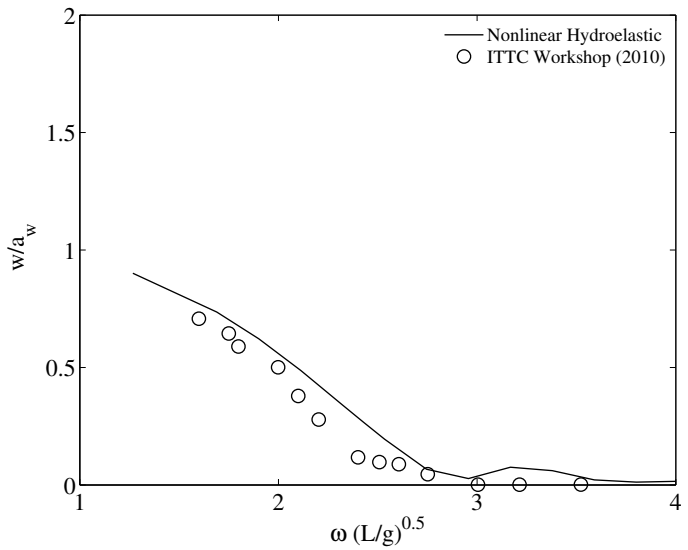

Figure 4.15: Comparison for the non dimensional heave response for the S-175, in stern sea at $F_n = 0.275$, against experimental points (ITTC, 2010).

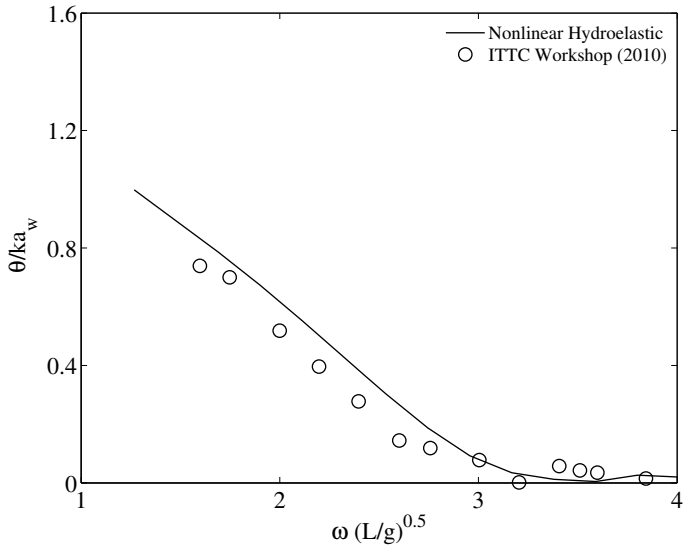

Figure 4.16: Comparison for the non dimensional pitch response for the S-175, in stern sea at $F_n = 0.275$, against experimental points (ITTC, 2010).

A comparison between the proposed numerical approach and linear numerical techniques is presented in Figures 4.17 and 4.18. Simulations are conducted in head sea at Froude number $F_n = 0.275$. Responses predicted by the proposed method show a good comparison against other numerical techniques (frequency domain strip theory and frequency domain free-surface Green's function methods). In small amplitude waves, the motions responses given by the two dimensional nonlinear hydroelastic method tend to the predictions of the frequency domain strip theory, proving a correct modelling of the proposed method, for small amplitude waves. Pitch response by the nonlinear hydroelastic method results larger than the one given by the linear strip-theory for small wave frequencies. This is not due to any nonlinear behaviour, it is only related to the small differences in the formulation of the forward speed effects.

Figures 4.19 and 4.20 show a comparison between the previously described numerical techniques and experimental points (ITTC, 2010) in head sea at Froude number $F_n = 0.275$. In Figure 4.19 heave motion predicted by PRECAL presents the higher peak around resonant region, while results obtained by the two dimensional approaches show a overall good agreement with experimental results. Similar comment can be formulated for the pitch motion in Figure 4.20 where the maximum response predicted by PRECAL occurs at smaller frequencies compared to the experimental results.

The studies reported in Figures 4.17, 4.18, 4.19 and 4.20 are useful to understand the effectiveness of the proposed methodology in small amplitude waves. The motions predicted in small amplitude waves by the proposed nonlinear hydroelastic approach are in agreement with the results of linear frequency domain methods. The comparison against experimental points shows the effectiveness of the proposed methodology within the limits of its theory (ideal fluid).

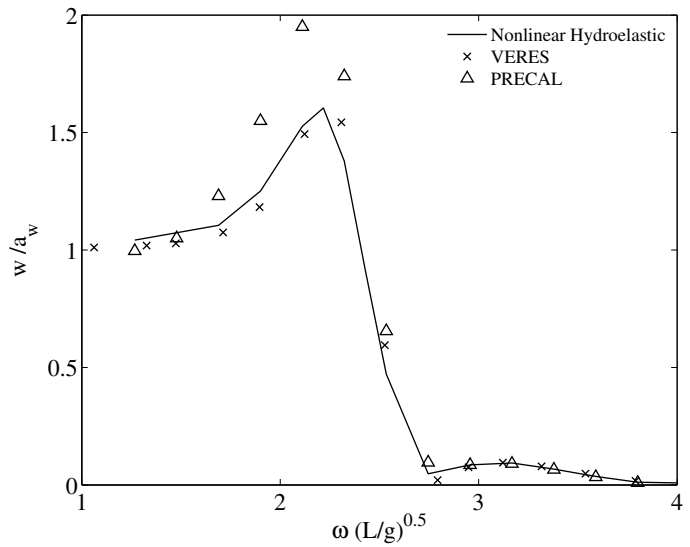

Figure 4.17: Comparison for the non dimensional heave response for the S-175, in head sea at $F_n = 0.275$, between the proposed nonlinear hydroelastic method, a frequency domain strip-theory (VERES) and a three-dimensional free-surface Green's function approach (PRECAL).

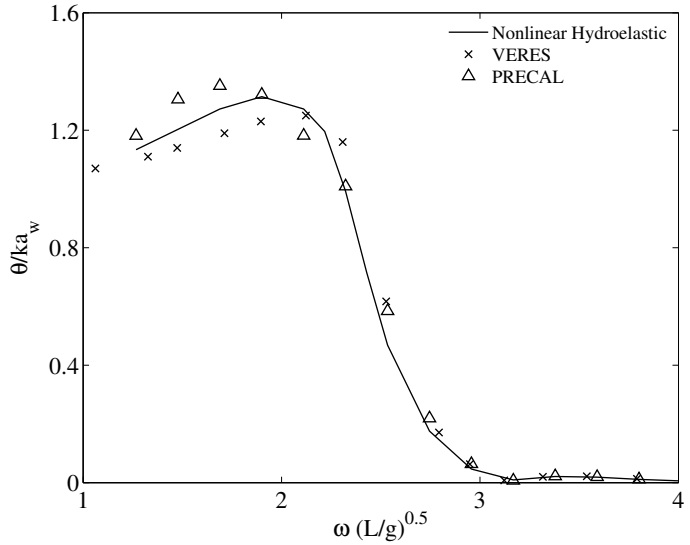

Figure 4.18: Comparison for the non dimensional pitch response for the S-175, in head sea at $F_n = 0.275$, between the proposed nonlinear hydroelastic method, a frequency domain strip-theory (VERES) and a three-dimensional free-surface Green's function approach (PRECAL) .

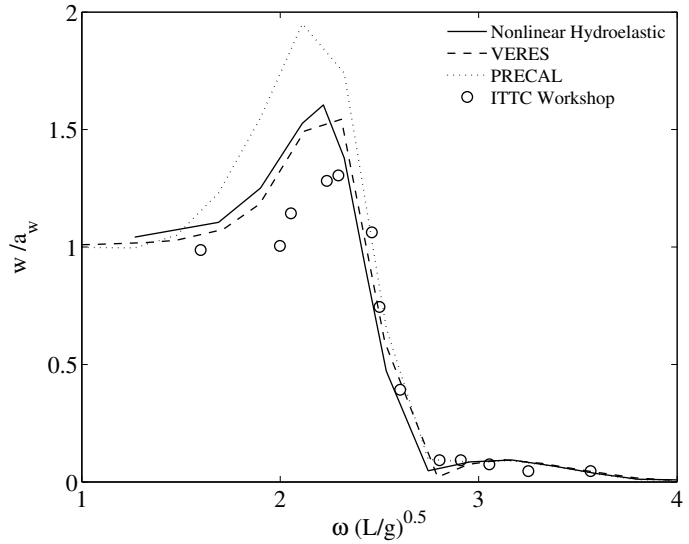

Figure 4.19: Comparison for the non dimensional heave response for the S-175, in head sea at $F_n = 0.275$, between different numerical approaches(nonlinear hydroelastic, VERES and PRECAL) and experimental points (ITTC, 2010).

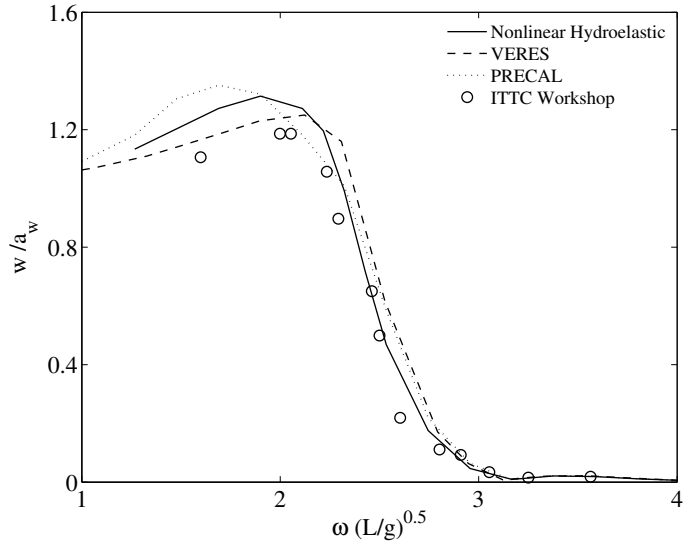

Figure 4.20: Comparison for the non dimensional heave response for the S-175, in pitch sea at $F_n = 0.275$, between different numerical approaches(nonlinear hydroelastic, VERES and PRECAL) and experimental points (ITTC, 2010).

Similar analysis and comparisons are conducted for the vertical shear force at station 15 ($L_{BP}/4$ from FP) and the midship vertical bending moment (station 10). The wave induced loads are presented in non dimensional form as follow: the vertical shear force and bending moment are divided by $\rho g a_w L B$ and $\rho g a_w L^2 B$ respectively.

Figures 4.21 and 4.22 show the vertical shear force and bending moment for the different Froude numbers $F_n = 0.25, 0.275$, in regular waves having steepness $H_w/\lambda = 1/120$ in head sea condition.

A comparison between the predicted wave induced loads and experimental points (Fonseca and Guedes Soares, 2004) is reported in Figures 4.23 and 4.24. The simulations are conducted at Froude number $F_n = 0.25$ in head sea condition at wave steepness $H_w/\lambda = 1/120$. Figures 4.25 and 4.26

Figures 4.25 and 4.26 compare the midship vertical bending moment with experimental trials (ITTC, 2010). The first figure reports the results in head sea, while the second one collects the comparison for the stern sea case. The Froude number considered is $F_n = 0.275$ with wave steepness $H_w/\lambda = 1/120$.

The comparisons show good agreement with experimental results, especially for the case with higher Froude number. Vertical shear force at station 15 ($F_n = 0.25$) predicted by the proposed methodology is smaller than experimental points, but the behaviour of the response is well predicted. Similar observations can be made for the vertical bending moment, for the same Froude number, but in this case the response results slightly over predicted around its peak. This shift between numerical and experimental results for the comparison at $F_n = 0.25$ could be due to uncertainties about the actual longitudinal distribution of mass and stiffness of the model. Numerical results at $F_n = 0.275$ present good agreement with experimental points, especially around the peak of the response.

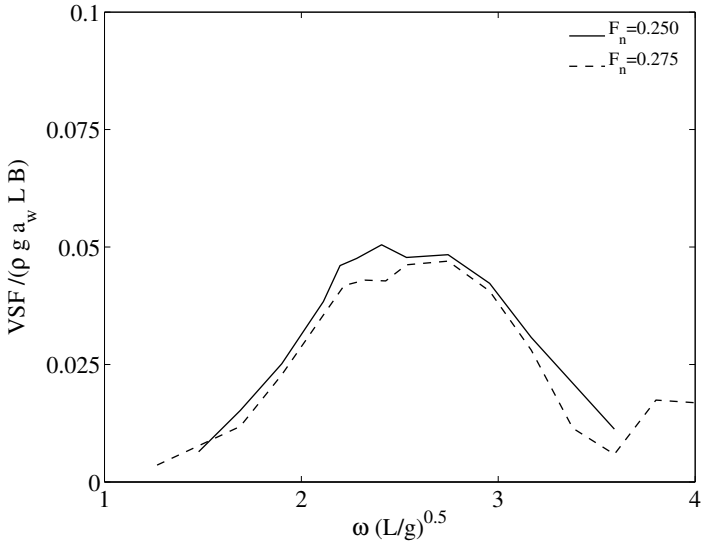

Figure 4.21: S-175, non dimensional vertical shear force at station 15 in head sea for different Froude numbers for $H_w/\lambda = 1/120$.

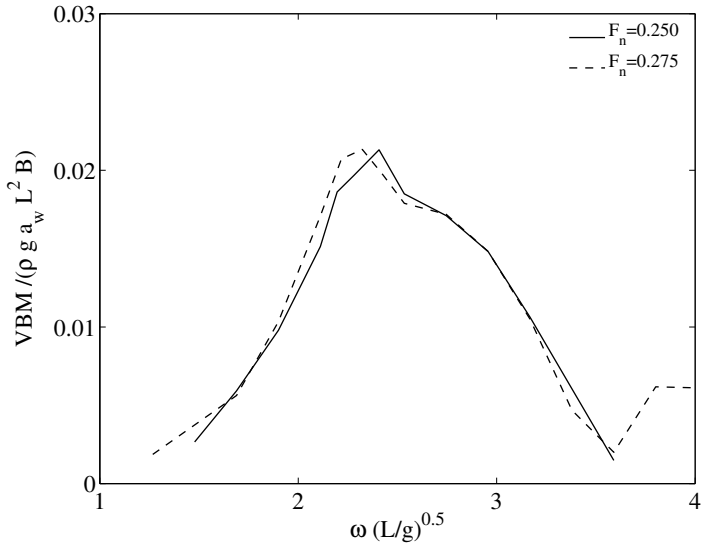

Figure 4.22: S-175, non dimensional vertical bending moment at station 10 in head sea for different Froude numbers for $H_w/\lambda = 1/120$.

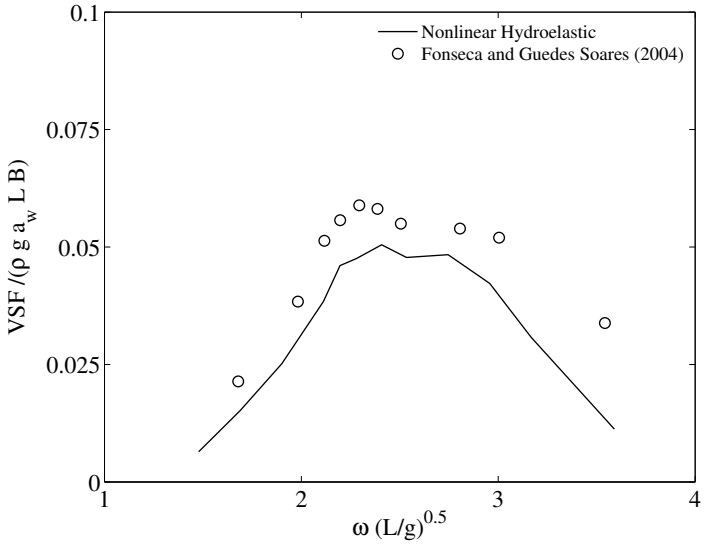

Figure 4.23: Comparison for the non dimensional vertical shear force at station 15 for the S-175, in head sea at $F_n = 0.25$ and $H_w/\lambda = 1/120$, against experimental points (Fonseca and Guedes Soares, 2004).

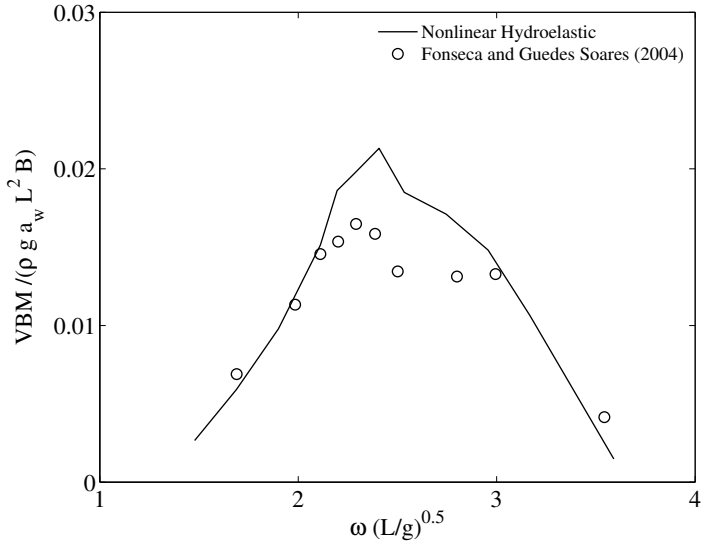

Figure 4.24: Comparison for the non dimensional vertical bending moment at station 10 for the S-175, in head sea at $F_n = 0.25$ and $H_w/\lambda = 1/120$, against experimental points (Fonseca and Guedes Soares, 2004).

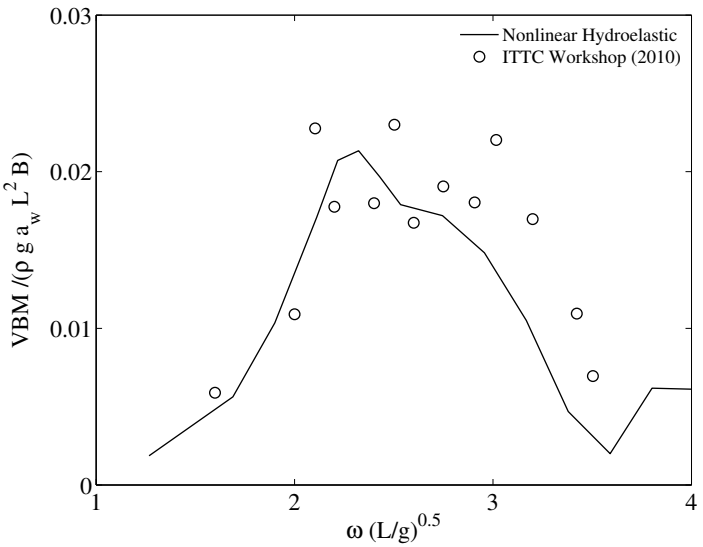

Figure 4.25: Comparison for the non dimensional vertical bending moment at station 10 for the S-175, in head sea at $F_n = 0.275$ and $H_w/\lambda = 1/120$, against experimental points (ITTC workshop, 2010).

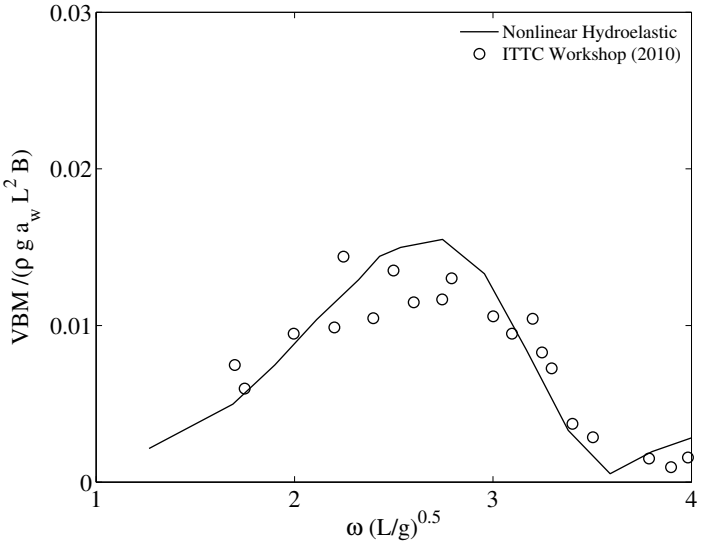

Figure 4.26: Comparison for the non dimensional vertical bending moment at station 10 for the S-175, in stern sea at $F_n = 0.275$ and $H_w/\lambda = 1/120$, against experimental points (ITTC workshop, 2010).

Figures 4.27 and 4.28 show a comparison for the vertical shear force at station 5 ($L_{BP}/4$ from AP) and the vertical bending moment at station 10 between the proposed methodology and the linear frequency domain numerical techniques (VERES and PRECAL) at Froude number $F_n = 0.275$ in head sea condition. For small amplitude waves, the load responses predicted by the nonlinear hydroelastic strip-theory are in good agreement with results from the frequency domain strip theory. Results from the three-dimensional free-surface Green's function methods predict the maximum values for vertical shear force and bending moment at slightly higher frequencies, resulting in a shift of the response in the low frequencies region ($\omega(L/g)^{0.5} \leq 2.5$), while the responses in the high frequencies region ($\omega(L/g)^{0.5} \geq 2.5$) are similar for all three methodologies.

Comparison between the previously described numerical methods and experimental results from ITTC (2010), for the vertical bending moment at midship (station 10) are presented in Figure 4.29, in head sea condition, for Froude number $F_n = 0.275$. The proposed nonlinear technique and the frequency domain strip-theory gives a good prediction of the maximum of the response in terms of value and location within the frequency range. All the numerical techniques are not able to predict properly the second peak in the experimental points and underestimate the response in the high frequency region. This phenomena could be due to the uncertainties in the longitudinal distribution of mass and structural properties for the model used in the experimental campaign.

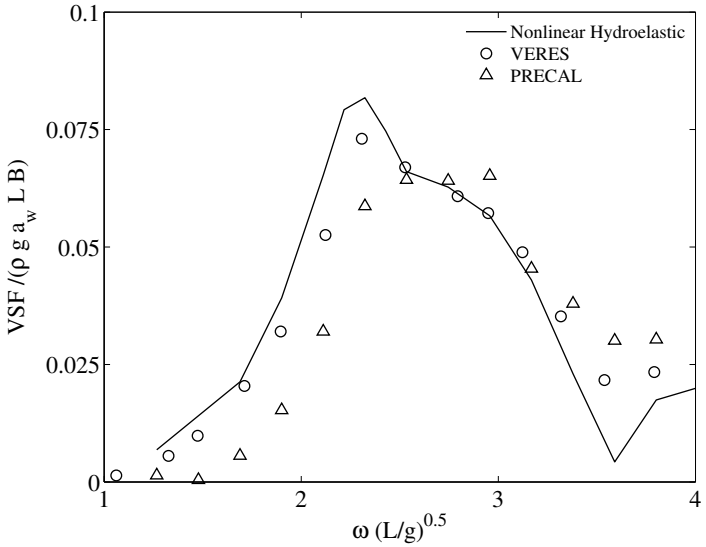

Figure 4.27: Comparison for the non dimensional vertical shear force at station 5 for the S-175, in head sea at $F_n = 0.275$, between the proposed nonlinear hydroelastic method, a frequency domain strip-theory (VERES) and a three-dimensional free-surface Green's function approach (PRECAL).

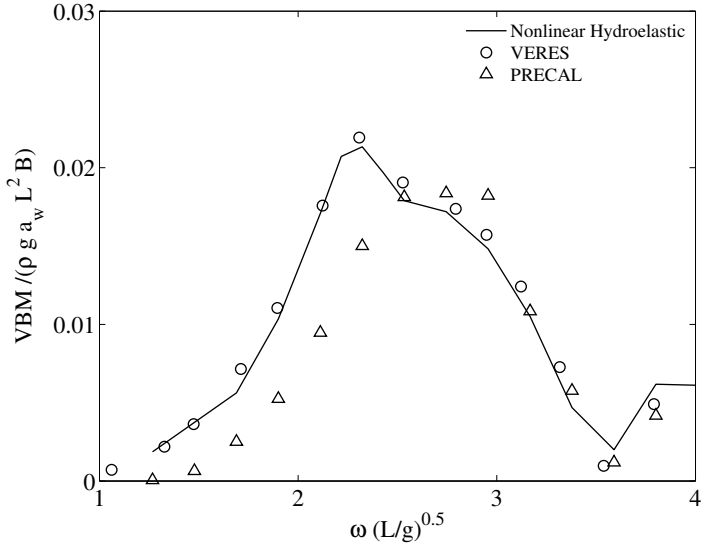

Figure 4.28: Comparison for the non dimensional vertical bending moment at station 10 for the S-175, in head sea at $F_n = 0.275$, between the proposed nonlinear hydroelastic method, a frequency domain strip-theory (VERES) and a three-dimensional free-surface Green's function approach (PRECAL).

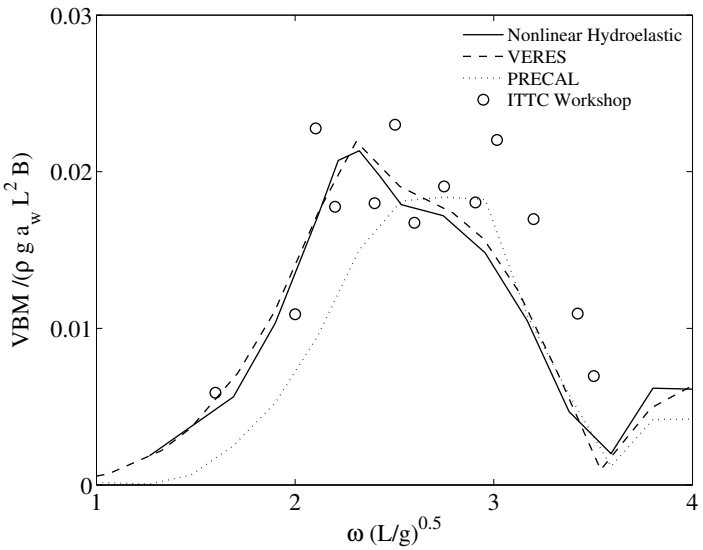

Figure 4.29: Comparison for the non dimensional vertical bending moment at station 10 for the S-175, in head sea at $F_n = 0.275$, between the proposed nonlinear hydroelastic method, a frequency domain strip-theory (VERES) and a three-dimensional free-surface Green's function approach (PRECAL) and experimental points (ITTC, 2010).

In the previous analysis the vertical motions and loads predicted by the proposed nonlinear hydroelastic method have been compared against results from experimental trials and other numerical techniques for small amplitude waves. In the following pages, the responses of the S-175 container ship are reported for different wave steepness with the intention to study the effectiveness of the nonlinear methodology when wave elevation rises.

Figures 4.30 and 4.31 show the heave and pitch motions as function of the wave steepness for different wave lengths: (a) $\lambda/L = 1.00$, (b) $\lambda/L = 1.20$, (c) $\lambda/L = 1.40$ in head sea at Froude number $F_n = 0.20$. Numerical results are compared against experimental points by O'Dea et al. (1992). Similar analysis for $F_n = 0.25$ and $F_n = 0.275$ are presented in Figures 4.32 and 4.33, for $F_n = 0.25$ and Figures 4.34 and 4.35, for $F_n = 0.275$. For the case when $F_n = 0.25$, numerical results are compared against experimental trial published by Fonseca and Guedes Soares (2004), while for $F_n = 0.275$ results by O'Dea et al. (1992) are used.

For all three forward speed heave motion for the shorter wave length ($\lambda/L = 1.00$) shows excellent agreement with experimental results, while for other cases it is slightly over predicted. For the cases when $\lambda/L = 1.20, 1.40$ numerical response is significantly larger than experimental points for small wave steepness. This is due to the resonance effect that are visible in the high peaks of Figure 4.9, where the numerical non dimensional heave response reaches sometimes the value of 1.5. The magnitude of the damping forces is important around resonance and in the current model only damping resulting form the wave radiation (ideal fluid) is considered. This effect is reduced when wave elevation rises due to the nonlinear formulation of the fluid actions.

Pitch motions predicted by the numerical technique shows excellent agreement with experimental points, for all the wave steepness, since it is less affected by non-linear behaviour. For both heave and pitch the reduction of the non dimensional response when the wave steepness increases is in agreement with the experimental points. The behaviour of the responses as function of the wave steepness is important and, it can be used to represent the ratio between the linear and the nonlinear predictions.

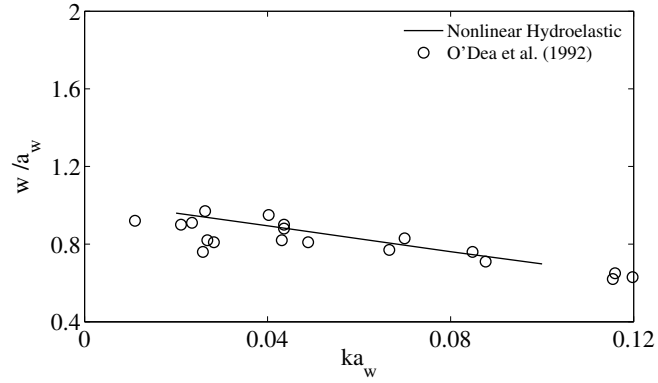

(a) $\lambda/L = 1.00$

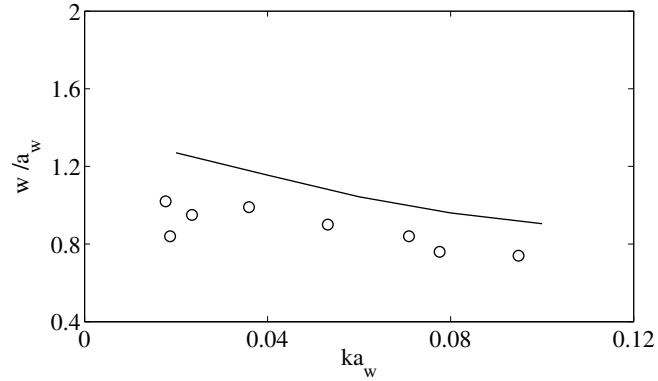

(b) $\lambda/L = 1.20$

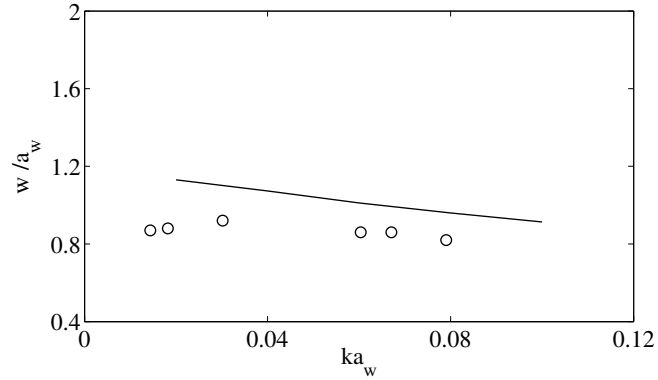

(c) $\lambda/L = 1.40$

Figure 4.30: Comparison between calculated and experimental (O'Dea et al., 1992) heave amplitude respect wave steepness for the S-175 container ship, in head sea at $F_n = 0.20$.

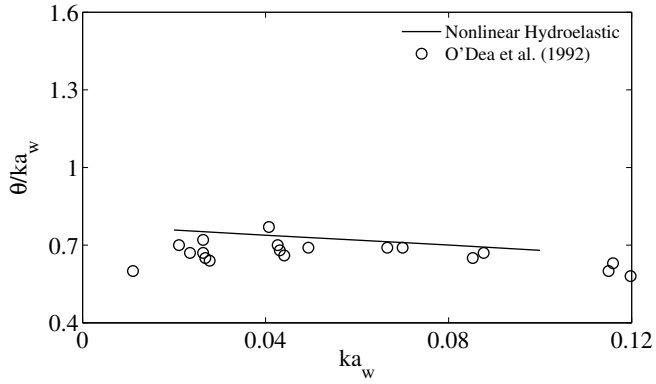

(a) $\lambda/L = 1.00$

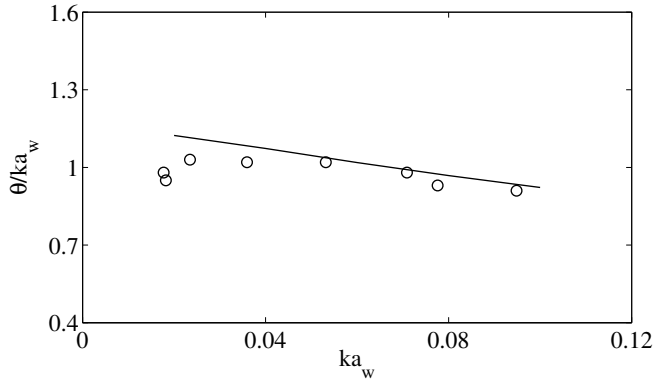

(b) $\lambda/L = 1.20$

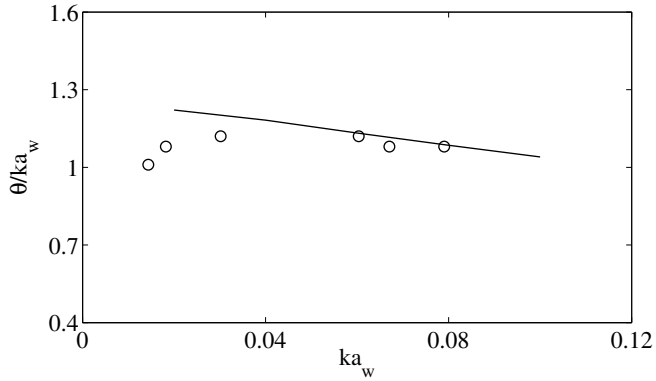

(c) $\lambda/L = 1.40$

Figure 4.31: Comparison between calculated and experimental (O'Dea et al., 1992) pitch amplitude respect wave steepness for the S-175 container ship, in head sea at $F_n = 0.20$.

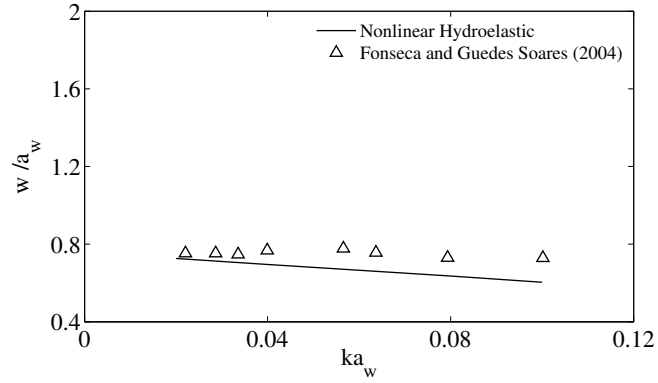

(a) $\lambda/L = 1.00$

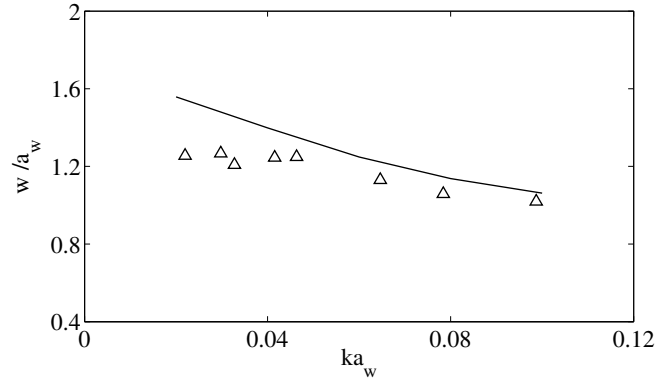

(b) $\lambda/L = 1.20$

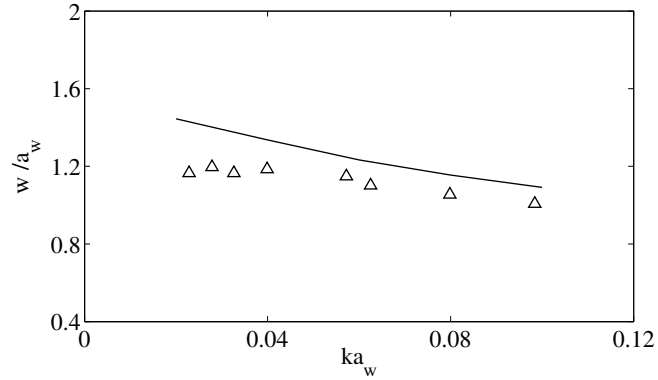

(c) $\lambda/L = 1.40$

Figure 4.32: Comparison between calculated and experimental (Fonseca and Guedes Soares, 2004) heave amplitude respect wave steepness for the S-175 container ship, in head sea at $F_n = 0.25$.

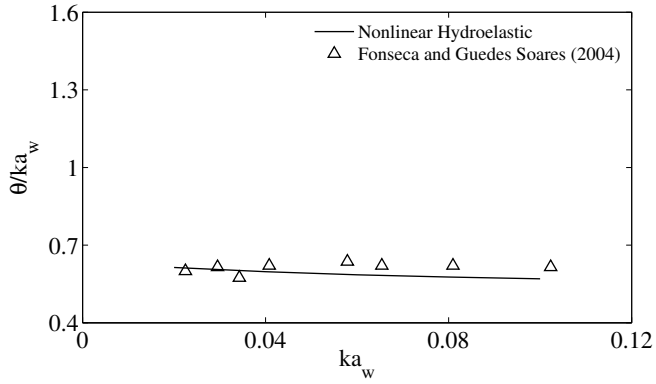

(a) $\lambda/L = 1.00$

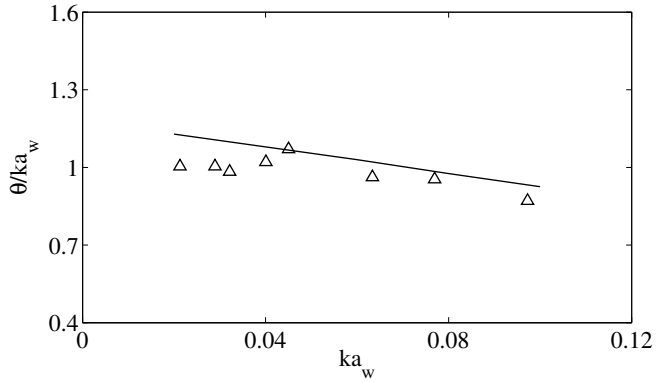

(b) $\lambda/L = 1.20$

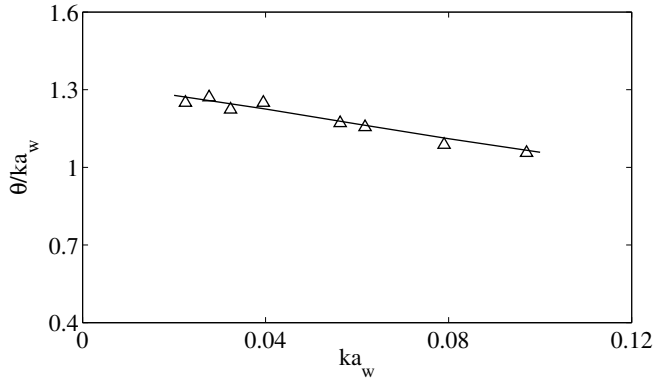

(c) $\lambda/L = 1.40$

Figure 4.33: Comparison between calculated and experimental (Fonseca and Guedes Soares, 2004) pitch amplitude respect wave steepness for the S-175 container ship, in head sea at $F_n = 0.25$.

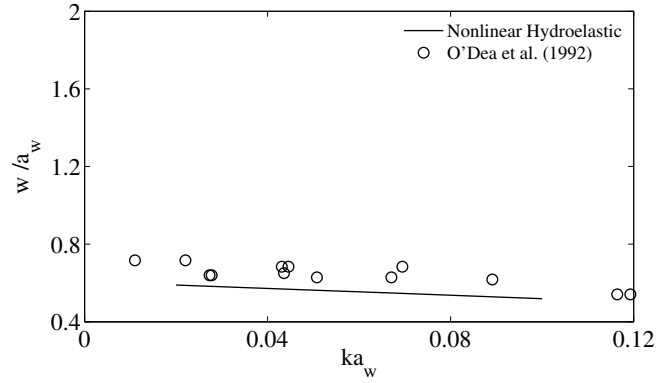

(a) $\lambda/L = 1.00$

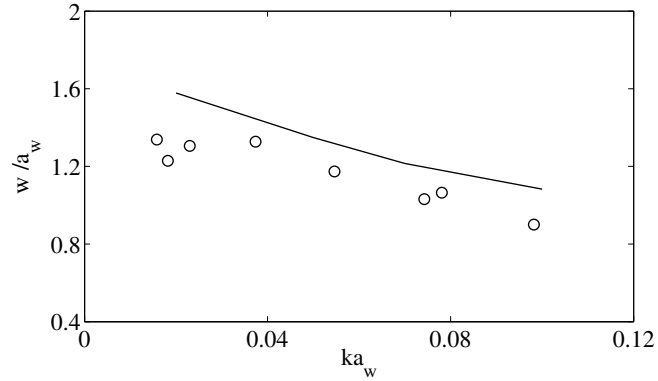

(b) $\lambda/L = 1.20$

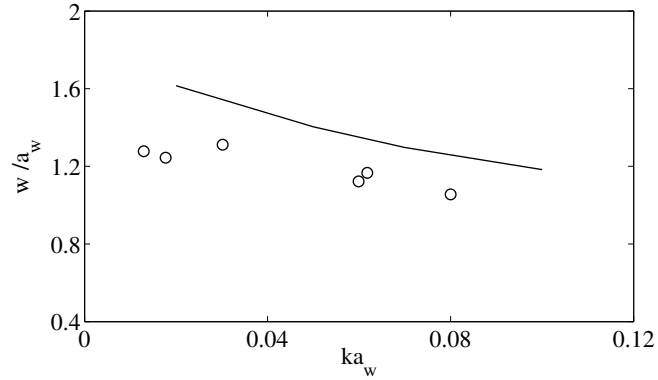

(c) $\lambda/L = 1.40$

Figure 4.34: Comparison between calculated and experimental (O'Dea et al. 1993) heave amplitude respect wave steepness for the S-175 container ship, in head sea at $F_n = 0.275$.

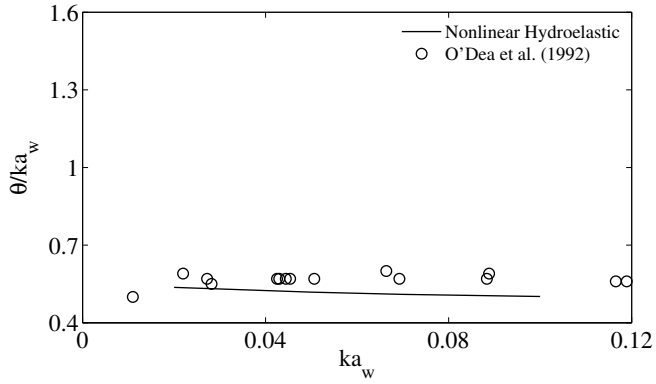

(a) $\lambda/L = 1.00$

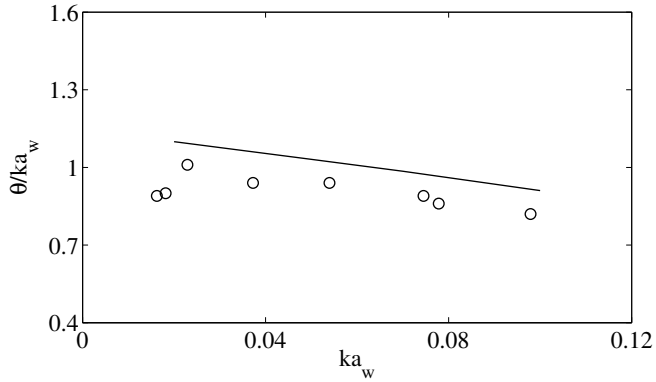

(b) $\lambda/L = 1.20$

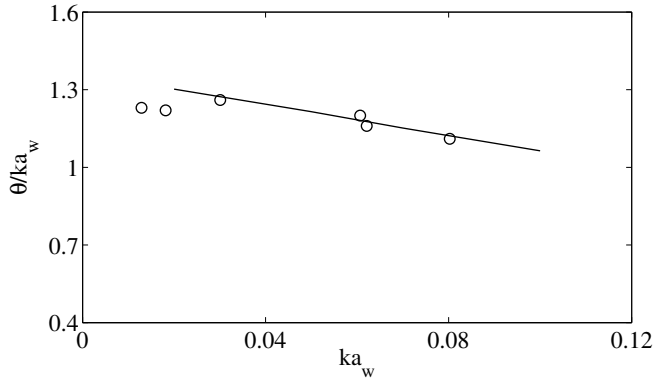

(c) $\lambda/L = 1.40$

Figure 4.35: Comparison between calculated and experimental (O'Dea et al. 1993) pitch amplitude respect wave steepness for the S-175 container ship, in head sea at $F_n = 0.275$.

Figure 4.36 shows a comparison between numerical and experimental points (Fonseca and Guedes Soares, 2004) for vertical shear force at station 15 in head sea for Froude number $F_n = 0.25$. Similar comparison is presented in Figure 4.37 for the vertical bending moment at station 10 also in head sea for Froude number $F_n = 0.25$.

The numerical positive, negative amplitudes and mean loads values are compared against experimental points. Vertical shear force and bending moments are in good agreement for the shorter waves $\lambda/L = 1.00$ for both positive and negative amplitudes. When wave length increases ($\lambda/L = 1.20, 1.40$), numerical positive peaks, of vertical shear force and bending moment, are sensibly larger than the experimental points for the highest values of wave steepness. For smaller values of ka_w they agree well with experimental points.

The experimental positive peaks show a reduction of non dimensional response for the larger values of wave steepness, changing the behaviour that they present at smaller waves. On the other hand numerical results in large amplitude waves are affected by hydroelasticity that causes vibrations of the hull girder. These increase the magnitude of the response, especially for positive values of vertical bending moment (sagging).

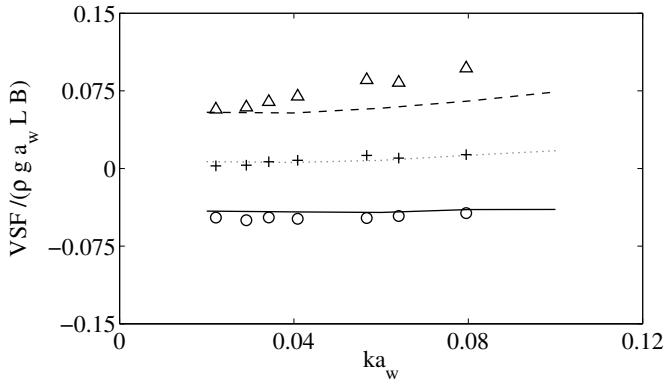

(a) $\lambda/L = 1.00$

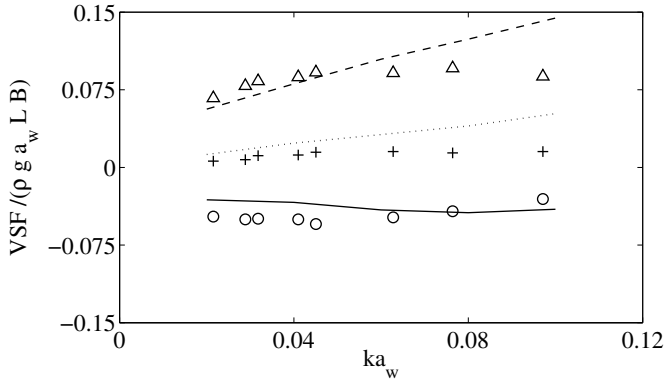

(b) $\lambda/L = 1.20$

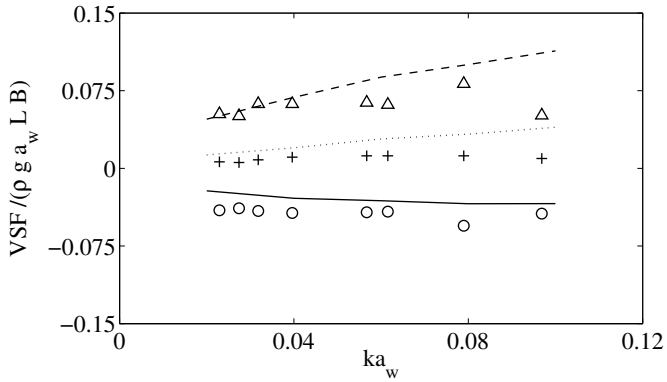

(c) $\lambda/L = 1.40$

Figure 4.36: Comparison between calculated and experimental (Fonseca, 2004) vertical shear force amplitude at station 15 respect wave steepness for the S-175 container ship, in head sea at $F_n = 0.25$. Numerical positive peaks (———), numerical negative peaks (– – –), numerical mean (·····); experimental positive peaks (△), experimental negative peaks (○) and experimental mean (+).

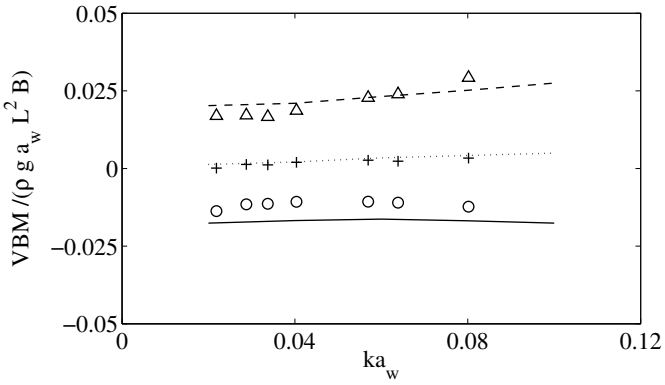

(a) $\lambda/L = 1.00$

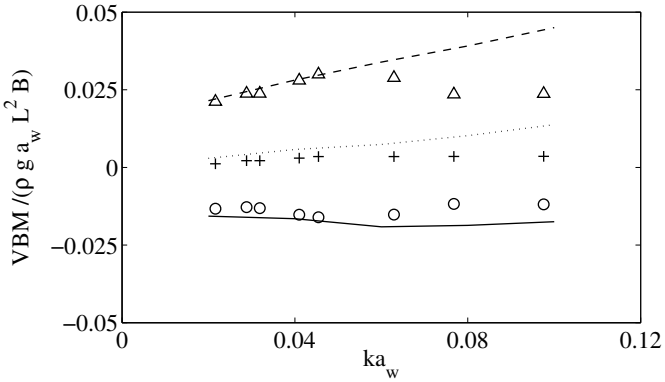

(b) $\lambda/L = 1.20$

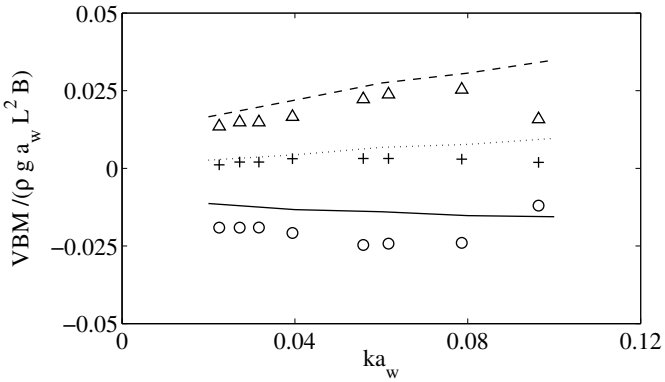

(c) $\lambda/L = 1.40$

Figure 4.37: Comparison between calculated and experimental (Fonseca, 2004) vertical bending moment amplitude at station 10 respect wave steepness for the S-175 container ship, in head sea at $F_n = 0.25$. Numerical positive peaks (——), numerical negative peaks (– – –), numerical mean (·····); experimental positive peaks (△), experimental negative peaks (○) and experimental mean (+).

Figure 4.38 shows pitch motion in head sea at Froude number $F_n = 0.25$ for waves amplitude $a_w = L_{BP}/60$. Predicted motions are compared with experimental points published by Watanabe et al. (1989), displaying good agreement between numerical and experimental points.

Figure 4.39 shows the longitudinal distribution of vertical bending moment in head sea at $F_n = 0.25$,$\lambda/L = 1.20$ and $a_w = L/60$. Numerical results are compared against experimental points by Watanabe et al. (1989). Sagging values present good agreement with experimental results for both magnitude and longitudinal distribution, while hogging results to be over predicted in terms of magnitude, but displays the same longitudinal location of peak of the experimental points.

Comparisons for the vertical bending moment at different sections are presented in Figures 4.40 and 4.41. The stations of the analysis are: (a) 6, (b) 10 and (c) 15. Comparisons are conducted for the same conditions of Figure 4.38. Figure 4.40 shows the results for the 1^{st} harmonic and Figure 4.41 for the 2^{nd} one. Comparisons show good agreement, also for the 2^{nd} harmonic, except for the second peak for the 1^{st} harmonic at station 6 (Figure 4.40a), that is not visible in the numerical results, while it clearly appears in the experimental points.

Watanabe's experimental trials are conducted at constant wave amplitude ($a_w = L_{BP}/60$), while O'Dea and Fonseca presented results considering constant wave steepness ($H_w/\lambda = 1/120$, for example). This implies that nonlinear effects are more relevant for shorter waves than long ones.

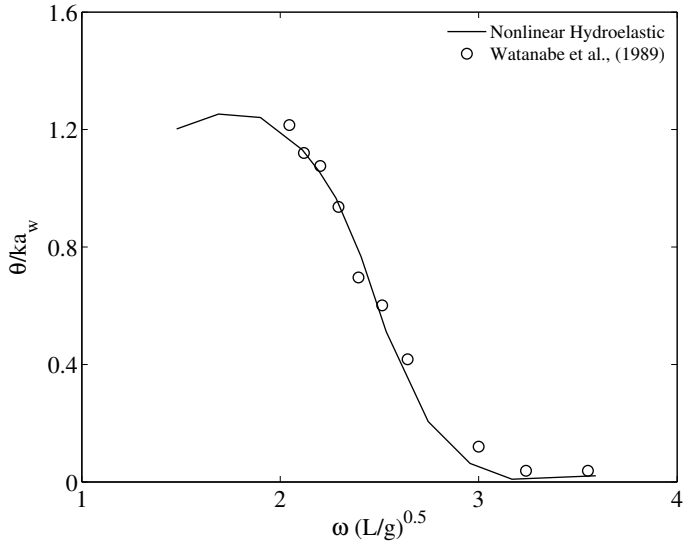

Figure 4.38: Comparison between numerical and experimental (Watanabe et al., 1989) pitch amplitude for the S-175 container ship, in head sea at $F_{=}0.25$ and $a_w/L = 1/60$.

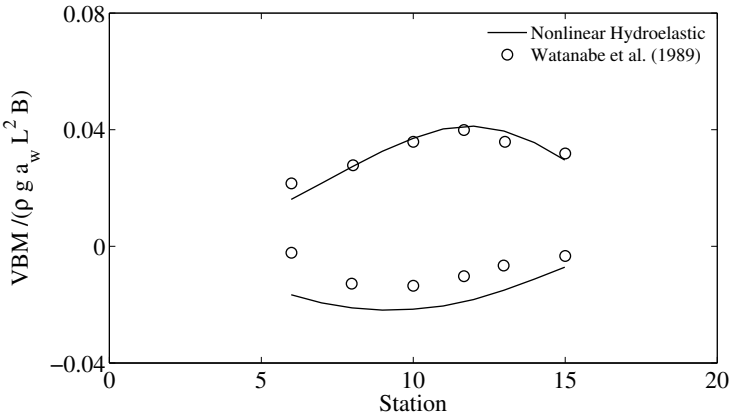

Figure 4.39: Comparison between numerical and experimental (Watanabe et al., 1989) longitudinal distribution of the vertical bending moment for the S-175 container ship, in head sea at $F_{=}0.25$ and $\lambda/L = 1.20$ $a_w/L = 1/60$.

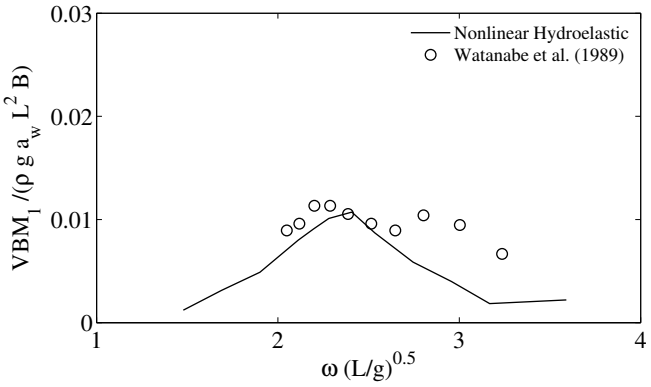

(a) Station 6

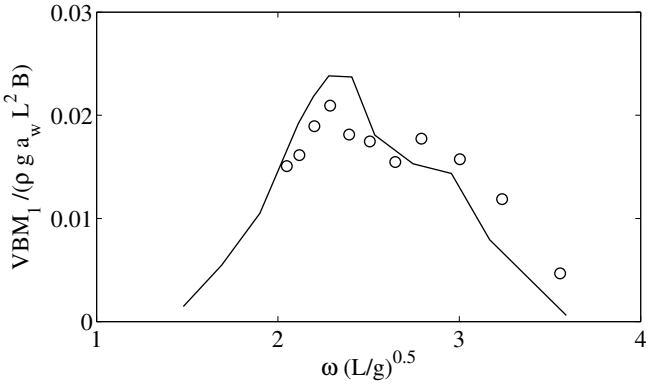

(b) Station 10

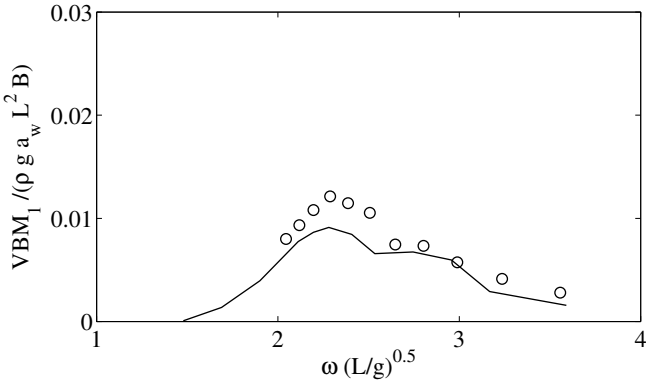

(c) Station 15

Figure 4.40: Comparison between numerical and experimental (Watanabe et al., 1989) 1^{st} harmonic of vertical bending moment for the S-175 container ship, in head sea at $F_{=}0.25$ and $a_w/L = 1/60$.

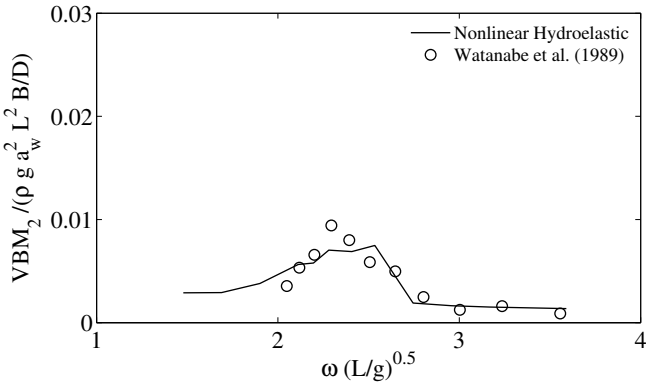

(a) Station 6

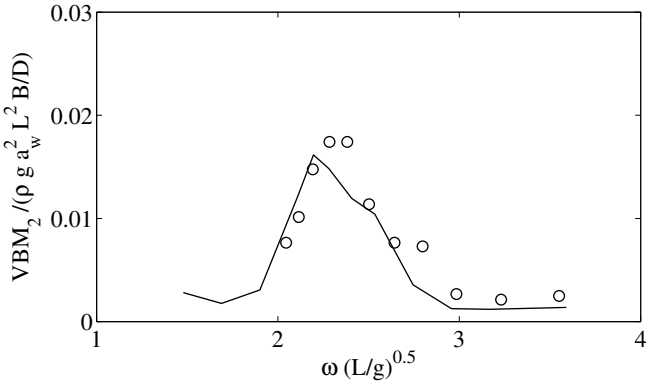

(b) Station 10

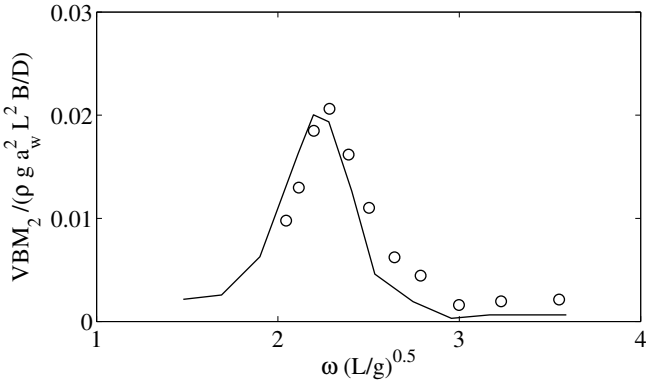

(c) Station 15

Figure 4.41: Comparison between numerical and experimental (Watanabe et al., 1989) 2^{nd} harmonic of vertical bending moment for the S-175 container ship, in head sea at $F_{=}0.25$ and $a_w/L = 1/60$.

Figure 4.42 reports the time history of the heave motion in head sea condition at $F_n = 0.20$, $\lambda/L = 1.20$ for different wave steepnesses ($H_w/L = 1/120$, $1/60$ and $1/30$). The comparison of heave elevation for different wave amplitude (considering the same wave length) shows that the principal nonlinear effects are associated with the reduction of response from the linear prediction. This effect can also be observed in Figure 4.43, that describes the Fourier transform of the time histories of the heave response of Figure 4.42. From an analysis of the frequency components of the heave response it is possible to state that the effect of an increment of the wave steepness is a reduction of the $1st$ harmonic of the heave response. The pitch motion, reported in figures 4.44 and 4.45, presents behaviour similar to the heave one and in this case the reduction of the 1^{st} harmonic of the response is less significant.

A similar analysis is conducted for the vertical bending moment at stations 10 and 15 at the same environmental conditions. Figures 4.46 and 4.47 show results for station 10, while Figures 4.48 and 4.49 describe the analysis at station 15. Time histories of the wave induced loads show a behaviour that is different from the one of the motions. In large amplitude waves, load responses are characterised by multi harmonic shape; this is clearly visible from the Fourier analysis of the loads, displayed in Figures 4.47 and 4.49 for vertical bending moment at station 10 and 15 respectively. When the wave elevation rises the amplitude of the a^{st} harmonic of the response increases from the linear prediction and higher harmonics components appears.

Rigid body motions and wave induced loads have different characteristics in large amplitude waves. For large wave elevations, the amplitude of the motions is reduced compared to the linear prediction, but they preserve an almost simple harmonic shape (in terms of time history). Loads on the other-hand present an increase of the 1^{st} harmonic components, compared to linear predictions and they

are characterised by multi harmonic responses. These difference could be due to the fact that, in an hydroelastic approach, heave and pitch are associated with the first two principal coordinates, and wave induced loads are functions and combinations of all the flexural principal coordinates (Bishop and Price, 1979).

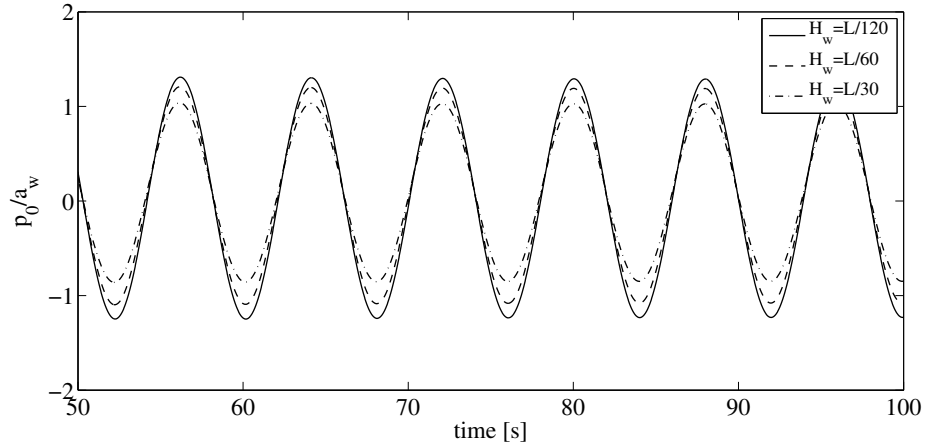

Figure 4.42: Time history of heave motion for the S-175 container ship, in head sea at $F_n = 0.20$, $\lambda/L = 1.20$ and for different wave steepnesses.

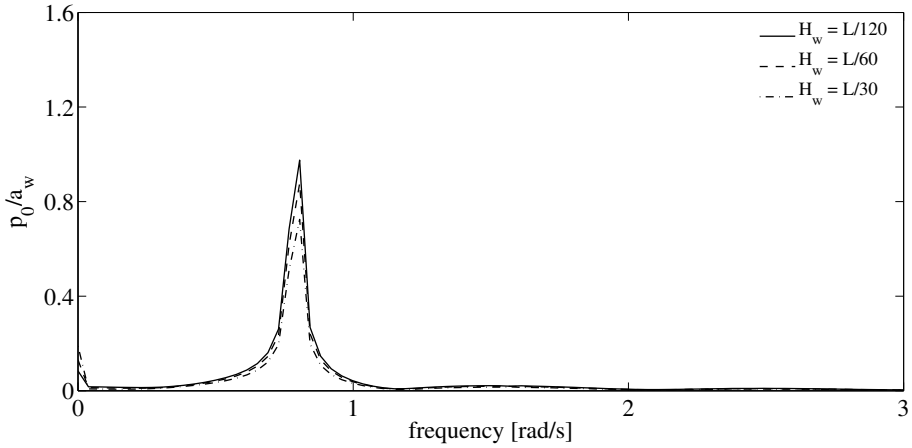

Figure 4.43: Amplitude of the Fourier transform for the heave response of the S-175 container ship in head sea at $F_n = 0.20$, $\lambda/L = 1.20$ and for different wave steepnesses.

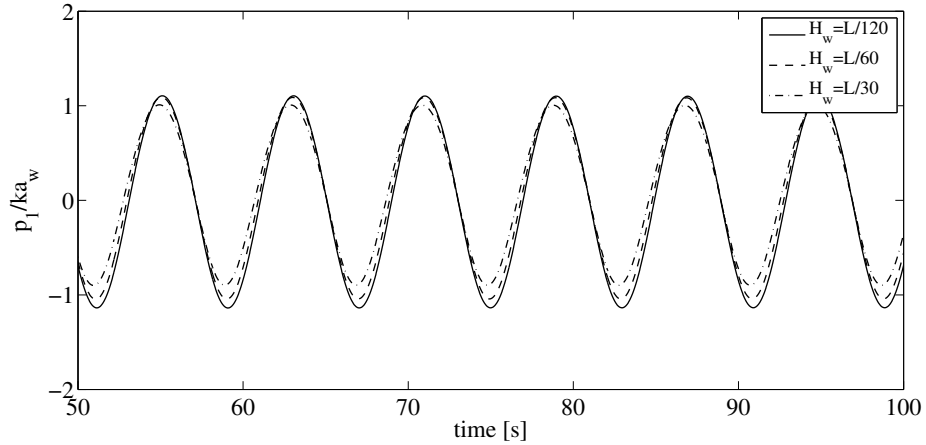

Figure 4.44: Time history of pitch motion for the S-175 container ship, in head sea at $F_n = 0.20$ and $\lambda/L = 1.20$ and for different wave steepnesses.

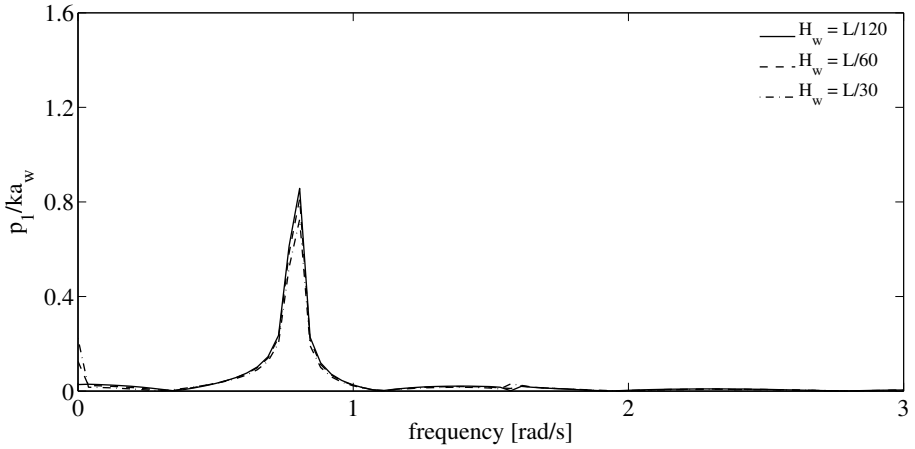

Figure 4.45: Amplitude of the Fourier transform for the pitch response for the S-175 container ship in head sea at $F_n = 0.20$, $\lambda/L = 1.20$ and for different wave steepnesses.

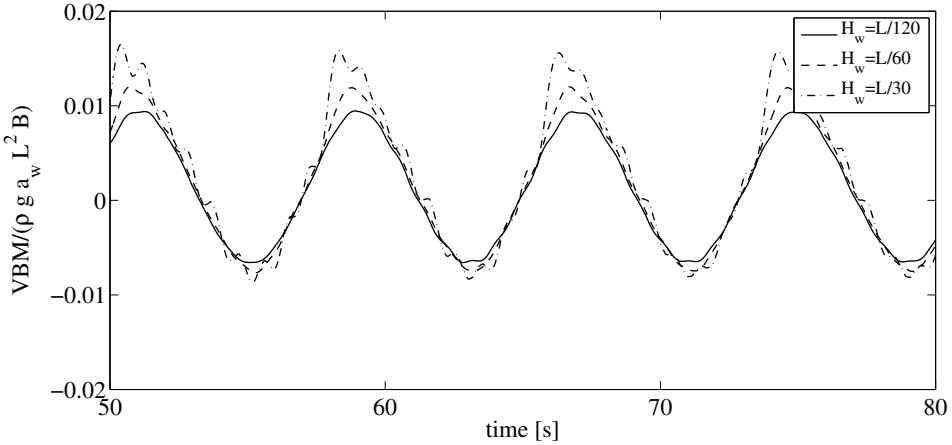

Figure 4.46: Time history of the vertical bending moment at station 10 for the S-175 container ship, in head sea at $F_n = 0.20$ and $\lambda/L = 1.20$ and for different wave steepnesses.

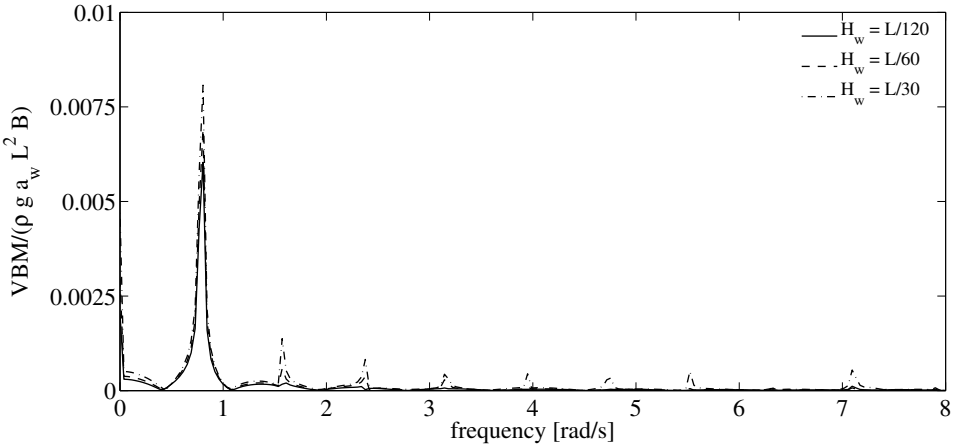

Figure 4.47: Amplitude of the Fourier transform for the vertical bending moment at station 10 for the S-175 container ship in head sea at $F_n = 0.20$, $\lambda/L = 1.20$ and for different wave steepnesses.

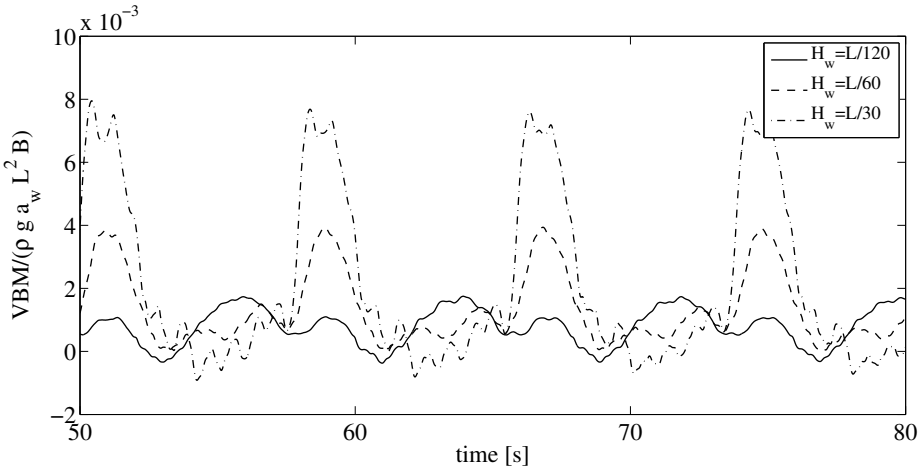

Figure 4.48: Time history of the vertical bending moment at station 15 for the S-175 container ship, in head sea at $F_n = 0.20$ and $\lambda/L = 1.20$ and for different wave steepnesses.

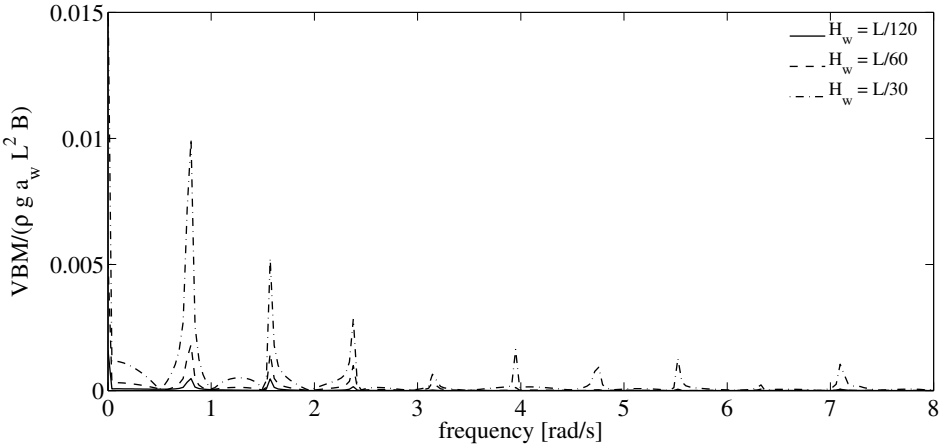

Figure 4.49: Amplitude of the Fourier transform for the vertical bending moment at station 15 for the S-175 container ship in head sea at $F_n = 0.20$, $\lambda/L = 1.20$ and for different wave steepnesses.

The longitudinal distribution of vertical bending moment for different wave steepness is shown in Figure 4.50. The non-dimensional sagging bending moment (positive) increases for larger wave steepnesses and the peak shifts forward. The hogging bending moment displays a small increment in term of values, but the absolute maximum of the response remains at the same longitudinal position for all the wave conditions.

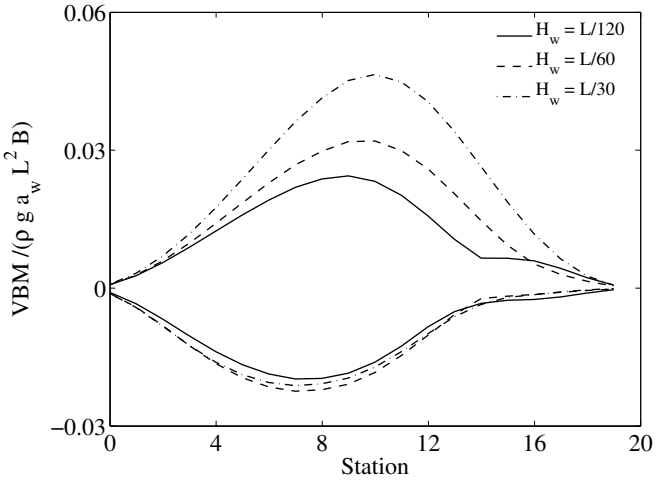

Figure 4.50: Longitudinal distribution of the amplitudes of the vertical bending moment for the S-175 container ship in head sea at $F_n = 0.20$, $\lambda/L = 1.20$ and for different wave steepnesses.

From a comparison of vertical bending moment at different stations, reported in Figures 4.46 and 4.48, it is possible to notice that the time histories present different shapes. The bending moment at station 10 is characterised by a strong 1^{st} harmonic with disturbances associated with both geometrical nonlinearities (asymmetric response) and with structural dynamic (rapid fluctuation). The bending moment at station 15 presents a strong multi-harmonic behaviour with strong vibration due to the hydroelastic modelling.

In order to understand these phenomena it is important to study the effect of the different mode of shapes on the loads. Figure 4.51 shows the time histories of the first four flexural principal coordinates ($r = 2, \ldots, 5$) in head sea for $F_n = 0.20$, $\lambda/L = 1.20$ and $H_w/L = 1/30$.

Figure 4.52 shows the vertical bending moment as station 10, considering the contributions of the different principal coordinates. From an observation of the time history, it is visible that the vertical bending moment at station 10 is mainly function of the first flexural mode of shape (two nodes, $r = 2$). This is even more visible in Figure 4.53, where a detail of a positive peak of the time history of the

vertical bending moment is reported. Only the first and the third flexural modes affect the vertical bending moment at station 10, while the second and the fourth modes do not modify the response.

A similar analysis for the vertical bending moment at station 15 is presented in Figure 4.54. In this case the first and the second mode of shapes are the larger contributors. The second mode (three nodes) affects more significantly the hogging response, where it significantly reduces the amplitude of the response.

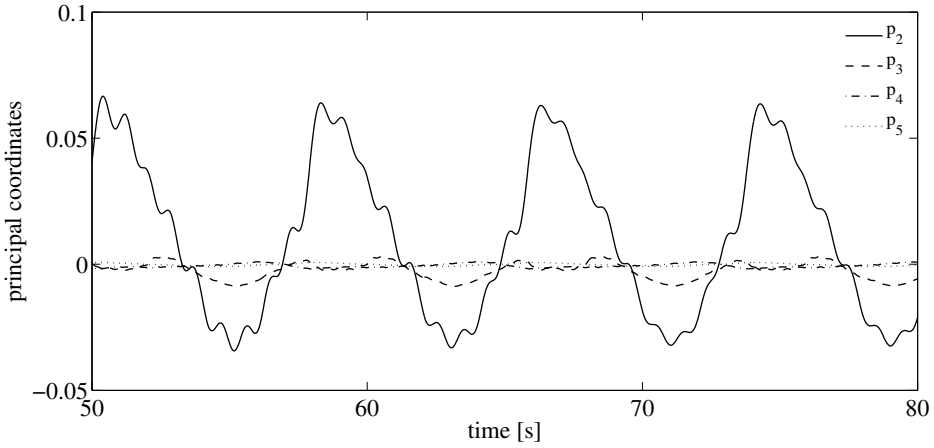

Figure 4.51: Time histories of the flexural principal coordinates for the S-175 container ship in head sea at $F_n = 0.20$, $\lambda/L = 1.20$ and $H_w/L = 1/30$.

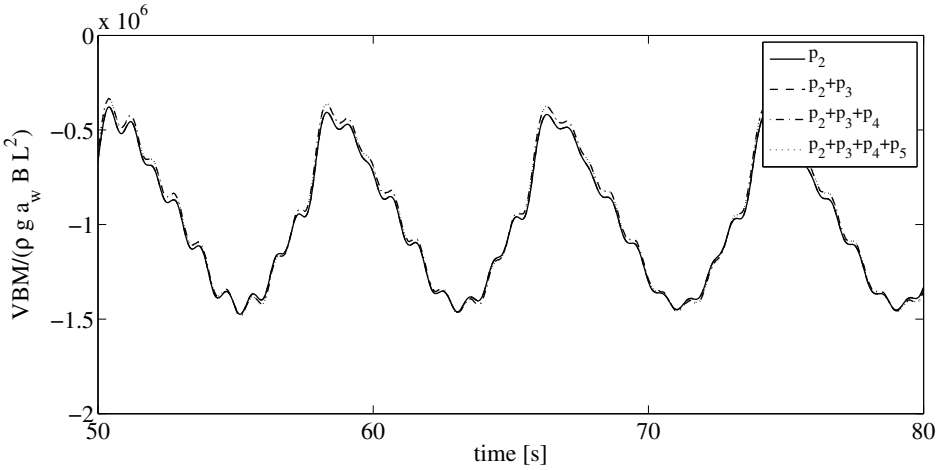

Figure 4.52: Time history of the vertical bending moment at station 10 as combination of its different mode of shapes for the S-175 container ship in head sea at $F_n = 0.20$, $\lambda/L = 1.20$ and $H_w/L = 1/30$.

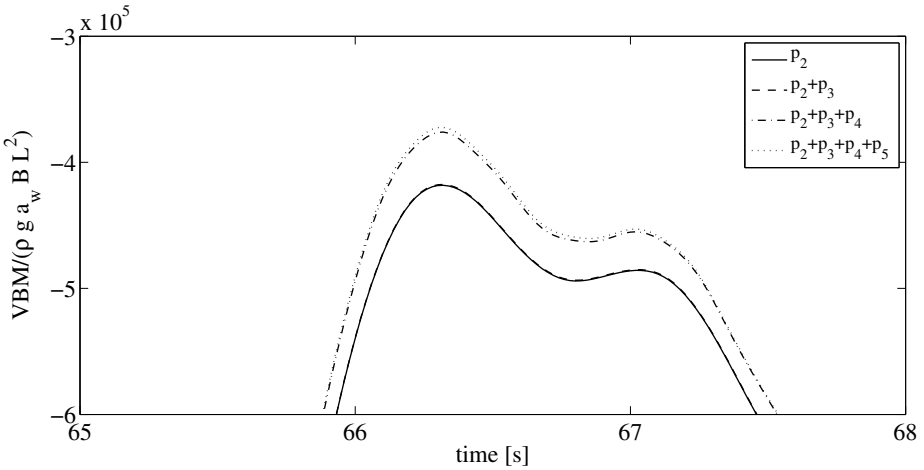

Figure 4.53: Detail of one positive peak of the time history of the vertical bending moment at station 10 as combination of its different mode of shapes for the S-175 container ship. In head sea at $F_n = 0.20$, $\lambda/L = 1.20$ and $H_w/L = 1/30$.

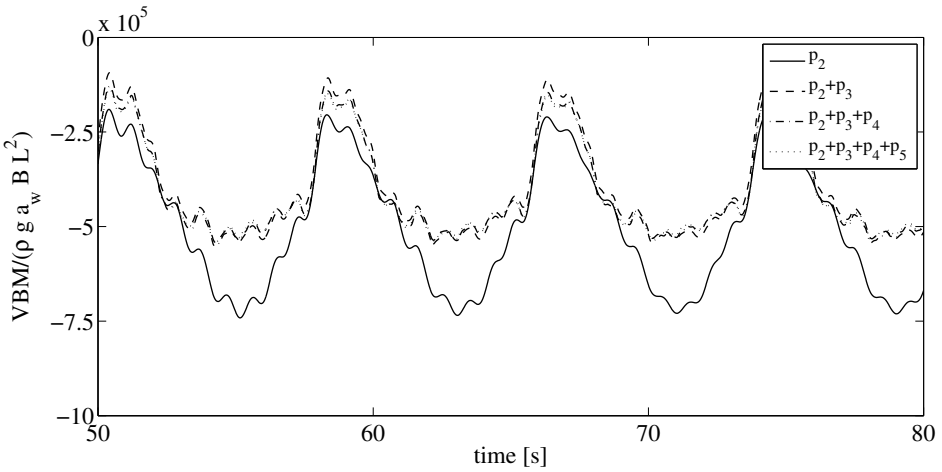

Figure 4.54: Time history of the vertical bending moment at station 15 as combination of its different mode of shapes for the S-175 container ship in head sea at $F_n = 0.20$, $\lambda/L = 1.20$ and $H_w/L = 1/30$.

Figure 4.55 describes the time histories of the sectional impulsive force at station 17 in head sea for a Froude number $F_n = 0.20$, at $\lambda/L = 1.20$ for different wave amplitudes. For the two smaller waves ($H_w = L/60$ and $H_w = L/30$) the impulsive force is governed by bow flare slamming. For $H_w = L/30$ water entry events occur, but the magnitude of the relative vertical velocity is not large enough to produce any significant bottom impact force. For the larger waves ($H_w = L/20$) relative vertical velocity allows significant bottom impact force.

This is visible in Figure 4.55, where the first steep peak is due to bottom impact.

For Froude number $F_n = 0.20$ the maximum value of sectional impulsive force is due to bow flare slamming. Figure 4.56 shows the time history of the section impulsive force at station 17, in head sea at $\lambda/L = 1.20$ and $H_w = L/30$ for different Froude numbers ($F_n = 0.20$ and 0.25). From this comparison it is possible to assess the effect of forward speed on slamming. A small increment of forward speed results in a small increment of maximum sectional force due to bow flare slamming, but corresponds to a large increment of force related to bottom impact phenomena. For this reason, while for $F_n = 0.20$ the maximum force is obtained when the flare enters the water, for $F_n = 0.25$ the maximum values are obtained when the bottom of the hull hits the free-surface.

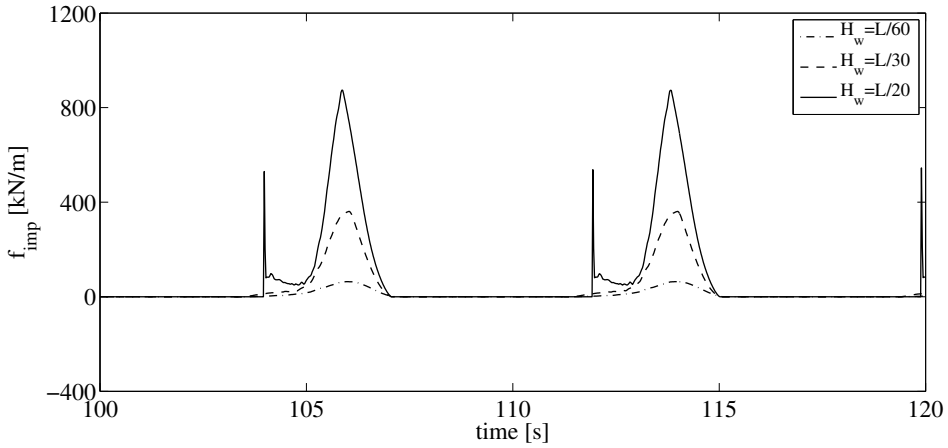

Figure 4.55: Time history of the sectional impulsive force at station 17 for different wave steepness for the S-175 container ship. In head sea at $F_n = 0.20$, $\lambda/L = 1.20$.

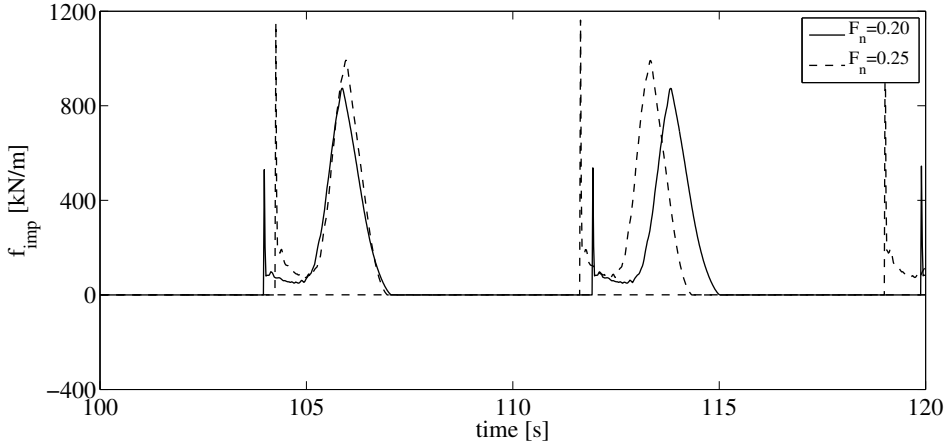

Figure 4.56: Time history of the sectional impulsive force at station 17 at $F_n = 0.20$ and 0.25 for the S-175 container ship. In head sea at $H_w = L/30$ and $\lambda/L = 1.20$.

Figure 4.57 describes the time history of the vertical bending moment at station 10 for $F_n = 0.20$ in head sea at $H_w = L/30$ and $\lambda/L = 1.20$. For this simulation conditions slamming is severe and leads to large rapid vibration of the vertical bending moment response: whipping. From the amplitude of the Fourier transformation of the time trace, reported in Figure 4.58, it is possible to notice that these fluctuations occur at $\omega = 7.1 rads$. Thus the vibrations are associated with the two nodes mode of shape (p_2).

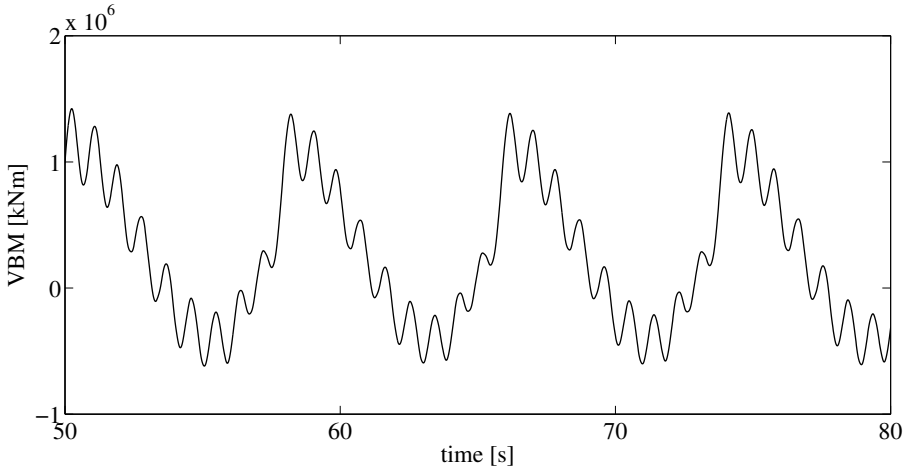

Figure 4.57: Time history of the vertical bending moment as station 10 for the S-175 container ship, in head sea at $F_n = 0.20$ and $\lambda/L = 1.20$ and $H_w = L/30$.

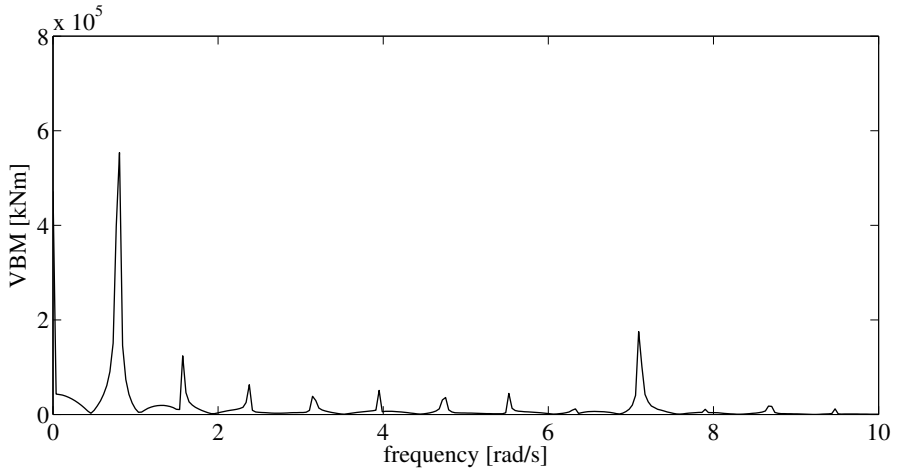

Figure 4.58: Amplitude of the Fourier transform for the vertical bending moment as station 10 for the S-175 container ship in head sea at $F_n = 0.20$, $\lambda/L = 1.20$ and $H_w = L/30$.

Longitudinal distributions of sectional impulsive force are presented in Figure 4.59. Simulations were conducted for $F_n = 0.20$ in head sea at $\lambda/L = 1.20$ for different wave amplitudes. The figure shows the effect of wave amplitude over the sectional impulsive force, and allows to identify the critical regions along the hull. As expected, slamming is more significant at the bow, where the relative motions are larger and the flare is significant. Significant contribution to the global impulsive force comes from the stern region. At the stern values of the sectional impulsive force are almost half of the one at the bow, but they still can contribute significantly to the force.

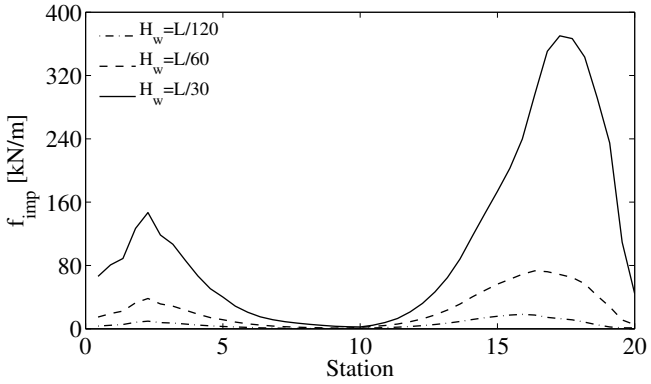

Figure 4.59: Longitudinal distribution of the maximum sectional impulsive force for different wave steepness for the S-175 container ship. In head sea at $F_n = 0.20$, $\lambda/L = 1.20$.

4.3 Concluding Remarks

In this chapter the proposed nonlinear hydroelastic approach is applied to the S-175 container ship sailing in regular waves. Wave induced motions and loads are compared against experimental points and the predictions from other numerical techniques, in both small and large amplitude waves.

In small amplitude waves, the motions and loads predicted by the nonlinear hydroelastic method show good agreement with experimental results, within the limits of the theory. Heave responses are usually over predicted around resonance; this is due to the lack of damping arising from the ideal fluid model. Empirical coefficients can be used to increase damping; this approach has not been used in this dissertation, since the effect of heave over prediction do not deteriorate the quality of the other variables. In fact, prediction for pitch and vertical shear force and bending moments present good agreement among the whole frequency range.

The proposed method is compared against a linear frequency domain strip-theory (VERES) and a linear frequency domain free-surface Green's function method.

All the three methodologies give comparable results, in particular results from the nonlinear strip theory tends to compare better with the prediction of VERES; since in small amplitude waves the formulation of the nonlinear hydroelastic approach is similar to the one used in the frequency domain strip-theory.

Comparison against experimental points for large amplitude waves displays the capability of the methodology to correctly predict the responses of the vessel. The heave over prediction, around resonance region, reduces when wave elevation rises, and the numerical values agree better with the experimental points.

The analysis of the loads at $F_n = 0.25$ is presented in Figures 4.36 and 4.37. It shows a good agreement for the negative peaks; positive responses compare generally well up to $ka_w = 0.05$, after that wave steepness the experimental points change their trend, while the numerical prediction do not show any change of behaviour. Sagging responses (positive peaks) are influenced by whipping in large amplitude waves. The experimental setup used by Fonseca and Guedes Soares (2004) consist of a wooden model in scale 1/40 composed by three segments. This type of model does not allow for vibrations due to slamming (Fonseca and Guedes Soares, 2004). Therefore the experimental values in large waves do not take into account whipping resulting in a smaller values of sagging responses. The discrepancy between the numerical values and the experiment could be due to the fact that hull vibrations were not allowed in the experimental trials, while they are considered into the numerical approach.

Figure 4.42 to 4.45 analyse heave and pitch for different wave amplitude. From the study of the time histories and their frequency components it is possible to observe that the nonlinear effects for rigid body motions is principally a reduction of the responses from their linear counterpart, this decrease is more pronounced for heave than in pitch.

Similar analysis is conduced for wave induced loads from Figure 4.46 to 4.49. In

this case the nonlinear responses are characterised by an increment from the linear prediction for the 1^{st} harmonic component and by a multi harmonic behaviour. The study reports also a different behaviour of the vertical bending moment at different sections. The previously described effects are more significant at the bow (station 15) compared to mid ship (station 10).

Differences between rigid body motions and loads can be justified by looking into the details of the fluid structure interaction problem. Heave and pitch are associated with the first two mode of shape ($r = 0, 1$) while vertical shear force and bending moments are evaluated as superposition of contribution among all the flexural mode shapes (Bishop and Price, 1979). From the magnitude of the forces involved the coupling between the flexural and the rigid modes into the equations of motion of heave and pitch is of small magnitude. Therefore flexural modes do not significantly affect rigid body motions.

Figures 4.52 and 4.54 show that the contribution of each mode shape to the total value of vertical bending moment is different at different sections. Vertical bending at station 10 is mainly function of the two and the four nodes mode shapes ($r = 2, 4$), while at station 15 the two and three nodes mode of shapes ($r = 2, 3$) give the larger contribution. This is associated with the shape of the principal vertical bending moments, visible in Figure 4.8. In fact, at station 10 the two node mode has its maximum, while at station 15 the maximum value correspond to the three nodes mode.

Analysis of the time histories of the sectional impulsive force at different station shows the effect of wave amplitude and forward speed. Maximum values of the momentum slamming (bow flare) force varies almost quadratically with the wave amplitude and the bottom impact forces are largely affected by forward speed.

The time history of vertical bending moment at station 10 and its Fourier transform of Figures 4.57 and 4.58 displays whipping effect associated with vibration

in the two nodes mode of shape. The frequency analysis shows that the frequency of vibration is around $7.1 rads$. The first dry natural frequency of the structure is equal to 9.268 (Table 4.2). The actual frequency of vibration is smaller due to the effect of fluid added mass and stiffness that are not considered in the dry analysis. For a linear system, natural frequencies for the wetted hull can be evaluated in an iterative procedure, but this cannot be done for a nonlinear model in which hydrodynamic coefficients change at each time step as function of the under water hull geometry.

Chapter 5

Application of the Methodology in a Seaway and Long Term Predictions

5.1 Introduction

In this chapter the proposed methodology is applied in irregular seas, focusing on the prediction of long term maximum expected values of wave induced loads. A procedure, used to extrapolate extremes from the time histories of the responses and to conduct the long term analysis, is described and applied to the S-175 and Wils II container ships.

Long term analyses are performed considering the entire wave scatter diagram and using the equivalent design sea state method. Maximum expected wave induced loads are calculated using different combinations of forward speeds and return periods, with the aim to understand the effect of these parameters over long term analysis via time domain nonlinear methods.

5.2 Irregular Sea Model

In a time domain analysis of the behaviour of the vessel in irregular seas, the ambient wave profile and its kinetics characteristics need to be defined everywhere in both time and space within the numerical domain. The time history of the sea elevation η for a long crested irregular sea is described as the superposition of a finite set of regular plane progressive waves. These are combined utilising a uniform distributed random phase angle ϵ_i as follow.

$$\eta(x, y; t) = \sum_i A_i(\omega_i) cos\big[k_i\big(x\cos\beta + y\sin\beta\big) - \omega_i t + \epsilon_i\big] \tag{5.1}$$

where A_i, ω_i and k_i are the amplitude, frequency and the wave number of the $i-th$ sinusoidal component. ϵ_i is the normal distributed phase angle of the $i-th$ regular wave.

From Equation 5.1 it is possible to define the wave profile and if the same formulation is applied to the definition of the velocity potential in Equation 3.29, it is possible to calculate excitation forces in irregular sea.

The amplitude A_i in Equation 5.1 is defined via spectral analysis, evaluating the wave spectrum at ω_i.

$$A_i(\omega_i) = \sqrt{2S(\omega_i)\Delta\omega_i} \tag{5.2}$$

where $S(\omega)$ is the wave spectrum and $\Delta\omega$ is the frequency step around ω. The wave spectrum, used in the present analysis, is defined following the ISSC formulation as function of the significant wave height H_s and the mean wave crossing period T_0.

$$\begin{aligned} S(\omega) =& \frac{A}{\omega^5}\exp\left[-\frac{B}{\omega^4}\right] \\ A =& 0.11 H_s^2 \left(\frac{2\pi}{T_0}\right)^4 \\ B =& 0.44 \left(\frac{2\pi}{T_0}\right)^4 \end{aligned} \tag{5.3}$$

5.3 Short Term Analysis From Nonlinear Seakeeping Method

Characteristics of the response of a vessel in a short term, when a linear seakeeping method is involved, are obtained via spectral analysis. In the case of a nonlinear time domain approach spectral techniques do not represent an advantage anymore. Statistical properties should be obtain by a direct study of the time histories of the responses.

One of the principal interests of this thesis is to understand the effect of nonlinearties over the prediction of extreme responses in large amplitude waves. For this reason the focus of this section is the evaluation of maximum and minima from the time histories of motions and loads.

To properly evaluate the probability density function of the extremes it is important to correctly identify the peaks of the signals, both positive and negative. Responses evaluated using a nonlinear approach usually present more than one local extreme for positive zero crossing period; a clear example is the vertical bending moment response when whipping is considered. Tuitman (2010) presented a comparison between several approaches to count extremes from nonlinear time domain hydroelastic method. The author compared results by counting one peak per mean zero crossing period, one peak per rigid body zero crossing period and by counting all the maximum and minima of the time histories. Tuitman concluded that the approach used to identify the peaks does not significantly affect the results.

In the current work peaks are extrapolated from the time history by counting only one positive and negative maximum per zero crossing period of the linear response. The linear methodology used in this analysis is described in section 3.4.4. This approach has been chosen to ensure consistency with results obtained

by rigid body methods. Nonlinear analysis are conducted in parallel to linear ones considering the same set of normal distributed phase angle ϵ of Equation 5.1. Figure 5.1 shows an example of the used approach to count extremes.

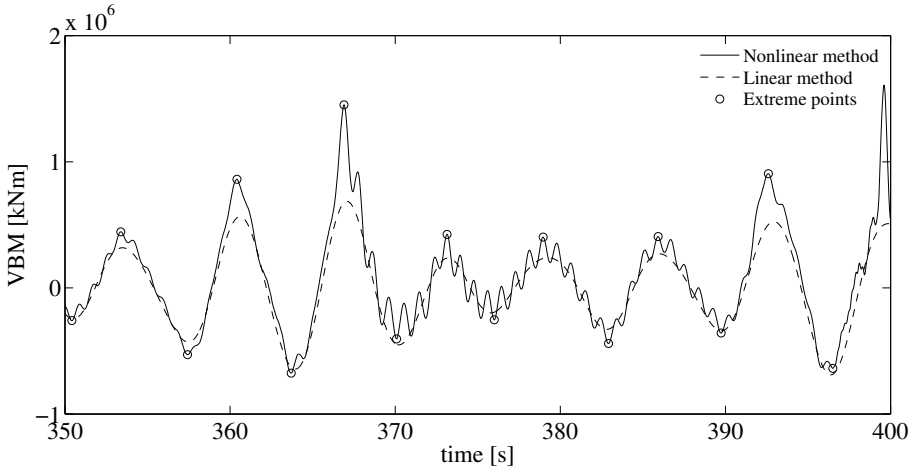

Figure 5.1: Example of counting method for extremes for the vertical bending moment time history

Once extremes are found, statistical properties can be evaluated directly from the histogram, or by fitting the values using a mathematically well-known probability density function. If the response characteristics in the short term are the only interest of the analysis, statistics can be evaluated directly from the histogram. If the short term analysis is incorporated into the evaluation of the maximum expected values in long term, probability distributions of the counted extremes should be fitted with a mathematical defined function. In this study, a Weibull probability density function is used to fit the histogram of the extreme responses.

Positive and negative peaks (especially for loads) must be studied separately to include asymmetric behaviours. An example of the differences between sagging and hogging peaks for the vertical bending moment response at station 10 for the S-175 container ship is reported in Figures 5.2 and 5.3 where the sagging and hogging extremes are respectively plotted.

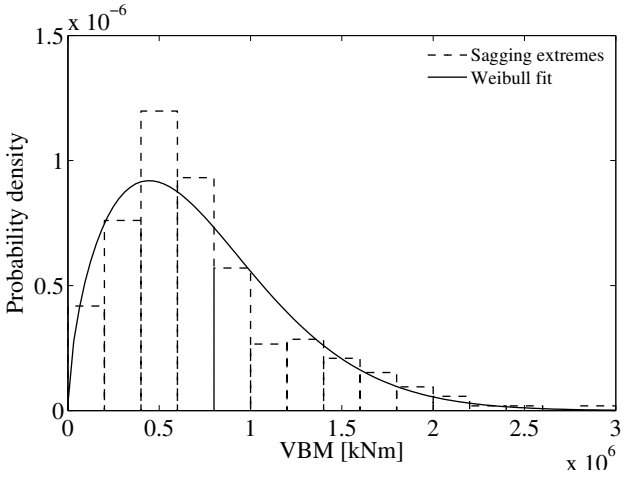

Figure 5.2: Example of short term analysis of the sagging extremes for the S-175 container ship, sailing in irregular sea $H_s = 13.5m$ and $T_p = 12.5s$ for $F_n = 0.25$ in head sea

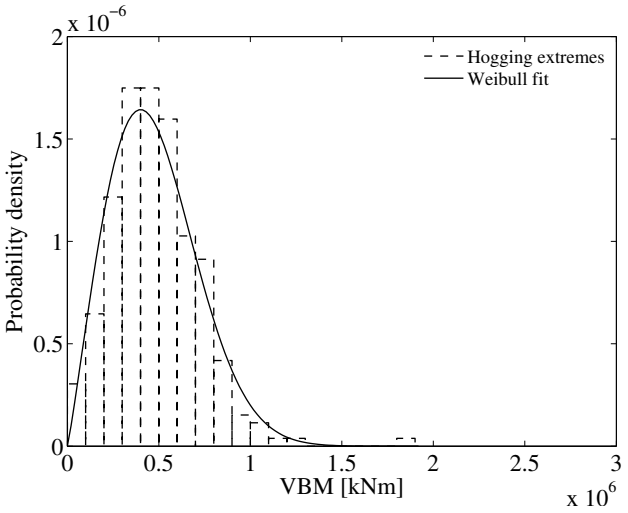

Figure 5.3: Example of short term analysis of the hogging extremes for the S-175 container ship, sailing in irregular sea $H_s = 13.5m$ and $T_p = 12.5s$ for $F_n = 0.25$ in head sea

Short term is usually defined as a three hours duration in which the characteristics of the sea state and of the vessel can be considered constant. In the present analysis the short term is simulated via three hours of time domain computation. This period is divided into six sets of thirty minutes simulations each. This subdivision allows to avoid the dependency of the response from the actual set of normal distributed phase angles ϵ and it also allows to parallelise the procedure

and hence reducing the computational time.

5.4 Long Term Analysis From the Nonlinear Seakeeping Method

The principal aim of the present analysis is to investigate the effect of whipping over the prediction of maximum expected wave induced loads. Results from nonlinear seakeeping approaches are often used to evaluate a correction factor that needs to be applied to the more popular linear methodologies. This correction factor is quantified as the ratio between the response, positive or negative, obtained by the nonlinear approach and the one calculated using the linear method, as described in Equation 5.4. Once this is evaluated, calculations are conducted using linear methods and nonlinearities are taken into account via the nonlinear correction.

$$C^{nl} = \frac{X_{nonlinear}}{X_{linear}} \tag{5.4}$$

A single value for the ratio between the nonlinear and the linear response does not characterise the whole behaviour of the vessel and it is strongly related to the parameters chosen for the calculation. For example, wave induced motions and loads are functions of the heading angles and the forward speed. Due to limitations in time, only a small number of headings and forward speeds can be considered for the nonlinear time domain analysis, and the actual set of values that is used influences the results.

When the wave body interaction problem is modelled using a linear approach the long term probability of exceedance of a certain value P for the variable p is

given as follow

$$Q_{LT}(P) = \iiiint_{H_s,T_z,\beta,U} Q_{ST}(p > P|h_s, t_z, b, u) f_{H_s,T_z}(h_s, t_z) \\ f(\beta, u|h_s, t_z)\bar{T}_z dh_s dt_z dbdu \tag{5.5}$$

where H_s is the significant wave height, T_z is the positive zero crossing period, f_{H_s,T_z} is the probability of occurrence of a combination of H_s and T_z, $f(\beta, u|h_s, t_z)$ is the probability of occurrence of a combination of wave heading angles and forward speed in a given sea state, and $\bar{T}_z = T_z^{avg}/T_z(h_s, t_z)$ is the weight parameter that takes into account the zero crossing period of the response in the short term defined as the average zero crossing period divided by the zero crossing period in the current sea state. Q_{ST} represents the commutative probability of the extremes in the short term, for a linear system it is defined as a Rayleigh distribution.

In the current analysis only head sea is considered therefore $\beta = 180$ degrees and the relation between forward speed and sea states is completely defined, thus Equation 5.5 can be simplified.

$$Q_{LT}(P) = \iint_{H_s,T_z} \widetilde{Q}_{ST}(p > P|h_s, t_z) f_{H_s,T_z}(h_s, t_z)\bar{T}_z dh_s dt_z \tag{5.6}$$

In Equation 5.6 $\widetilde{Q}_{ST}$ is the commutative probability of the extremes in the short term defined using the fitted Weibull functions described in section 5.3. $\bar{T}_z$ is formulated considering the actual number of positive zero crossing in the time histories.

Using a nonlinear approach, long term analysis can be performed following a procedure analogous to the linear one or, can be performed using the *"equivalent design sea state"* approach. In the equivalent design sea state method only the combination of H_s and T_z that gives the larger contribution to the maximum expected values for a probability of exceedance of 10^{-8} is considered. This par-

ticular sea state is usually identified using linear methodologies, considering the assumption that the combination of significant wave height and zero crossing period that mostly contributes to the linear response is the same combination that gives the maximum contribution for the nonlinear one. The sea state that gives the higher contribution to the probability of exceedance is identified using the coefficients of contribution approach described by Baarholm and Moan (2000). The coefficient of contribution C_r of the $si-th$ sea state to the probability of exceed P, $Q_{LT}(P)$, is defined as follow.

$$C_r(si) = \frac{Q_{ST}^{si}(p > P|h_s, t_z, b, u) f_{H_s,T_z}^{si}(h_s, t_z) \bar{T_z}^{si} \Delta h_s \Delta t_z}{Q_{LT}(P)} \tag{5.7}$$

where Δh_s and Δt_z are the finite step in the wave scatter diagram of significant wave heights and mean positive zero crossing period respectively.

5.5 Analysis in Irregular Waves for the S-175 Container Ship

In this section results in irregular seas for the S-175 are presented. The analysis is focused on the study of the long term maximum expected values of wave induced vertical bending moment. Results from the proposed time domain nonlinear hydroelastic approach are compared against prediction given by linear frequency domain methods, that are the current industry standards.

The principal particulars of the S-175 container ship together with its structural and mass properties are summarised in section 4.2. A single loading condition and a single wave heading angle (head sea) are considered for the long term analysis, instead of different configurations associated with the operational profiles and routes of the vessel. These assumptions are introduced to simplify the analysis

and to reduce the computational cost.

A different approach is taken for the vessel forward speed. The actual sailing speed of the vessel is function of the sea state in which the vessel is operating. Rougher seas requires the master to reduce the speed of the ship in order to avoid undesired events, such as slamming and green water. To understand the effect of forward speed on the nonlinear long term prediction, different speed profiles are used. Firstly the vessel is considered to sail at design speed (20 knots for the S-175) in all the sea conditions, in a second analysis the forward speed is function of the significant wave height as described in Figure 5.4

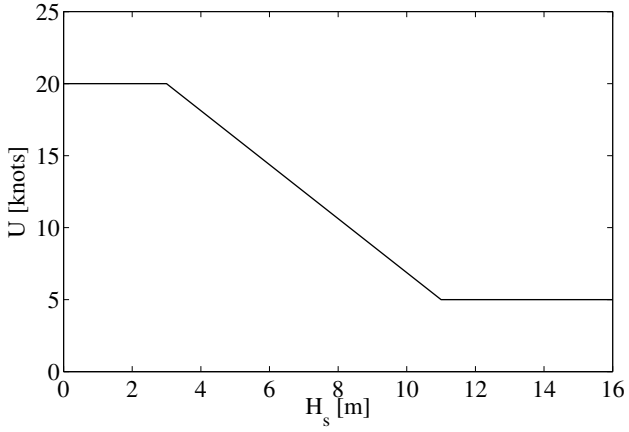

Figure 5.4: Ship speed in different sea states for the S-175 container ship.

The first approach is unrealistic, especially for large values of significant wave heights, but it helps to highlight the importance of choosing the correct value of an important parameters such as the speed of the vessel.

Figures 5.5 show the responses of the vessels sailing at $F_n = 0.25$ in an irregular sea with $H_s = 8.5m$ and $T_z = 11.5s$. Heave, pitch, vertical shear force at station 15 and vertical bending moment amidships are presented together with the time history of the wave elevation at the bow (Figure 5.5a). From the plots it is possible to observe the effect of slamming due to bottom and bow flare impact. When the simulated time reach almost 260 seconds, the bow enters into the water and

the time histories of the loads present large vibrations due to the impact showing the effect of whipping in irregular seas. Vibrations rapidly decay in two positive zero crossing periods due to structural and fluid damping.

Figure 5.6 presents the amplitude of the Fourier transform of the vertical bending moment amidships for the case in Figure 5.5. The spectral density shows that the larger amount of response is concentrated in the frequency range of the ocean waves, but a significant contribution is given at frequencies close to the first (two nodes) vertical wetted natural frequency of the hull. This contribution describes high frequency vibrations due to whipping. Springing could be also a cause of rapid fluctuations, but for a vessel of this size in a sea state with average positive zero crossing period $T_z = 11.5s$ springing does not affect the loads responses.

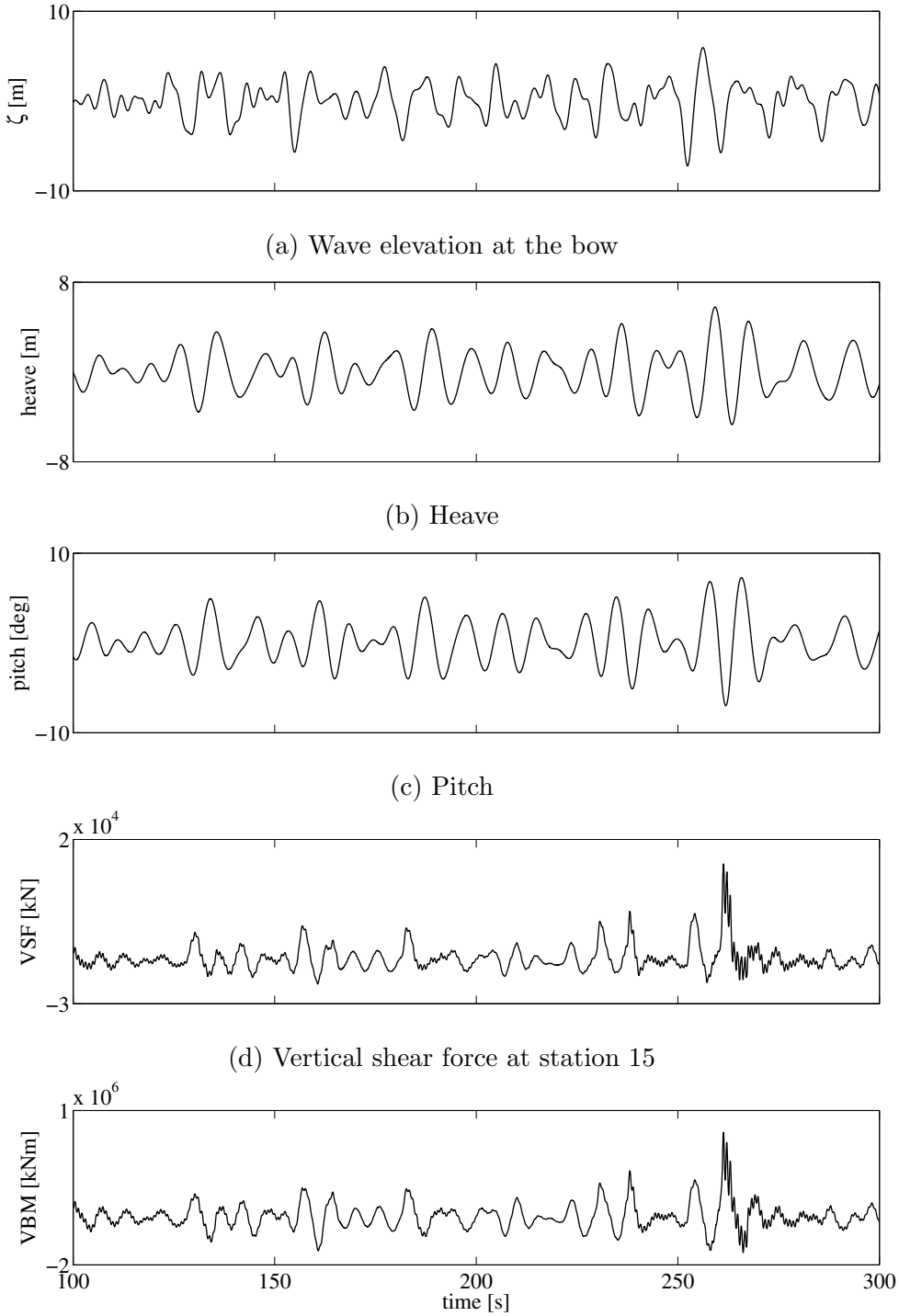

(a) Wave elevation at the bow

(b) Heave

(c) Pitch

(d) Vertical shear force at station 15

(e) Vertical bending moment amidsips

Figure 5.5: Time histories for the S-175 container ship sailing sea at $F_n = 0.25$ in irregular, $H_s = 8.5m$ and $T_z = 11.5s$.

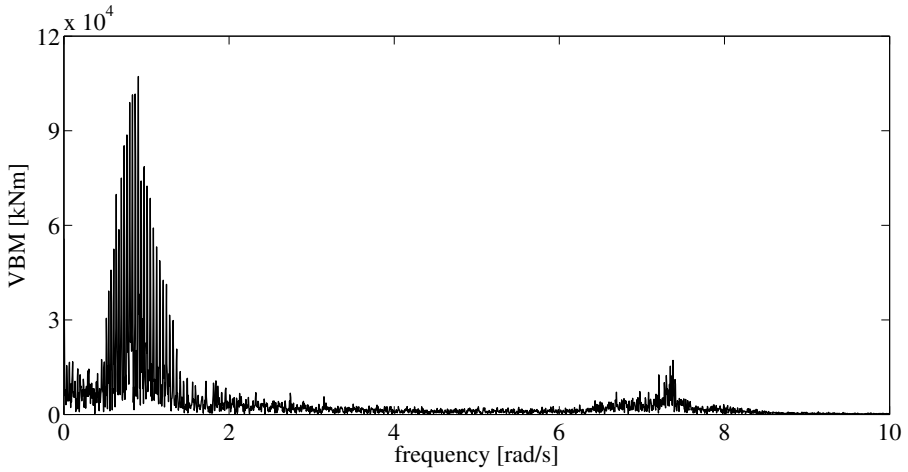

Figure 5.6: Amplitude of the Fourier transform for the vertical bending moment amidships for the S-175 container ship sailing sea at $F_n = 0.25$ in irregular, $H_s = 8.5m$ and $T_z = 11.5s$.

The present analysis is focused on the study of the maximum expected vertical bending moment amidships. The wave scatter diagram used in all the following long term calculations is the North Sea scatter diagram (IACS, 2000). Extreme expected values for sagging and hogging are calculated using the proposed nonlinear hydroelastic approach and compared against values calculated using a frequency domain strip theory (VERES). Long term analysis is conducted as described in the previous sections.

Table 5.1 describes the maximum expected values of vertical bending moment for the return periods of 3, 20 hours and 20 year. Linear and nonlinear results are compared using the correction factor described in Equation 5.4. This analysis is conducted considering the entire wave scatter diagram.

Return period	3 hours	20 hours	20 years
Prob. of exceedance	6.10110^{-4}	$9.152\ 10^{-5}$	$1.045\ 10^{-8}$
Linear VBM [kNm]	$5.275\ 10^{5}$	$6.457\ 10^{5}$	$1.246\ 10^{6}$
Sagging VBM [kNm]	$7.895\ 10^{5}$	$9.954\ 10^{5}$	$2.192\ 10^{6}$
Hogging VBM [kNm]	$6.332\ 10^{5}$	$8.009\ 10^{5}$	$1.632\ 10^{6}$
Sagging ratio	1.497	1.542	1.759
Hogging ratio	1.200	1.240	1.309

Table 5.1: Maximum expected values for different return periods of vertical bending moment amidships for the S-175 container ship with velocity profile described in Figure 5.4 considering the entire wave scatter diagram.

Results in Table 5.1 show a large asymmetry between nonlinear sagging and hogging response. Sagging amplitudes are usually larger compared to the hogging ones, due to the impulsive forces at the bow. It is also visible that the nonlinear correction factor is a function of the return period, especially for the sagging case, where it increments from 1.497 to 1.759 for return periods varying from 3 hours to 20 years. This behaviour is displayed in Figure 5.7 where the maximum expected values of Table 5.1 are plotted against the associated probability of exceedance (in logarithmic scale).

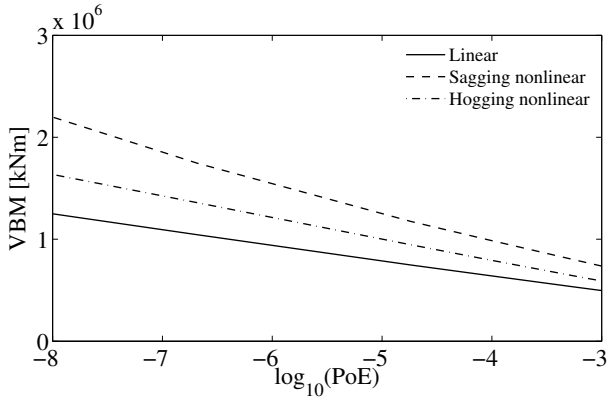

Figure 5.7: Long term probability of exceedance for vertical bending moment amidships, for the S-175; the whole scatter diagram is considered and the velocity varies accordingly to Figure 5.4.

The sagging vertical bending moment increases more rapidly with the return period, compared to the hogging one, and this affects the nonlinear correction factor.

In this calculation the entire wave scatter diagram is used. This approach is rather time consuming but allows to analyse the contribution of each sea state to the maximum response. The contribution of each combination of H_s and T_z is described using the coefficient of contribution reported in Equation 5.7. Figures 5.8 describe the results considering a return period of 20 hours, while in Figures 5.9 a return period of 20 years is applied. For each analysis results are presented for the linear, nonlinear sagging and hogging response.

For the smaller return period the values of C_r for the linear and the nonlinear cases are similar. For all three cases the maximum occurs at $H_s = 8.5m$ and $T_z = 9.5s$. Differences can be seen in the overall distribution of the coefficient of contribution. In the linear case the distribution is regular and spreads around a prevalent wave steepness (H_s/T_z). Distributions for nonlinear sagging present a steeper surface in which the sea states that give the higher contribution are more concentrated around the peak ($H_s = 8.5m$ and $T_z = 9.5s$); C_r for nonlinear hogging is similar to linear one, but in this case the majority of sea state that give a relevant contribution have values of H_s that are higher compared to the peak one; while the linear response present a almost symmetrical distribution (respect H_s).

For 20 years return period the maximum value of C_r for the linear response occurs at $H_s = 13.5m$ and $T_z = 9.5s$, while for the nonlinear sagging and hogging is at $H_s = 15.5m$ and $T_z = 10.5s$. The distribution of C_r around its peak is similar for all three cases. From Figure 5.9b seems that the distribution of C_r for the nonlinear sagging response presents two local maxima: they are a single peak and the plot displays separate peaks due to the steps in the wave scatter diagram.

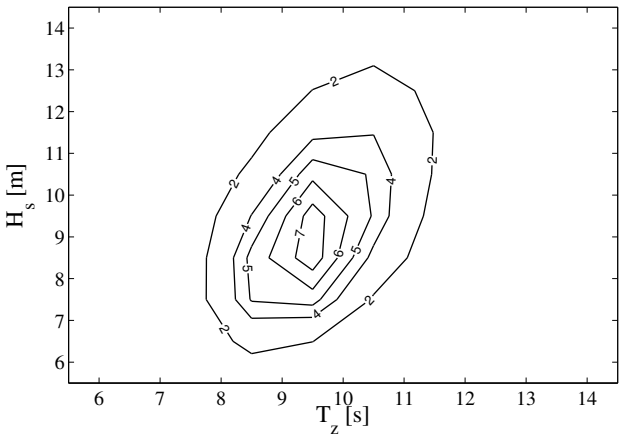

(a) Linear

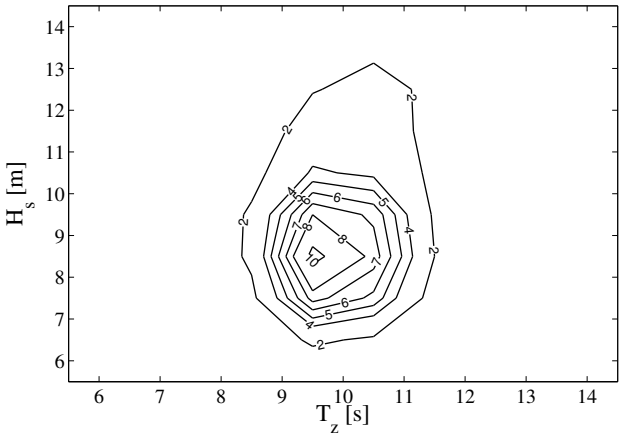

(b) Nonlinear sagging

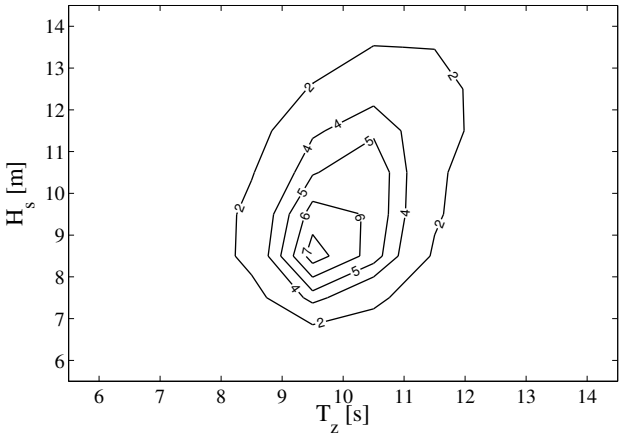

(c) Nonlinear Hogging

Figure 5.8: Coefficients of contribution C_r for the S-175 container ship for the linear, nonlinear sagging and hogging vertical bending moment amidships. Reduced speed profile of Figure 5.4, for a return period of 20 hours.

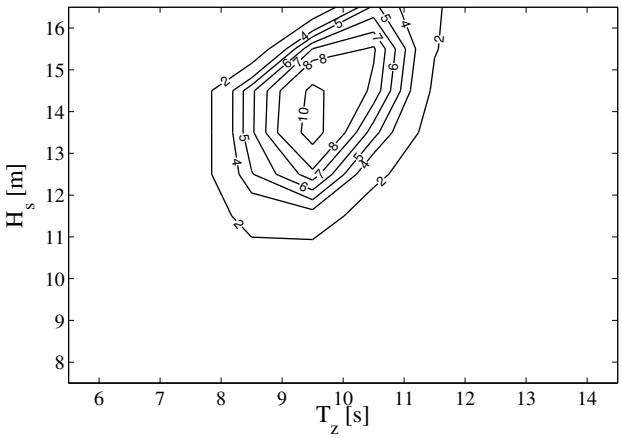

(a) Linear

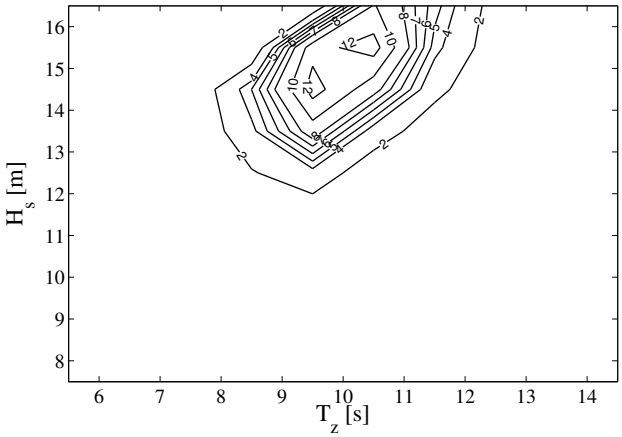

(b) Nonlinear sagging

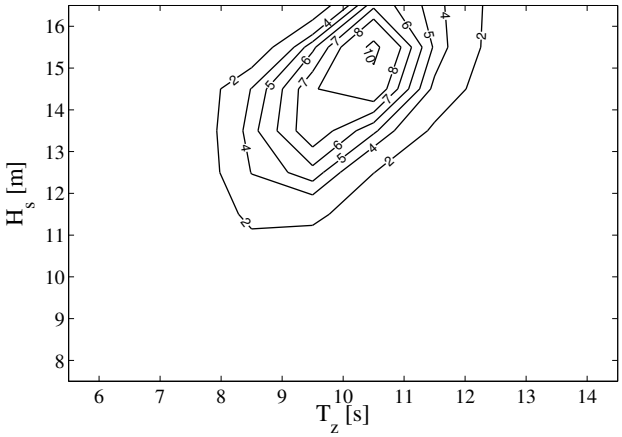

(c) Nonlinear hogging

Figure 5.9: Coefficients of contribution C_r for the S-175 container ship for the linear, nonlinear sagging and hogging vertical bending moment amidships. Reduced speed profile of Figure 5.4, for a return period of 20 years.

The analysis of the maximum expected vertical bending moment amidships conducted using the equivalent design sea state approach (EDS) is summarised in Table 5.2. The sea state used in the analysis has $H_s = 13.5m$ and $T_z = 9.5s$, since this is the combination of significant wave height and wave positive zero crossing period that gives the higher contribution to the probability of exceedance of 10^{-8}.

In the current case, the ratios between the linear and the nonlinear sagging response are higher compared to the results in Table 5.1, while for hogging the ratio is almost invariant. This could be due to the fact that the distribution of the coefficient of influence for nonlinear sagging is the one that presents larger differences between the all three distributions (see Figures 5.8 and 5.9).

Return period	3 hours	20 hours	20 years
Prob. of exceedance	$8.409\ 10^{-4}$	$1.261\ 10^{-4}$	$1.440\ 10^{-8}$
Linear VBM [kNm]	$1.100\ 10^{6}$	$1.239\ 10^{6}$	$1.757\ 10^{6}$
Sagging VBM [kNm]	$1.871\ 10^{6}$	$2.149\ 10^{6}$	$3.231\ 10^{6}$
Hogging VBM [kNm]	$1.408\ 10^{6}$	$1.592\ 10^{6}$	$2.283\ 10^{6}$
Sagging ratio	1.701	1.735	1.840
Hogging ratio	1.280	1.285	1.300

Table 5.2: Maximum expected values for different return periods of vertical bending moment amidships for the S-175 container ship with velocity profile described in Figure 5.4, using the EDS approach.

The values of maximum expected vertical bending moment in Table 5.2 are presented in graphical form in Figure 5.10. The figure shows the different behaviour of nonlinear sagging moment compared to Figure 5.7 in both terms of magnitude and curvature. Linear and nonlinear hogging response are almost parallel for all the probability values, while the sagging response is steeper.

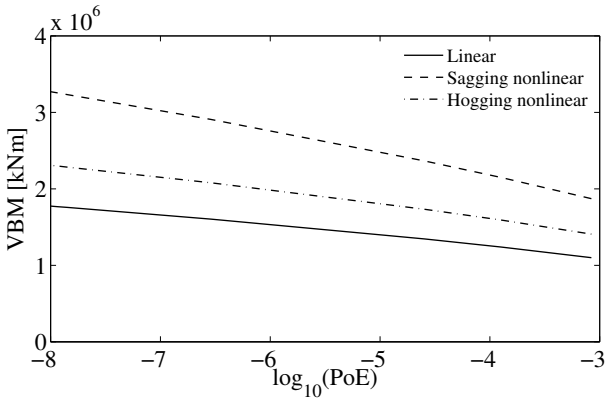

Figure 5.10: Long term probability of exceedance for vertical bending moment amidships, for the S-175; the EDS approach is considered and the velocity varies accordingly to Figure 5.4.

The nonlinear hydroelastic correction ratios, calculated using the entire wave scatter diagram and the EDS approach are compared in Table 5.3. For the sagging response the nonlinear correction ratio is larger when the EDS approach is used, for the hogging one the values obtained by the two approaches are similar for all the return periods. For both methods the ratios increase with the return period.

Tables 5.2 and 5.3 shows that EDS method over predicts the maximum expected bending moment for all the return periods. Also if that results in an inaccurate response, it improves the safety increasing the design loads. It can be seen as a useful compromise, especially if a nonlinear method is applied, because it reduces significantly the computational cost of the analysis.

Nonlinear analysis is based on the statistical study of three hours long time histories. Therefore the most accurate ratio should be the one based on the 3 hours return period, since the others extrapolate the maximum vertical bending moment from range of values that do not contain any actual simulated points. On the other hand this is a limitation, because the return period for design interest is at least 20 years long, and as described in Table 5.3 the nonlinear-linear response ratio is not constant (as function of the return period).

Return period	3 hours	20 hours	20 years
	Sagging VBM		
Whole scatter diagram	1.497	1.542	1.759
Equivalent design sea state	1.701	1.735	1.840
	Hogging VBM		
Whole scatter diagram	1.200	1.240	1.309
Equivalent design sea state	1.280	1.285	1.300

Table 5.3: Comparison of the nonlinear correction ratios obtained by using the entire wave scatter diagram and the EDS approach. For the S-175 with velocity profile described in Figure 5.4.

In the previous study the forward speed of the vessel is function of the significant wave height. In the current case the forward speed is constant for all the values of significant wave heights and equal to the design value of 20.15 knots ($F_n = 0.25$). Maximum expected vertical bending moment amidships is evaluated considering the entire wave scatter diagram. Results for different return periods are collected in Table 5.4 and plotted in Figure 5.11.

Results show large correction factor for nonlinear sagging that is 2.015 and 2.247 for a return period of 3 and 20 hours respectively. Correction for hogging is similar to previous case. The different behaviour of sagging and hogging response for different probability of exceedance can be seen in Figure 5.11. The sagging response increases more rapidly compared to the hogging one.

Return period	3 hours	20 hours	20 years
Prob. of exceedance	$5.892\ 10^{-4}$	$8.838\ 10^{-5}$	$1.009\ 10^{-8}$
Linear VBM [kNm]	$6.268\ 10^{5}$	$7.820\ 10^{5}$	$1.537\ 10^{6}$
Sagging VBM [kNm]	$1.263\ 10^{6}$	$1.757\ 10^{6}$	$4.640\ 10^{6}$
Hogging VBM [kNm]	$7.761\ 10^{5}$	$9.900\ 10^{5}$	$2.219\ 10^{6}$
Sagging ratio	2.015	2.247	3.019
Hogging ratio	1.238	1.266	1.444

Table 5.4: Maximum expected values for different return periods of vertical bending moment amidships for the S-175 container ship with constant velocity (20.15 knots), considering the entire wave scatter diagram.

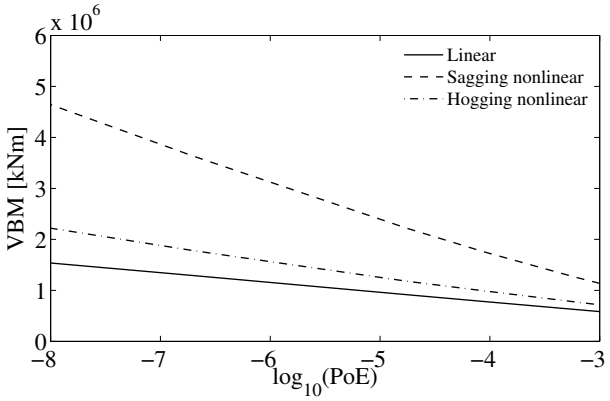

Figure 5.11: Long term probability of exceedance for vertical bending moment amidships, for the S-175 container ship with constant velocity (20.15 knots), considering the entire wave scatter diagram.

A comparison between the long term analysis considering the two different forward speed operational profiles is presented in Table 5.5. Forward speed of the vessel affects especially the sagging response. For 3 hours return period the nonlinear sagging correction increases from 1.497 to 2.015, as effect of considering the forward speed constantly equal to 20 knots. The hogging response shows a small increment due to the forward speed (from 1.2 to 1.238, for 3 hours return period).

This analysis underlines the problem of the selection of the correct relation be-

tween the velocity of the vessel and the severity of the sea states.

Return period	3 hours	20 hours	20 years
	Sagging VBM		
Speed reduction	1.497	1.542	1.759
Constant design speed	2.015	2.247	3.019
	Hogging VBM		
Speed reduction	1.200	1.240	1.309
Constant design speed	1.238	1.266	1.444

Table 5.5: Comparison of the nonlinear correction ratios obtained by using the velocity profile described in Figure 5.4 and the constant design speed (20.15 knots), for the S-175 considering the entire wave scatter diagrams.

The numerical method applied in the previous analyses is a nonlinear hydroelastic method, this approach takes into account nonlinear phenomena associated with slow varying forces.

In order to understand the nonlinear effects associated with wave frequency forces (nonlinear restoring forces, for example) a nonlinear rigid body model should be applied. To reproduce the results of a rigid body nonlinear approach the time histories of the vertical bending moment are post processed using a low pass filter that remove the high frequency vibrations associated with whipping.

Table 5.6 summarises the analysis for the maximum vertical bending moment amidships filtered from the high frequency response. The relationship between the forward speed of the vessel and the significant wave height is described in Figure 5.4. The EDS approach is used, limiting the analysis to a single combination sea state ($H_s = 13.5m$ and $T_z = 9.5s$).

The maximum expected sagging vertical bending moments calculated using the nonlinear rigid body technique is still larger than the one obtained using the linear approach. Also the nonlinear hogging response is larger than the linear

one. In this case the ratio between the nonlinear and the linear response varies slowly with the return period.

Return period	3 hours	20 hours	20 years
Prob. of exceedance	$8.409\ 10^{-4}$	$1.261\ 10^{-4}$	$1.440\ 10^{-8}$
Linear VBM [kNm]	$1.100\ 10^{6}$	$1.239\ 10^{6}$	$1.757\ 10^{6}$
Sagging VBM [kNm]	$1.574\ 10^{6}$	$1.807\ 10^{6}$	$2.712\ 10^{6}$
Hogging VBM [kNm]	$1.239\ 10^{6}$	$1.404\ 10^{5}$	$2.032\ 10^{6}$
Sagging ratio	1.431	1.458	1.544
Hogging ratio	1.126	1.134	1.157

Table 5.6: Maximum expected VBM amidships considering a nonlinear rigid body model. Considering different return periods, for the S-175 container ship, with velocity profile described in Figure 5.4 and using the EDS approach.

A comparison between the nonlinear correction factor obtained using the two different nonlinear approaches is presented in Table 5.7. Figures 5.12 and 5.13 display the maximum expected vertical bending moment for different levels of probability of exceedance for the linear, nonlinear rigid body and the nonlinear hydroelastic methods. Figure 5.12 describes the sagging response and Figure 5.13 the hogging one. Values predicted by the nonlinear hydroelastic approach are larger compared to the rigid body in both sagging and hogging response. The increment in response due to hydroelastic effects seems constant for all the return periods; the difference in sagging is 0.27 for 3 hours and 0.296 for 20 years, and in hogging varies from 0.154 to 1.43 for the same return periods.

Return period	3 hours	20 hours	20 years
	Sagging VBM		
Nonlinear rigid body	1.431	1.458	1.544
Nonlinear hydroelasticity	1.701	1.735	1.840
	Hogging VBM		
Nonlinear rigid body	1.126	1.134	1.157
Nonlinear hydroelasticity	1.280	1.285	1.300

Table 5.7: Comparison between nonlinear rigid body and nonlinear hydroelasticity correction ratios of the VBM amidships for the S-175 container ship. With velocity profile described in Figure 5.4 and using the EDS approach.

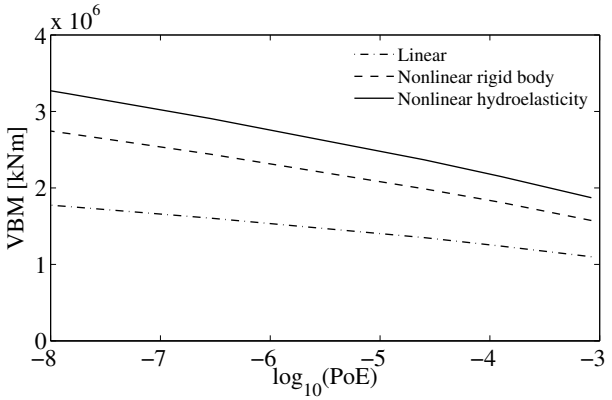

Figure 5.12: Long term probability of exceedance for sagging VBM amidships, for the S-175 container ship velocity profile described in Figure 5.4 and using the EDS approach. Comparison between linear, nonlinear rigid body and nonlinear hydroelastic methods.

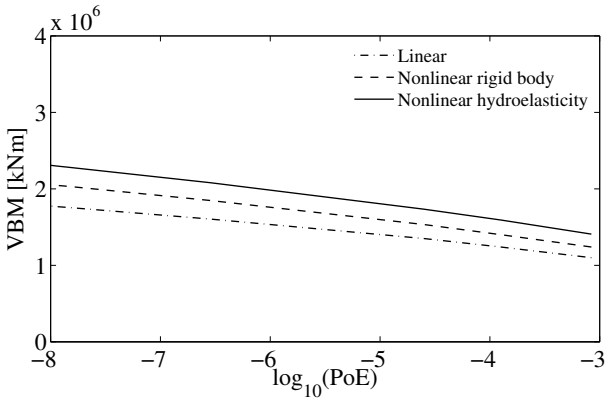

Figure 5.13: Long term probability of exceedance for hogging VBM amidships, for the S-175 container ship velocity profile described in Figure 5.4 and using the EDS approach. Comparison between linear, nonlinear rigid body and nonlinear hydroelastic methods.

5.6 Analysis in Irregular Waves for the WILS II Ultra Large Container Ship

The following section focus on the analysis of maximum expected vertical bending moment amidships for the WILS II 10,000 TEU container ship. The geometry of the vessel and its main particulars are described in Figure 5.14 and Table 5.8.

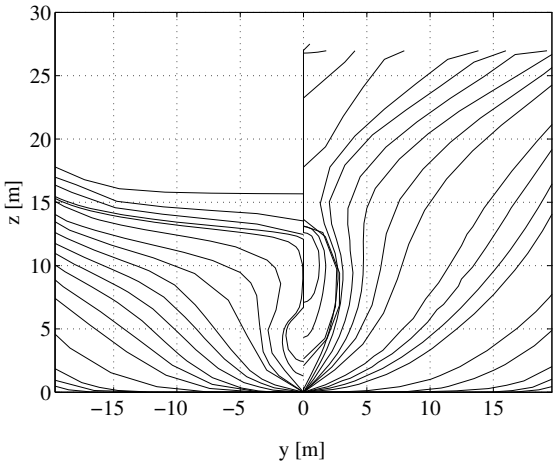

Figure 5.14: WILS II, lines plan.

Parameters	Values
Length between the perpendiculars	321.00 m
Beam amidships	48.40 m
Depth amidships	27.20 m
Draught amidships	15.00 m
Displacement	145200 tonnes
LCG from MP	-8.00 m
Pitch radius of gyration	80.51 m

Table 5.8: WILS II, main particulars.

The mode shapes and the natural frequencies of the structure of the vessel are evaluated using a finite element scheme as described in section 3.5. The natural frequencies for symmetric modes, used in the simulations, are summarised in Table 5.9. The calculation of structural characteristics of the hull is conducted using 50 longitudinal elements, while the nonlinear time domain seakeeping analysis is conducted using 40 stations.

Modes	Values [rad/s]
2	3.584
3	8.7505
4	15.6129
5	23.392

Table 5.9: WILS II, dry hull natural frequencies.

The analysis of the maximum expected vertical bending moment amidship is conducted using the EDS approach. The forward speed of the ship is considered function of the significant wave height as described in Figure 5.4. Analysis conducted with linear frequency domain strip theory identifies that the sea state

that gives the maximum contribution to the 10^{-8} probability of exceedance has $H_s = 15.5m$ and $T_z = 11.5s$. Time domain simulations for the selected sea state and statistical analysis of the time histories are conducted using the methodology described in section 5.3.

Table 5.10 compares the maximum expected vertical bending moment obtained using the proposed nonlinear technique against the results of the linear approach, for different return periods. Figure 5.15 plots the predicted extreme loads against the associated probability of exceedance.

Return period	3 hours	20 hours	20 years
Prob. of exceedance	1.14910^{-3}	$1.724\ 10^{-4}$	$1.967\ 10^{-8}$
Linear VBM [kNm]	$8.738\ 10^{6}$	$9.887\ 10^{6}$	$1.415\ 10^{7}$
Sagging VBM [kNm]	$1.475\ 10^{7}$	$1.690\ 10^{7}$	$2.505\ 10^{7}$
Hogging VBM [kNm]	$1.393\ 10^{7}$	$1.579\ 10^{7}$	$2.267\ 10^{7}$
Sagging ratio	1.689	1.709	1.770
Hogging ratio	1.595	1.597	1.602

Table 5.10: Maximum expected values for different return periods of vertical bending moment amidships for the WILS II container ship with velocity profile described in Figure 5.4, using the EDS approach.

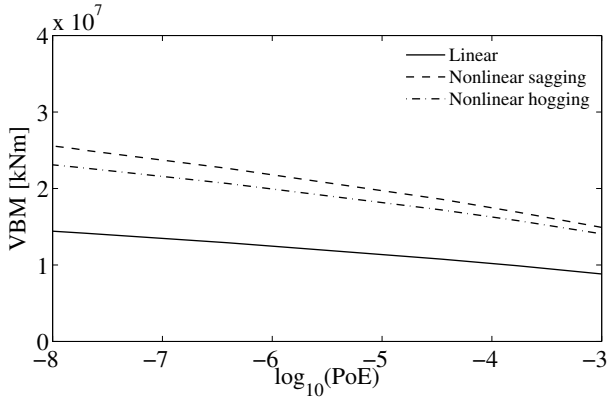

Figure 5.15: Maximum expected values for different return periods of vertical bending moment amidships for the WILS II container ship with velocity profile described in Figure 5.4, using the EDS approach.

Sagging and hogging bending moment predicted by the nonlinear hydroelastic approach are almost 1.7 and 1.6 times the ones obtained by the linear approach, respectively. The ratio between the nonlinear and the linear responses remains almost constant for the different return periods. This is clearly visible in Figure 5.15, where the curves that represent the nonlinear responses seem almost parallel and very close to each other. Hogging correction factor is larger compared to the S-175. For the S-175 it is 1.280 for 3 hours return period while for the Wils II is 1.595.

Storhaug et al. (2011) present experimental results for extreme and fatigue analysis of a 13,000 TEU container ship. Simulations where conducted in large sea states, the trials show that the amplification of vertical bending moment due to hydroelastic effect in severe seas has values similar to the one obtained via the proposed methodology. This publication cannot be considered as a validation of the proposed methodology, since the vessel and the conditions (forward speed and sea states) are different, but shows that the proposed methodology can improve the prediction of extreme wave induced loads in large amplitude waves.

5.7 Concluding Remarks

In the previous section the developed time domain nonlinear hydroelastic approach is used to assess extreme values of vertical bending moment amidships for the S-175 and the Wils II container ships. The vessels have different lengths, 175 and 320 metres respectively. Calculations are conducted considering different operational profile for the forward speed and using both the entire wave scatter diagram and the EDS approach for the long term calculations.

The comparison between the calculations performed using the entire wave scatter diagram and the EDS approach shows that EDS methods gives a higher prediction

for both the linear and the nonlinear response: 10% of the linear case 37% for nonlinear sagging and 22% for the nonlinear hogging (for 3 hours return period). Limiting the calculation to the sea states that give the maximum contribution does not allow to consider less severe sea states that tend to reduce the long term values. Convergency between the long term prediction obtained using the whole possible sea states and the EDS approach can be obtained using the iterative approach proposed by Baarholm and Moan (2000).

As described in the previous paragraph, the EDS approach tends to increase the prediction of the maximum expected loads. The increment is larger for the non-linear responses than for the linear one. From Figures 5.8 and 5.9 it is noticeable that the coefficient of contribution C_r has a steeper distribution for the nonlinear cases, this means that a smaller number of sea states, compared to the linear case, contributes significantly to the maximum expected values. The only case in which the distribution of C_r spreads in more sea states than the linear case is for the hogging with 20 years of return period, and in this case the correction factor calculated using the entire wave scatter diagram is slightly larger than the one obtained via EDS approach (1.309 and 1.300, respectively).

The analysis considering the vessel sailing at design speed in all the possible sea states shows the importance of selecting the correct velocity profile. Impulsive forces are extremely sensible to any change in forward speed, as described in Figure 4.56. The principal issue is that it is not possible to obtained a accurate relation between the forward speed and the significant wave height. The actual sailing speed of the vessel is function of the loading condition, route, sea state, economical condition and of master of the ship. An over estimation of the forward speed can lead to a not realistic correction factor, on the other hand an under estimation can under predict design loads.

Same consideration can be obtained for the wave heading angle. In this case the

assumption of limiting the analysis to head seas increase the safety margin, but if springing is considered for fatigue analysis, bow and quartering seas are critical due to the small natural periods of asymmetric modes (Hirdaris et al., 2003). This thesis focuses on extreme loads evaluation considering whipping, therefore the assumption of limiting the analysis to head seas can be considered reasonable.

All the long term prediction presented in sections 5.5 and 5.6 are conducted for different return periods. The ratio between the linear and nonlinear predictions increases with the return period. This is related to the increment of the importance of larger sea states for longer return periods. In these sea conditions nonlinear responses are higher than linear ones and therefore the maximum expected values, obtained via nonlinear methods, increase.

The Weibull probability density function that characterised the statistical properties of short term extreme responses is obtained by fitting up to 3 hours of numerical simulations. On the other hand the return period of interest for extreme wave induced loads is no less than 20 years. Calculating the maximum expected values, in 20 years, from the fitted Weibull distributions could lead to inaccurate results, since the fitting is obtained with values that have a larger probability of exceedance (compared to 20 years). On the other hand the calculation of the nonlinear correction ratio, considering 3 hours of return period, could under predict the correction factor. In this case the EDS approach represents a good compromise, because the sea state on which the calculations are based on is found considering a probability of exceedance of 10^{-8} and the maximum expected values are obtained, from the fitted Weibull distribution, for 3 hours return period.

The results for the Wils II container ship show the effect of the length of the vessel over the nonlinear wave induced loads. Both sagging and hogging response increases, compared to the S-175. The larger increment occurs to the hogging

vertical bending moments. Large wave induced hogging response can be critical for a container ship, since this type of ships usually have a large hogging still water vertical bending moment.

Chapter 6

Conclusions and Future Works

6.1 Conclusions

In this thesis a nonlinear time domain hydroelastic approach is presented. The hull is modelled as a one dimensional Timoshenko beam. Modal superposition method is used to solve the fluid structure interaction problem. The fluid actions on the hull are modelled using a nonlinear strip theory that considers the actual wetted hull portion and the relative velocity between the vessel and the waves. Impulsive forces are taken into account with a combination of analytical and empirical formulations.

Applying the methods described the following conclusions can be drawn:

- The validation of the methodology in both small and large amplitude waves in regular seas shows the capability of the proposed method to correctly assess the wave induced motions and loads.
- Analyses in large amplitude waves highlight the importance of high frequency vibrations due to water impact, in the calculation of wave induced loads

- Wave induced loads at different longitudinal sections depend upon different combinations of principal coordinates and mode of shapes, and modal superposition methods allow to study their relationship in details.
- The analysis of the longitudinal distribution of impulsive forces shows that impact forces at the stern have a significant magnitude and should therefore be included in the formulation of the equations of motion.

A procedure to apply the proposed methodology to long term analysis for wave induced loads is described. Extreme values are selected from the time history of wave induced motions and loads using the positive zero crossing period of the linear predictions. A Weibull probability density function is used to fit the histogram of the extreme. The long term analysis is conducted using both the entire wave scatter diagram and the Equivalent design sea state approach.

- Analysis of the maximum expected vertical bending moments shows that nonlinear rigid body motions effect and whipping lead to an increment to the sagging and hogging moment amplitudes compared to the equivalent linear case.
- The equivalent design sea state approach can give higher predictions, compared to considering the entire wave scatter diagram.
- A comparison between the nonlinear correction factors between the s-175 and the Wils II container ships, shows that nonlinear effects on wave induced vertical bending moment are more relevant for bigger vessels.

6.2 Future Works

Future research and applications of the proposed methodology could be conducted on several topics as follows:

- Introduction of more accurate methodologies for the evaluation of water impact that are able to take into account forward speed and asymmetrical impact.
- Modelling of green water on the deck.
- Implementation of asymmetrical modes to properly model arbitrary wave headings.
- Intensive parametric study to understand the effect of size of the dimension of the vessel and its operational profile over the nonlinear wave induced motions and loads.

References

Andersen, P. and Wuzhou, H. (1985). On the Calculation of Added Mass and Damping Coefficients by Simple Green's Function Technique, *Ocean Engineering* **12**(5): 425–451.

Baarholm, G. S. and Moan, T. (2000). Estimation of nonlinear long-term extremes of hull girder loads in ships, *Marine Structures* **13**: 495–516.

Bandyk, P. (2009). *A Body-Exact Strip Theory Approach to Ship Motion Computations* , PhD thesis, Department of Naval Architecture and Marine engineering, University of Michigan.

Beck, R. F. (1994). Time-domain computations for floating bodies, *Applied Ocean Research* **16**: 267–282.

Beck, R. F. (2001). Modern Computational Methods for Ship in a Seaway, *Transactions SNAME* **109**: 1–51.

Bishop, R. and Price, W. G. (1979). *Hydroelasticity of Ships*, Cambridge University Press.

Bruzzone, D., Gironi, C. and Grasso, A. (2011). Nonlinear Effects on Motions and Loads Using an Iterative Time Frequency Solver, *International Journal of Naval Architecture and Ocean Engineering* **3**: 20–26.

Bruzzone, D. and Grasso, A. (2007). Time Domain Evaluation of Vertical Motions of High-Speed Dispalcement Hulls, *Second International Conference*

on Marine Research and Transportation, Naples, Italy.

Chang, M.-S. (1977). Computations of Three-dimensional ship motions with forward speed, *2nd International Conference on Numerical Ship Hydrodynamics*, USA, p. 124/135.

Cummins, W. (1956). *The Wave Resistance of a Floating Slender Body*, PhD thesis, American University, Washington DC.

Cummins, W. (1962). The Impulse Response Function and Ship Motions, *Schiffstechnik* **9**(47).

Dawson, C. (1977). A practical method for solving ship-wave problems, *2nd International Conference on Numerical Ship Hydrodynamics*, USA.

Dessi, D. and Mariani, R. (2008). Analysis and Prediction of Slamming-Induced Loads of a High-Speed Monohull in Regular Wave, *Journal of Ship Research* **52**(1): 71–86.

Dommermuth, D. and Yue, D. (1987). Numerical Simulation of Nonlinear Axisimmetric Flows with Free-Surface, *Journal of Fluid Mechanics* **178**: 195–219.

Faltinsen, O. (1987). Numerical Techniques in Seakeeping, *18th ITTC Conference*, Kobe.

Faltinsen, O. M. (1978). A Numerical Nonlinear Method of Sloshing in Tanks with Two-dimansional Flow, *Journal of Ship Research* **22**(3): 193–202.

Fonseca, N. and Guedes Soares, C. (1998). Time-Domain Analysis of Large-Amplitude Vertical Ship Motions and Wave Loads, *Journal of Ship Research* **42**(2): 139–153.

Fonseca, N. and Guedes Soares, C. (2002). Comparison of Numerical and Experimental Results of Nonlinear Wave-Induced Vertical Ship Motions and Loads, *Journal of Marine Science and Technology* **6**: 193–204.

Fonseca, N. and Guedes Soares, C. (2004). Experimantal investigation of the nonlinear effects on the vertical motions and loads of a containership in regular waves, *Journal of Ship Research* **48**(2): 118–147.

Frank, W. (1967). On the Oscillation of Cylinders in or Below the Free Surface of Deep Fluid, *DTNSRDC, No2375* .

Froude, W. (1861). On the Rolling of Ships, *Transactions of the Institution of Naval Architects* **2**: 180–229.

Haskind, M. (1946). The Hydrodynamic Theory of Ship Oscillations inRolling and Pitching, *Prikl. Mat. Mekh.* **10**: 33–66.

Hirdaris, S. E., Price, W. G. and Temarel, P. (2003). Two- and Three-Dimensional Hydroelastic Modelling of a Bulker in Regular Waves, *Marine Structures* **16**(8): 627–658.

Huang, Y. (1997). *Nonlinear Ship Motions by a Rankine Panel Method*, PhD thesis, Department of Ocean Engineering, Massachusetts Institute of Technology.

IACS (2000). Rec. 2000. No. 34. Standard Wave Data.

ISSC (2009). 17th ISSC Committee 1.2 Load, *Technical report*, Seoul, Korea.

ITTC (2010). ITTC Workshop on Seakeeping , *in* Y. Kim (ed.), *ITTC Towing Tank Conference*, Seoul.

ITTC (2011). The Seakeeping Committee, *Technical report*, Rio de Janeiro, Brazil.

Jensen, J. and Dogliani, M. (1996). Wave-Induced Ship Full Vibrations in Stochastic Seaways, *Marine Structures* **9**: 353–387.

Jensen, J. and Pedersen, P. (1979). Wave-Induced Bending Moments in ships - a Quadratic Theory, *Transactions of the Royal Institution of Naval Architects* **121**: 151–161.

Joosen, W. (1964). Oscillating Slender Ships at Forward Speed, *Publ. No. 268 Neth. Ship Model Basin* .

Kim, Y.-H., Kim, K.-H., Kim, J.-H., Kim, T.-Y., Seo, M.-G. and Kim, Y.-I. (2011). Time-domain analysis of nonlinear motion responses and structural loads on ships and offshore structures: development of WISH programs, *International Journal of Naval Architecture and Ocean Engineering* **3**(1): 37–52.

Kim, Y., Kim, K.-H. and Kim, Y. (2009a). Analysis of Hydroelasticity of Floating Shiplike Structure in Time Domain Using a Fully Coupled Hybrid BEM-FEM, *Journal of Ship Research* **53**(1): 31–47.

Kim, Y., Kim, K.-H. and Kim, Y. (2009b). Linear and Nonlinear Springing Analysis in Time Domain Using Fully Coupled BEM-FEM, *International Workshop on Water Waves and Floating Bodies*, Zelenogorsk, Russia, pp. 1–4.

Kim, Y., Kim, K.-H. and Kim, Y. (2009c). Springing analysis of a seagoing vessel using fully coupled BEM–FEM in the time domain, *Ocean Engineering* **36**(11): 785–796.

Koo, W. and Kim, M.-H. (2004). Freely Floating-Body Simulation by a 2D Fully Nonlinear Numerical Wave Tank, *Ocean Engineering* **31**: 2011–2046.

Korsmeyer, F., Lee, C. H., Newman, J. N. and Sclavounos, P. (1988). The analysis of wave effects on tension-leg platforms, *7th Int'l. Conf. Offshore Mech. Artic Eng. (OMAE)*, Houston, TX, USA.

Korvin-Kroukovsky, B.V. (1955). Investigation of Ship motions in Regular Waves, *Transactions SNAME* **63**: 386–435.

Kring, D. C. (1994). *Time Domain Ship Motions by a Three-Dimensional Rankine Panel Method*, PhD thesis, Department of Ocean Engineering, Massachusetts Institute of Technology.

Krylov, A. (1896). A New Theory of the Pitching Motion of Ships on Waves, and on the Stresses Produced by this Motion, *Transactions of the Institution of Naval Architects* **37**: 326–368.

Kwon, Y. W. and Hyochoong, B. (1997). *The Finite Element Method Using MATLAB*, CRC Press.

Lewis, F. (1929). The Inertia of Water Surrounding a Vibrating Ship, *Transactions SNAME* **37**: 1–20.

Lin, W., Meinhold, M., Salvesen, N. and Yue, D. K. P. (1994). Large-Amplitude Motions and Waves Loads for Ship Design, *Proceedings of the Twentieth Symposium on Naval Hydrodynamics*, University of California, Santa Barbara, California, USA.

Longuet-Higgins, M. and Cokelet, E. (1976). The Deformation of Steep Waves on Water, *Proceedings of the Royal Society* **A(350)**: 1–28.

Maruo, H. (1967). Application of the Slender Body Theory to the Longitudianl Motion of Ships Among Waves, *Bull. Fac. Eng. Yokohama Natl. Univ.* **16**: 29–61.

Matthies, H. G. and Steindorf, J. (2003). Partitioned Strong Coupling Algorithms for Fluid-Structure Interaction, *Journal of Computers and Structures* **81**: 805–812.

Michell, J. (1898). XI. The Wave Resistance of a Ship, *Philosophical Magazine and Journal of Science* **45**: 106–123.

Nakos, D. E. (1990). *Ship Wave Patterns and Motions by a Three Dimensional Rankine Panel Method*, PhD thesis, Engineering, Massachusetts Institute of Technology.

Newman, J. N. (1961). A Linearized Theory of the Motion of a Thin Ship in Regular Waves, *Journal of Ship Research* **3**(1): 1–19.

Newman, J. N. (1964). A Slender-Body Theory for Ship Oscillations in Waves , *Journal of Fluid Mechanics* **18**: 602–618.

Newman, J. N. (1978). The Theory of Ship Motions, *Advances in Applied Mechanics* **18**: 221–283.

Newman, J. N. and Tuck, E. (1964). Current Progress in the Slender-Body Theory of Ship Motions, *Proc. Symp. Nav. Hydrodyn. 5th ACR-112*, Off. Nav. Res., Washington DC, pp. 129–167.

Nitta, A., Arai, H. and Magaino, A. (1992). Basis of IACS unified longitudinal strength standard, *Marine Structures* **5**: 1–21.

Ochi, M. K. and Motter, L. E. (1973). Prediction of Slamming Characteristics and Hull Responses for ship Design, *Transactions SNAME* **81**: 144–176.

O'Dea, J., Powers, E. and Zselecsky, J. (1992). Experimental Determination of Nonlinearities in Vertical Plane Ship Motions, *19th Symposium on Naval Hydrodynamics*, Seoul, Korea, pp. 73–91.

Ogilvie, T. (1964). Recent Progress Toward the Understanding and Prediction of Ship Motions, *5th Symposium on Naval Hydrodynamics*, Bergen, Norway.

Park, J. (2006). *Time Domain Simulation of Hydroelastic Response of Ships in Large Amplitude Waves*, PhD thesis, University of Southampton.

Pawlowski, J. S. and Bass, D. W. (1991). A Theoretical and Numerical Model of Ship Motions in Heavy Seas, *Transactions SNAME* **99**: 319–352.

Salvesen, N., Tuck, E. and Faltinsen, O. (1970). Ship Motions and Sea loads, *Transaction SNAME* **78**: 250–287.

Sclavounos, P. D. (2012). Nonlinear Impulse of Ocean Waves on Floating Bodies, *Journal of Fluid Mechanics* **697**: 316–335.

Singh, S. P. and Debabrata, S. (2007). A Comparative Linear and Nonlinear Ship Motion Study Using 3-D Time Domain Methods, *Ocean Engineering* **34**(13): 1863–1881.

St Denis, M. and Pierson, W. (1953). On the Motion of Ships in Confused Seas, *Transaction SNAME* **61**: 280–354.

Stavovy, A. B. and Chuang, S.-L. (1976). Analytical Determination of Slamming Pressure for High-Speed Vehicles in Waves, *Journal of Ship Research* **20**(4): 190–198.

Storhaug, G., Derbanne, Q., Choi, B.-K., Moan, T. and Hermundstad, O. (2011). Effect of Whipping on Fatigue and Extreme Loading of a 13000TEU Container Vessel in Bow Quartering Seas Based on Model Tests, pp. 1–10.

Storhaug, G., Malenica, S., Choi, B.-K., Zhu, S. and Hermundstad, O. A. (2010). Consequence of Whipping and Sprining on Fatique and Extreme Loading for a 13000TEU Container Vessel Based on Model Tests, *11th International Symposium on Practical Design of Ships and Other Floating Structures*, Rio de Janeiro, Brazil, pp. 1–101209.

Tuitman, J. (2010). *Hydro-Elastic Response of Ship Structures to Slamming Induced Whipping*, PhD thesis, Technische Universtiteit Delft.

Ursell, F. (1962). Slender Oscillating Ship at Zero Forward Speed, *Journal of Fluid Mechanics* **19**: 496–516.

Von Karman, T. (1929). The Impact on Seaplane Floats During Landing, *National Advisory Committee for Aeronautics, Technical Note No. 321* pp. 309–313.

Wagner, H. (1932). Phenomena Associated with Impacts and Sliding on Liquid Surfaces, *Z. Angrew. Math. Mech.* **12**: 193–215.

Watanabe, I., Keno, M. and Sawada, H. (1989). Effect of Bow Flare Shape to Wave Loads of a Container Ship, *Journal of the Society of Naval Architects Japan* **166**: 259–266.

Wehausen, J. and Laitone, E. (1960). Surface Waves, *Encyclopedia of Physics IX/Fluid Dynamics III* pp. 446–778.

White, N., Wang, Z. and Lee, Y. (2012). Guidance Notes on Whipping and springing Assessment, *International Marine Design Conference 2012*, Glasgow, pp. 279–293.

Wu, M. and Hermundstad, O. A. (2002). Time-Domain Simulation of Wave-Induced Non Linear Motions and Loads and Its Applications in Ship Design, *Marine Structures* **15**: 61–597.

Xia, J. (2005). A Consistent Strip-Theory Approach for Wave Loads and Ship Motions in Rough Seas, *20th Iinternational Workshop on Water Waves and Floating Bodies*, Longyearbyen, Norway.

Xia, J., Wang, Z. and Jensen, J. J. (1998). Non-Linear Wave Loads and Ship Responses by a Time-Domain Strip Theory, *Marine Structures* **11**: 101–123.

Zhang, X., Bandyk, P. and Beck, R. F. (2007). Large Amplitude Body Motion Computations in the Time-Domain, *9th International conference on numer-*

ical ship hydrodynamics, Ann Arbor, Michigan.

Zhang, X. and Beck, R. F. (2007). Computations for large-amplitude two-dimensional body motions, *Journal of Engineering Mathematics* **58**(1-4): 177–189.

Zhao, R. and Faltinsen, O. (1993). Water Entry of Two-Dimensional Bodies, *Journal of Fluid Mechanics* **246**: 593–612.

Zhao, R., Faltinsen, O. and Aarsnes, J. (1997). Water Entry of Arbitrary Two-Dimensional Sections with and Without Flow Separation, *21st Symposium on Naval Hydrodynamics*, pp. 408–423.

Appendix A

Evaluation of the Generalised Hydrodynamic Forces

Equations 3.34, 3.35 and 3.36 are applied to Equation 3.27 into the first and third terms of the right-hand side.

$$
\begin{aligned}
f_{hd}(x;t) = \sum_{r=0}^{\infty} \Bigg[& - a_z^{\infty} \Big(w_r \ddot{p}_r - 2U w_r' \dot{p}_r + U^2 w_r'' p_r - \ddot{\zeta} + 2U\dot{\zeta}' - U^2 \zeta'' \Big) \\
& + (a_z^{\infty})' U \Big(w_r \dot{p}_r - U w_r' p_r - \dot{\zeta} + U\zeta' \Big) \\
& - \frac{\partial a_z^{\infty}}{\partial T} \frac{dw}{dt} \frac{DW_{rel}}{Dt} \\
& - \int_0^t \dot{K}_z(\tau) \frac{DW_{rel}}{Dt}(t-\tau) d\tau + U \frac{\partial}{\partial x} \int_0^t K_z(\tau) \frac{DW_{rel}}{Dt}(t-\tau) d\tau
\end{aligned}
\tag{A.1}
$$

Then the sectional hydrodynamic force is defined by collecting the terms proportional to the principal coordinates p_r and its time derivatives, as presented

below.

$$
\begin{aligned}
f_{hd}(x;t) = \sum_{r=0}^{\infty} \Bigg[& - a_z^{\infty} w_r \ddot{p_r} + \Big(2a_z^{\infty} w_r' + (a_z^{\infty})' w_r\Big) U \dot{p_r} - \Big(a_z^{\infty} w_r'' + (a_z^{\infty})' w_r'\Big) U^2 p_r \Bigg] \\
& + a_z^{\infty} \frac{D^2\zeta}{Dt^2} - (a_z^{\infty})' \frac{D\zeta}{Dt} + \\
& - \frac{\partial a_z^{\infty}}{\partial T} \frac{dw}{dt} \frac{DW_{rel}}{Dt} \\
& - \int_0^t \dot{K}_z(\tau) \frac{DW_{rel}}{Dt}(t-\tau) d\tau + U \frac{\partial}{\partial x} \int_0^t K_z(\tau) \frac{DW_{rel}}{Dt}(t-\tau) d\tau
\end{aligned}
\tag{A.2}
$$

The first line of Equation A.2 collects the terms of the radiation forces that are directly proportional to the principal coordinates and their derivatives. The second line describes the impulsive diffraction force; the third line represents the impassive hydrodynamic force, while the last one collects the memory effect terms.

Equation 3.8 is used to formulate the generalised fluid action.

$$
\begin{aligned}
F_s^{HD}(t) = & \sum_{r=0}^{\infty} \Bigg[- \int_L a_z^{\infty} w_r w_s \; dx \; \ddot{p_r} \Bigg] \\
& + \sum_{r=0}^{\infty} \Bigg[U \int_L \Big(2a_z^{\infty} w_r' + (a_z^{\infty})' w_r\Big) w_s \; dx \; \dot{p_r} \Bigg] \\
& + \sum_{r=0}^{\infty} \Bigg[- U^2 \int_L \Big(a_z^{\infty} w_r'' + (a_z^{\infty})' w_r'\Big) w_s \; dx \; \dot{p_r} \Bigg] \\
& + \int_L \Big(a_z^{\infty} \frac{D^2\zeta}{Dt^2} - (a_z^{\infty})' U \frac{D\zeta}{dt}\Big) w_s \; dx + \\
& - \int_L a_z^{\infty} \frac{\partial a_z^{\infty}}{\partial T} \frac{dw}{dt} \frac{DW_{rel}}{Dt} w_s \; dx \\
& - \int_L \dot{\tilde{K}} w_s dx + U \int_L \tilde{K}' w_s dx \quad s = 0, 1, 2, \ldots
\end{aligned}
\tag{A.3}
$$

where the terms $\dot{\tilde{K}}$ and $\tilde{K}'$ describe the components of the convolution integrals.

$$\begin{aligned} \dot{\tilde{K}} &= \int_0^t \dot{K}(t-\tau)\frac{DW_{rel}}{Dt}(\tau)d\tau \\ \tilde{K}' &= \frac{\partial}{\partial x}\int_0^t K(t-\tau)\frac{DW_{rel}}{Dt}(\tau)d\tau \end{aligned} \tag{A.4}$$

Appendix B

Calculation of the Sectional Hydrodynamic Coefficients

The sectional frequency dependent hydrodynamic coefficients are evaluated following a BEM proposed by Andersen and Wuzhou (1985). The fluid is considered to be ideal, inviscid uniform and irrotational, therefore the velocity field within the fluid can be described by a velocity potential that has to satisfy the Laplace equation.

$$\nabla^2\phi = 0 \quad \text{in the fluid F} \tag{B.1}$$

Where ϕ is the velocity potential. This methodology utilises simple logarithmic Green functions and thus the entire boundary of the fluid domain has to be discretised into panels. The fluid boundary is composed by five different surface types over which different conditions are applied: body boundary S_1, free-surface S_2, bottom boundary S_5 (infinite water depth case), left and right radiation boundaries S_{4L} and S_{4R} respectively. Figure B.1 describes the fluid domain and its boundaries.

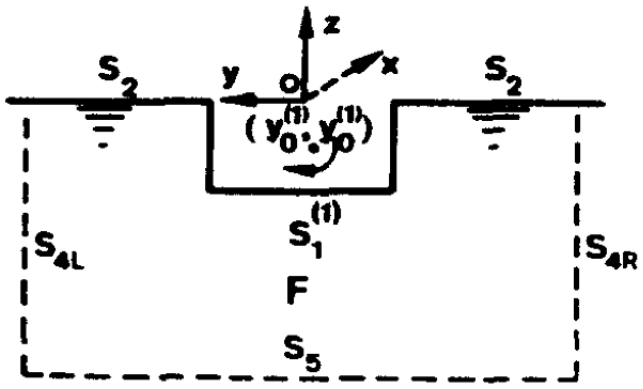

Figure B.1: The fluid Domain (Andersen and Wuzhou,1985)

The linearised set of boundary conditions for the case of a body vertically oscillating at frequency ω with unit amplitude in infinite water depth is described in Equation B.2

$$\begin{cases} \frac{\partial \phi}{\partial n} = i\omega n_z & \text{on } S_1 \\ \frac{\partial \phi}{\partial n} = \frac{\omega^2}{g}\phi & \text{on } S_2 \\ \frac{\partial \phi}{\partial n} = -i\frac{\omega^2}{g}\phi & \text{on } S_4 \\ \frac{\partial \phi}{\partial n} = -\frac{\omega^2}{g}\phi & \text{on } S_5 \end{cases} \tag{B.2}$$

where n_z is the z component of the normal vector to the boundary pointing outward the fluid domain. The condition over S_1 imposes that the normal component of the fluid velocity over the body section is equal to the normal velocity of the body. The second row of Equation B.2 describes the linearised free-surface boundary condition, while the last two lines assume that the potential at S_4 and S_5 is the one of a outgoing wave for infinite water depth.

By applying the Green's theorem the velocity potential of any point P inside the fluid and along its boundary can be found as follows

$$-V_p\phi(P) = -\int_S \big(\phi\frac{\partial lnr}{\partial n} - lnr\frac{\partial \phi}{\partial n}\big)ds + \int_{S_1}\big(i\omega n_z lnr\big)ds \tag{B.3}$$

where r is the distance between the point P and the integration point Q and V_p

is the angle between the half tangents in the fluid at point P.

Equation B.3 is solved by the method of discretisation. The boundary of the fluid is divided into a set of N linear panels. The potential of a point P located on the middle of $i-th$ panel is found adding the contribution of the integral along each panel S_j. Thus Equation B.2 can be approximated by the following equation.

$$-\pi\phi_i+\sum_{j=1}^{N}\int_{S_j}\phi\big(\frac{\partial lnr}{\partial n}-K_j lnr\big)ds=\sum_{m=1,S_m\in S_1}^{N}\int_{S_m}\big(i\omega n_{z,m}lnr\big)ds \quad i=1,2,...,N \tag{B.4}$$

where K_j is defined in Equation B.5

$$\begin{cases} K_j=0 & \text{if } S_j\in S_1 \\ K_j=\frac{\omega^2}{g} & \text{if } S_j\in S_2 \\ K_j=-i\frac{\omega^2}{g} & \text{if } S_j\in S_4 \\ K_j=-\frac{\omega^2}{g} & \text{if } S_j\in S_5 \end{cases} \tag{B.5}$$

The velocity potential ϕ is consider constant along a panel, therefore it can be moved out of the integral over S_j.

$$\begin{aligned} -\pi\phi_i+\sum_{j=1}^{N}\phi_j\Big[\int_{S_j}\big(\frac{\partial lnr}{\partial n}-K_j lnr\big)ds\Big]= \\ \sum_{m=1,S_m\in S_1}^{N} n_{z,m}\Big[\int_{S_m}\big(i\omega lnr\big)ds\Big] \quad i=1,2,...,N \end{aligned} \tag{B.6}$$

The integrals along S_j and S_m are numerical evaluated using a four points Gaussian quadrature method. Equation B.6 is a system of algebraic equations that can be solved to obtain the values of the velocity potential along the fluid domain boundary.

Once the values of ϕ are known everywhere along S the sectional added mass and

damping coefficients can be evaluated as follows

$$\begin{aligned} a_{33}(\omega) &= \frac{\rho}{\omega}\,\mathrm{Im}\left\{\int_{S_1}(\phi n_z)ds\right\} \\ b_{33}(\omega) &= \rho\,\mathrm{Re}\left\{\int_{S_1}(\phi n_z)ds\right\} \end{aligned} \tag{B.7}$$